Star Formation and Environmental Quenching of Group Galaxies from the GEEC2 Survey at $z \sim 1$

by

Angus Mok

A thesis
presented to the University of Waterloo
in fulfillment of the
thesis requirement for the degree of
Master of Science
in
Physics

Waterloo, Ontario, Canada, 2013

I hereby declare that I am the sole author of this thesis. This is a true copy of the thesis, including any required final revisions, as accepted by my examiners.

I understand that my thesis may be made electronically available to the public.

Declaration

The data from this work comes primarily from the Group Environment and Evolution Collaboration 2 (GEEC2) Survey. Observation, data reduction, and some initial analysis were done by the collaborators.

The figures and procedures outlined in Chapter 2 have been created and implemented by the members of the collaboration. Their work is included in this thesis where it is relevant to the proper understanding of my personal analysis in the subsequent chapters.

Abstract

This work presents detailed analysis from the GEEC2 spectroscopic survey of galaxy groups at $0.8 < z < 1$. This deep survey, which has a magnitude limit of $r_{AB} < 24.75$, had previously found a population of intermediate ('green') galaxies between the star-forming ('blue') and quiescent ('red') sequences. GMOS-S spectroscopy for the 11 X-ray selected galaxy groups was obtained and is highly complete ($> 66\%$) for eight of the eleven groups. Using an optical-NIR colour-colour diagram, the galaxies in the sample are separated with a dust insensitive method into the three categories, star-forming, quiescent, and intermediate. The strongest environmental dependence is observed in the fraction of quiescent galaxies, which is higher inside groups than in the field for all stellar masses. While intermediate galaxies represent $\sim 15-20$ per cent of the star-forming population in both the group and field, the average specific star formation rates (sSFR) of the group population is lower by a factor of ~ 3. The intermediate population also does not show the strong Hδ absorption that is characteristic of starburst galaxies. Inside groups, only $4.4-6.7$ per cent of star-forming galaxies are starbursts, which gives additional validity to the assumption that the quenching of star-formation is the primary process in the transition from the star-forming to the quiescent state. With the use of stellar synthesis models, two possible scenarios for the origins of the intermediate population are investigated, including the quenching of star-forming galaxies via environmental processes and the rejuvenation of star formation in early-type galaxies via mixed mergers. To model the quenching scenario, we have tested the use of different exponential quenching timescales (τ_2) and different types of delays between satellite accretion and the onset of quenching. We found that the fraction of intermediate galaxies depends most strongly on the value of τ_2. The relative fractions of galaxies rule out both the no-delay scenario, which would require a long τ_2 that over-produces intermediate galaxies, as well as the constant 3 Gyr delay model, which does not produce a sufficient number of quiescent galaxies. The observed fractions are best matched with a model that includes a dynamical delay time and a $\tau_2 = 0.25$ Gyr, but this model also predicts intermediate galaxies Hδ strength higher than that observed. For the rejuvenation scenario, we found that the time visible in the intermediate region is directly related to the size of the second 'burst' of star-formation, which can then be further constrained by the Hδ strength for the intermediate population. The observations are best matched to a burst size of ~ 1 per cent, at a rate of ~ 3 times per Gyr. In order to properly distinguish between the two scenarios, we will need to both increase the signal-to-noise ratio for the Hδ measurements and conduct a deeper survey of satellite galaxies both inside groups and in the field.

Acknowledgements

I would like to thank my supervisor, Michael Balogh, for his help throughout this process. His suggestions and insights have been invaluable in the research of this topic and the writing of this thesis.

I would like to thank the members of the GEEC2 and zCOSMOS collaborations. Without their contributions and prior efforts, this research would have been impossible.

Finally, I would like to thank my family and friends, for all their help and support along the way.

Table of Contents

List of Tables

List of Figures

Chapter 1

Introduction

1.1 What are Galaxies?

Galaxies are vast collections of stars, gas, dust, and dark matter bound together by the force of gravity. The luminous components of a galaxy lie at the centre of a spherical dark matter halo, which dominates the mass of the total system. Since dark matter is not yet detected directly, much of the historical observation and research have focused on the baryonic component of galaxies, which emits electromagnetic radiation that we can detect on Earth.

Several of the closest and brightest galaxies can be observed in the night sky as fuzzy patches of light. Historically, they have been called nebulae and were linked with the gas and dust clouds of the Milky Way, our home galaxy. The modern interpretation of these important objects only began in the early 20th century.

As part of the 'Great Debate' between Shapley and Curtis, there was a disagreement on the scale of the Universe. In particular, it had been unclear whether these special nebulae were nearby gas clouds inside the Milky Way or if they were separate galaxies or 'island universes'. In 1923, Erwin Hubble helped settle this debate by discovering that these objects were far too distant from the Earth to be part of the Milky Way, with the help of Celpheid variables in the Andromeda galaxy (Carroll & Ostlie, 2006).

This important discovery expanded the scale of the Universe by an enormous degree, as we now know that our Milky Way galaxy is just one galaxy out of many. As more and more galaxies have been discovered and catalogued, they have become ever more important tools for the field of astronomy. The study of galaxies has lead to many important discoveries, including the existence of dark matter.

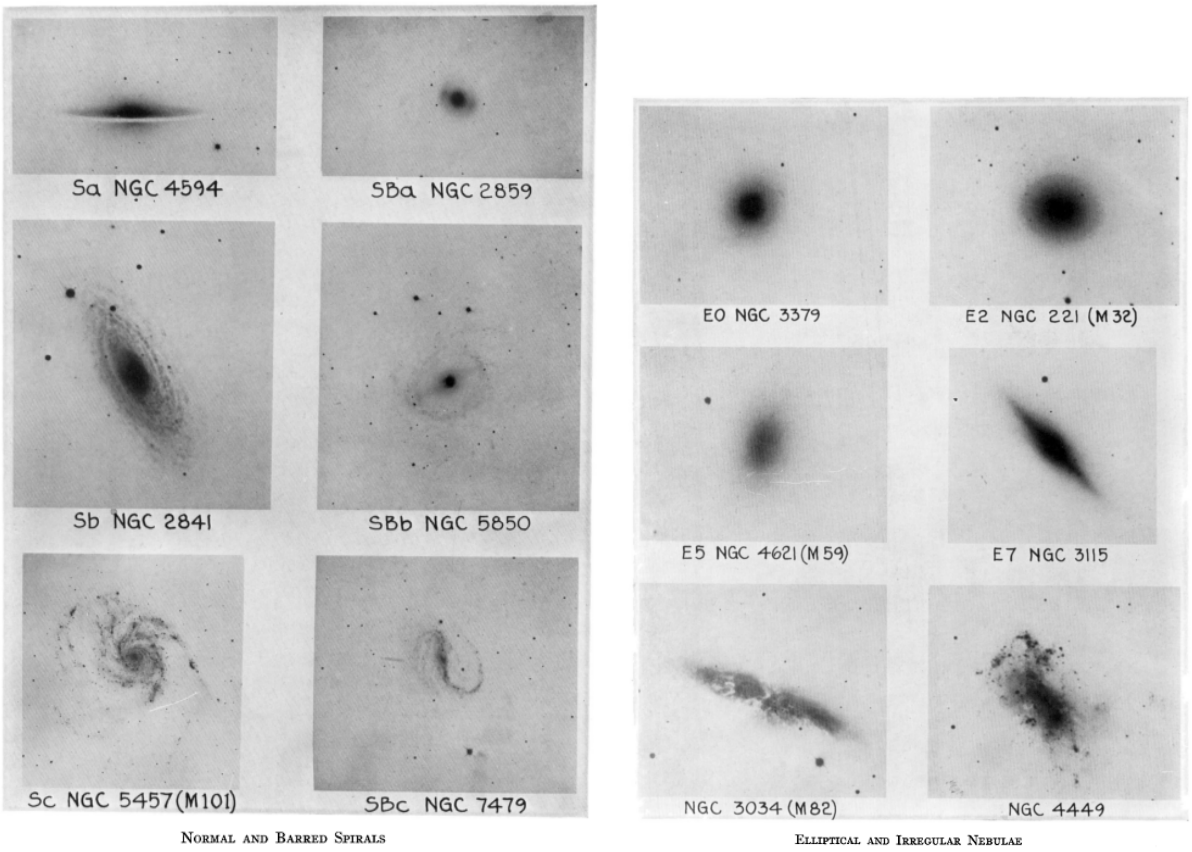

Figure 1.1: Hubble's galaxy morphology classifications from his original observations. Included are examples of spirals, ellipticals, and spirals. Reproduced from Hubble (1926).

Hubble first began to classify these extra-galactic collections of stars using their shapes, separating out elliptical, spiral, lenticular (a transitional category between spiral and elliptical) and irregular galaxies (Hubble, 1926). He later organized the elliptical, spiral, and lenticular galaxies into his Hubble sequence. In his well-known 'tuning fork' diagram, he also termed the spiral galaxies 'late-types' and the elliptical galaxies 'early-types'. Due to his enormous contributions to the study of extra-galactic objects, Hubble's classifications and conventions continue to be in use today.

Galaxies have also been traditionally classified according to their colours, into simple categories such as 'red' and 'blue'. With the advent of telescopes and the use of broad-band photometric filters, this process has been streamlined and quantified. The associated

measurement of the colours of individual stars have produced the Hertzsprung-Russell diagram and a vastly increased understanding of stellar evolution. When this technique was used on galaxies, it was found that spirals are typically bluer than ellipticals and giant ellipticals are typically redder than dwarf ellipticals (de Vaucouleurs, 1961). However, the relationship between photometry and morphology depends on multiple factors, which we will explore in later sections.

1.2 Galaxy Properties

In the 1970s, the global properties of galaxies were measured with great detail. They included the first measurement of the luminosity function for galaxies. Schechter (1976) pioneered the work of fitting an analytic function to this important distribution, which included a characteristic cut-off luminosity (L_*), a normalization (ϕ_*), and a power-law slope (α).

Other work focused on the scaling relations between the various physical properties of galaxies. For early-type galaxies, there is the Faber-Jackson relation, detailing a correlation between the mass (measured using the velocity dispersion) and the luminosity (Faber & Jackson, 1976). This was later generalized into the fundamental plane with the addition of the effective radius. For late-type galaxies, there is the Tully-Fisher relation, which correlates the rotational speed with the luminosity (Tully & Fisher, 1977). Both of these relationship are still quite useful in determining distances to galaxies.

Later, Dressler (1980) found one of the first hints of the relationship between morphology and their environment. With increasing local density, the fraction of ellipticals and lenticular increased while the fraction of spirals decreased. This relationship between morphology and density continues to be an important topic in the study of galaxy formation and evolution.

Systematic surveys of galaxies were soon proposed, studying a whole range of galaxy properties. They include wide-field surveys of large areas of the sky, as well as more detailed studies of select galaxies. The first large-scale redshift survey was the Center for Astrophysics (CfA) Redshift Survey, which was completed in 1982 and was made up of 2401 galaxies brighter than a magnitude of 14.5 (Huchra et al., 1983). The CfA survey provided the first clear picture of the large scale structure of the Universe.

Other large scale surveys were done, including the 2-degree Field Galaxy Redshift Survey (2dFGRS), completed in 2002 and the data released in 2003. In addition to measuring cosmological parameters like the power spectrum of galaxies and clustering, the 2dFGRS

also provided a detailed spectroscopic catalogue to aid in the study of galaxy properties (Percival et al., 2001).

For example, the luminosity function of star-forming galaxies was found to have a fainter characteristic magnitude than passive galaxies (-19.6 vs -19.2), as well as a steeper faint-end slope ($\alpha = -1.50$ vs -0.54) (Madgwick et al., 2002). This suggests that star-forming galaxies are, on the average, fainter than passive galaxies and more numerous in the faint-end.

By far the largest redshift survey conducted to date is the Sloan Digital Sky Survey (SDSS). With the latest Data Release 9, the data over 14000 square degrees and over a million galaxy spectra (released online at https://www.sdss3.org/dr9/). This wealth of new data has allowed detailed measurements of an unprecedented number of galaxies. Some of the key observations include:

First, after combining SDSS with the Two Micron All Sky Survey (2MASS), Bell et al. (2003) determined the luminosity functions and stellar mass functions for galaxies, separating out the early and late types using the concentration parameter. Similar to previous results, they found that late-type galaxies have a fainter characteristic magnitude than early-type galaxies and possessed a steeper faint-end slope.

Second, when these galaxies were separated by environment, i.e., into isolated, groups, and clusters, and their stellar mass functions measured, clear trends could be observed (Blanton & Moustakas, 2009). This is shown in Figure 1.2. More massive galaxies are found in denser environments. Furthermore, in denser environments such as clusters, early-type galaxies become the increasingly dominant population.

Third, the study of the distribution of galaxies in the $g - r$ and $u - g$ colour-colour diagrams, which is sensitive to star formation, has shown a clear bi-modality in the distribution, which morphologically corresponds to early and late type galaxies (Strateva et al., 2001). Furthermore, between the two peaks there is a clear minimum in the number of galaxies, which is sometimes referred to as the 'green valley'.

1.3 High Redshift Galaxy Properties

To aid in the understanding of galaxy formation and evolution, astronomers have focused on extending the study of galaxies to higher redshifts (i.e. looking further back in time). This work required much deeper surveys, such as the DEEP2 Galaxy Redshift Survey, the VIMOS-VLT Deep Survey (VVDS), and the Cosmic Evolution Survey (COSMOS).

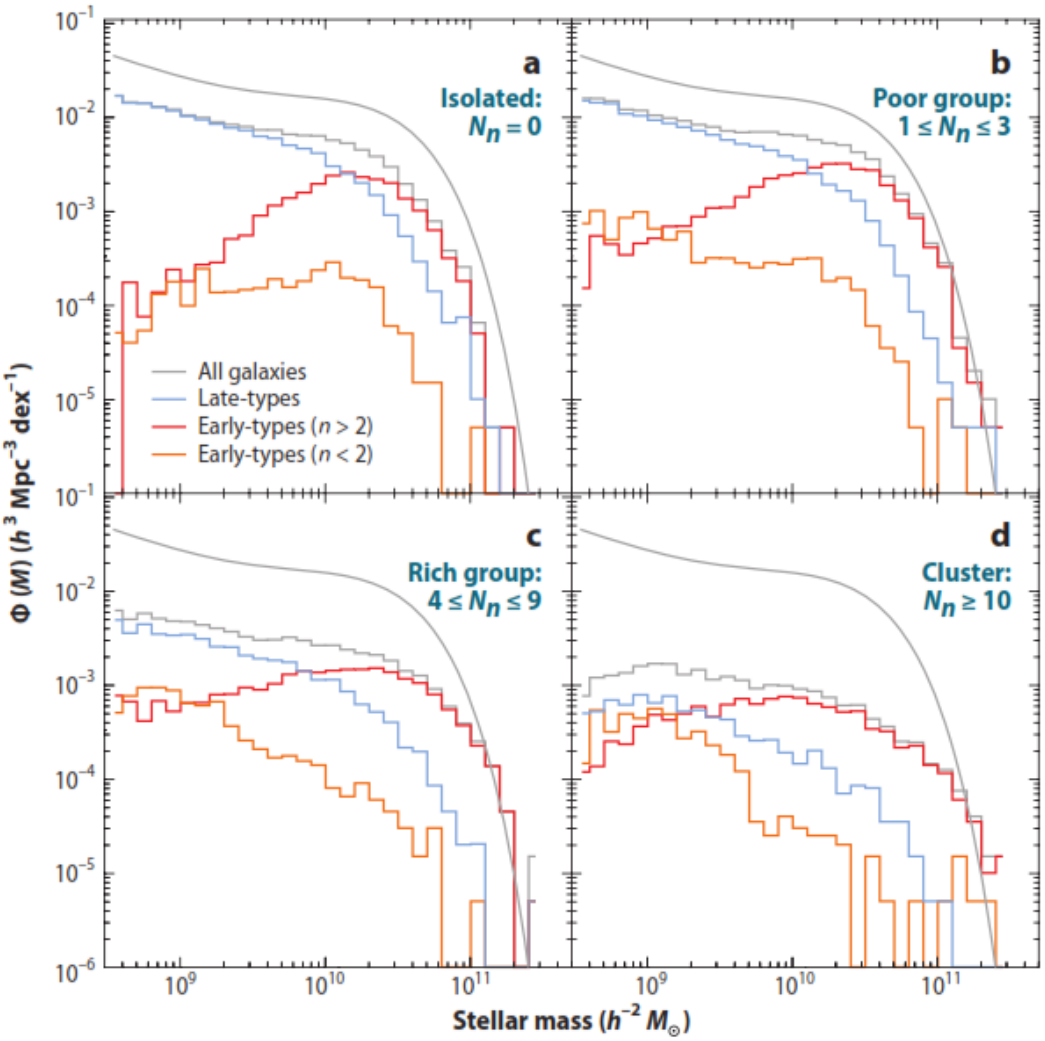

Figure 1.2: The stellar mass function of different morphological types, as a function of environment in the SDSS survey. Included are late-types, early-types with Sersic index ($n > 2$), and early-types with Sersic index ($n < 2$). Clockwise from the top left are plots for isolated galaxies, poor groups, rich groups, and clusters. The *gray curve* is a double Schechter fit to the whole sample. Reproduced from Figure 4 of Blanton & Moustakas (2009).

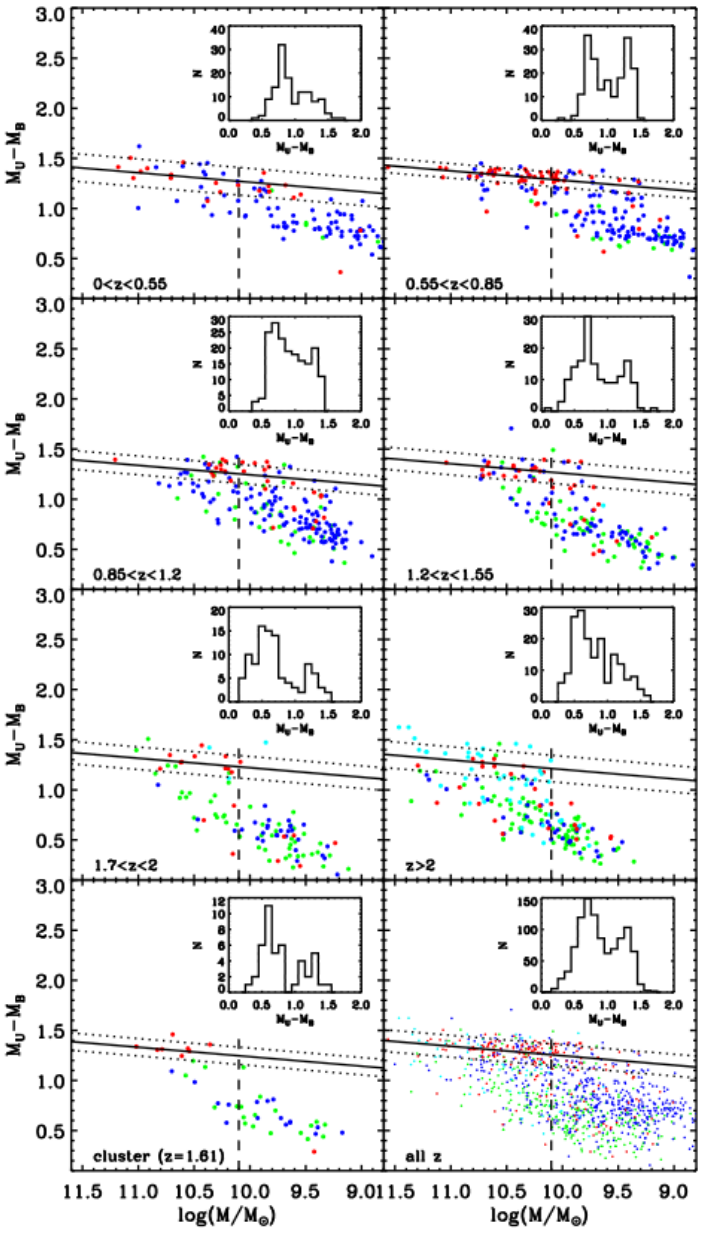

Figure 1.3: Colour-Mass diagram for galaxies from $0 < z \lesssim 3$ from the GMASS project. The bi-modal distribution is still seen at $z \sim 2$. Reproduced from Figure 1 of Cassata et al. (2008).

These surveys focus on using large telescopes to observe much fainter objects, down to $R_{\rm AB} < 24.1$ for DEEP2 (Davis et al., 2003), $I_{\rm AB} < 24$ for VVDS (Le Fèvre et al., 2005), and up to $I_{\rm AB} < 24$ for COSMOS-Deep (Lilly et al., 2007). Some of the key observations are presented below:

Inside the COSMOS field, the NEWFIRM Medium Band Survey (NMBS) have found that the bimodal distribution of galaxies observed in the local universe continue to be in place at $1 < z < 2.5$ (Brammer et al., 2009). They observed a red peak, a blue peak, and a much smaller population in between. Furthermore, in a colour-magnitude diagram, galaxies have been found to separate into a well-defined 'red sequence' and 'blue cloud', even at $z \sim 1$ (Bell et al., 2004).

With the GMASS project (Galaxy Mass Assembly Ultradeep Spectroscopic Survey), the bimodal nature of the distribution was found to exist up to $z \sim 2$, with the relative contribution of the passive galaxies decreased from $\sim 70\%$ at $z \sim 0.5$ to $\sim 50\%$ at $z \sim 2$ (Cassata et al., 2008). This result can be seen in Figure 1.3.

From the DEEP2 and COMBO-17 survey results, the normalization of the luminosity function for blue galaxies was found to remain almost the same over time, while it has doubled (~ 0.5 dex) for red galaxies since $z \sim 1$ (Faber et al., 2007). This is consistent with the results from the VVDS survey (Arnouts et al., 2007), where the stellar mass density for star-forming galaxies have remained constant, while it has doubled for passive galaxies. These results suggest that actively star forming galaxies must somehow transition to the quiescent population, 'building' up the red sequence.

This is also supported by measurements of the star formation density of the universe, which has been found to strongly depend on redshift. On the whole, star formation has peaked at $z \sim 2$ and has been decreasing until the present day (Cucciati et al., 2012). This is shown in Figure 1.4. For individual galaxies, this decrease in the star formation rate has been found to be linked to stellar mass, with more massive systems showing sharper decreases in star formation (Juneau et al., 2005). This process is also known as 'downsizing', where star formation gradually proceeds from higher mass to lower mass galaxies.

We also know that the star-forming galaxies continue to show a strong relationship between the specific star formation rate (sSFR) and stellar mass at $z \sim 1$, with moderate scatter (Noeske et al., 2007a; Salmi et al., 2012). Galaxies that lie above this sequence tend to either host an active galactic nucleus (AGN) or a short-lived burst of star formation, while those below the relation may be cases where the galaxy's star formation is shutting down (Whitaker et al., 2012b).

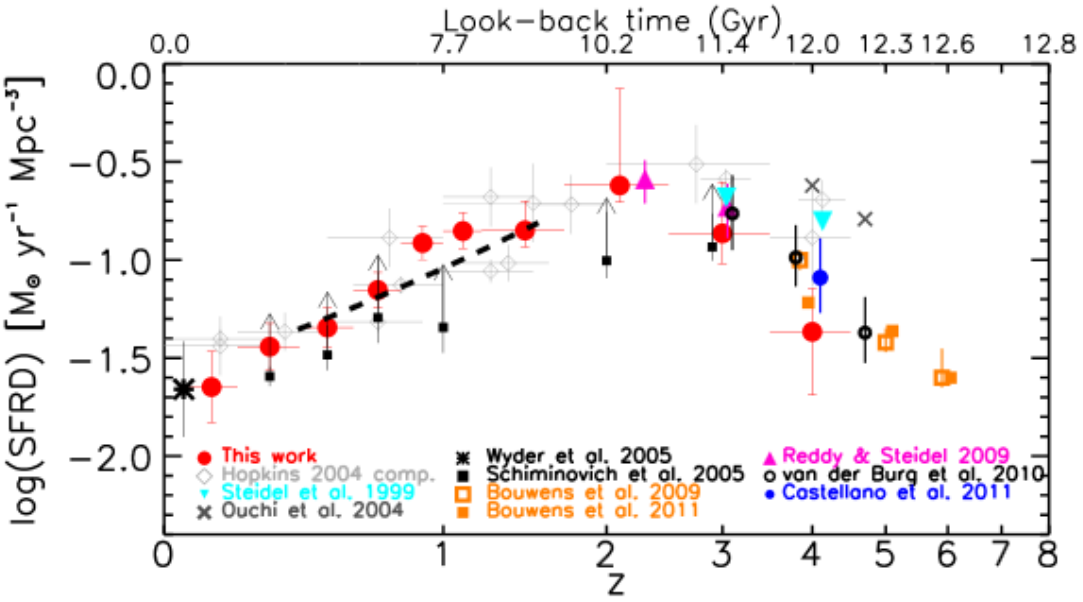

Figure 1.4: The star formation rate density of the Universe as a function of redshift, from various survey results. Reproduced from Figure 5 of Cucciati et al. (2012).

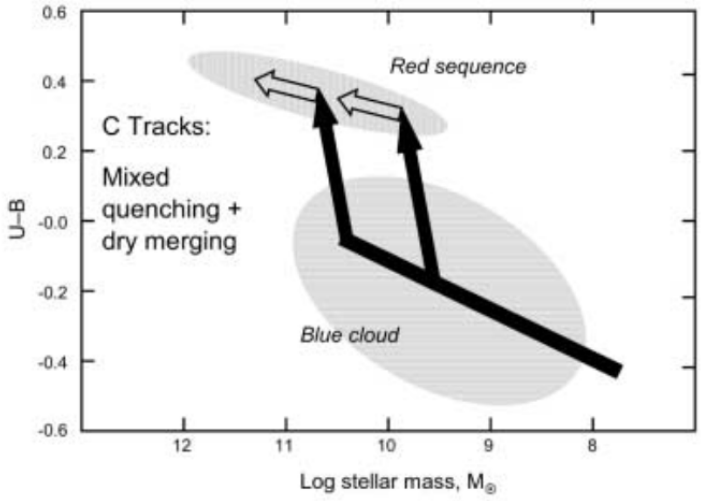

Figure 1.5: A possible scenario for the creation of the red sequence in a colour-mass diagram. Galaxies transition from star-forming to the quiescent state and gradually gain mass through dry (gas-less) mergers. Reproduced from Figure 10 of Faber et al. (2007).

How and why galaxies evolve from the star-forming sequence to the red sequence remains an important topic of research.

1.4 Evolution of Galaxies

From observations, we know that there is a clear bi-modality of galaxy colours and properties, which continues to exist at $1 < z < 2.5$. We also know that there has been a build up of the red sequence since that point, a 'dead' sequence that is characterized by a lack of star formation (Brammer et al., 2009).

A general process that fits the changes in the luminosity functions of star-forming and passive galaxies has been proposed by Faber et al. (2007) and is shown in Figure 1.5. Galaxies transition from the star-forming phase through quenching mechanisms and then potentially later merge through dry mergers.

1.4.1 Semi-Analytic Models

As well as studying galaxy evolution from the perspective of observations, we can also approach this problem from a more theoretical basis. From the current ΛCDM model of the Universe, we know that structure formation is hierarchical and largely determined by the distribution of dark matter. However, to form galaxies from numerical simulations is not a straight-forward matter. In general, this is done using semi-analytic models and requires the following steps, as discussed in Mo et al. (2010).

- From the cosmological model, use N-body simulations to determine the distribution of dark matter and the merger histories of dark matter haloes through Press-Schechter formalism.
- For each dark matter halo, keep track of the the baryonic contents (such as hot gas, cold gas, and stars) and convert between these different components through processes such as star formation, feedback, gas cooling, etc.
- Use stellar synthesis models to determine the colour, luminosity, and other observable properties of the galaxy.
- When necessary, model the outcome of halo mergers and the time when satellite galaxies enter a new halo. This requires a prescription of the environmental effects on the baryonic content, such as cold and hot gas.
- Finally, compare model results to the galaxy population both at the present day and at different redshifts. Refine model when necessary.

Many of these steps require a lot of additional physics, such as the procedure of turning cold gas into stars (e.g. Kennicutt, 1998) or determining the appropriate amount of feedback from AGN and supernovae reheating. Constant improvements in the semi-analytic models have created simulations that match the metallicity, cold gas fractions and the specific star formation rates of galaxies in the local universe, as well as the exponential cut-off in the stellar mass function (Somerville et al., 2008).

These semi-analytic models suggests that the quenching of massive galaxies observed ('downsizing') are caused primarily through AGN feedback, particularly after major merger events (Hopkins et al., 2006). For satellite galaxies, previous simulations have found that they tend to have colours redder than observed. However, more recent results have indicated that satellite galaxies are able to retain a significant fraction of their hot gas after in-fall, which allows them to continue forming cold gas and stars for several Gyr afterwards (Font et al., 2008).

1.4.2 Environmental Dependence

We know that other than epoch and stellar mass, a galaxy's environment can play a significant role in the quenching of star formation. We have seen this in Figure 1.2, where the stellar mass functions of SDSS galaxies in different environments was shown. Dense environments tend to have more massive galaxies and their galaxy populations are increasingly dominated by late-type galaxies.

Even at $z \sim 1$, surveys have found that the fractions of galaxies found along the 'red sequence' are higher for over-dense regions at fixed stellar masses (George et al., 2011; Muzzin et al., 2012; Tanaka et al., 2012; Presotto et al., 2012). Other results point to the existence of radial gradients in the fraction of quiescent and star-forming galaxies inside groups (Presotto et al., 2012), which may be further evidence of the work of environmental quenching upon in-fall.

Theoretically, many processes have been proposed to explain these inferred quenching of star formation in satellite galaxies. Inside groups, the process of strangulation may occur, where the satellite galaxy is stripped of its hot gas when entering a larger halo (van den Bosch et al., 2008). This removes the fuel for future star-formation and leads to the transition to a quiescent state.

In very dense environments, ram pressure stripping of the cold gas content of in-falling satellite galaxies could become an important factor (Combes, 2004). This leads to a rapid truncation of star formation in these galaxies. Finally, gravitational harassment from other group or cluster members may also help to quench star formation in satellite galaxies (Park & Hwang, 2009)

Since structure formation is dominated by dark matter, one method of interpreting the data is in the context of the halo model, in which the properties of the dark matter halo determines the properties of the galaxies inside. In this model, the evolution of satellite galaxies can be distinguished from that of central galaxies and quenching occurs when they enter a halo of a sufficient mass (through processes such as strangulation, harassment, or ram pressure striping). Therefore, the radial gradients of the quiescent fraction observed in groups and cluster is caused by the satellite galaxies' accretion history into the halo (Smith et al., 2012; De Lucia et al., 2012).

By trying to match the shape of the observed star formation rate distribution at $z = 0$, Wetzel et al. (2013) recently proposed that this environmental dependence should take the form of a long delay of $2 - 4$ Gyr, followed by rapid ($\tau < 1$ Gyr) satellite quenching timescale. This has also been previously suggested by simulations, where satellite galaxies are able to retain a significant fraction of their hot gas after in-fall (Font et al., 2008)

Another empirical model of galaxy evolution that seems to account for most of these observations was put forward by Peng et al. (2010, 2012). In this model, galaxy evolution is driven by two 'quenching rates', one factor that depends on stellar mass and another factor that is related to environment, in the form of the local density. While the efficiency of environmental quenching in this model is roughly independent of stellar mass and redshift, its effects should be most prominent amongst low-mass galaxies, $M < 10^{10.5} M_{\odot}$, for which mass-quenching is inefficient.

1.5 GEEC2 Survey

To study the effect of the environment on galaxy evolution, the Group Environment Evolution Collaboration 2 (GEEC2) survey have focused on low mass groups at $z \sim 1$. This is chosen for the reasons listed below:

First, the Peng et al. (2010) model and the physical effects of environment quenching both point towards low mass satellite galaxies as important area of study. Low mass galaxies have much shallower potential wells and would be more greatly impacted by the processes of harassment, strangulation, and ram pressure striping.

Second, groups are an important test of the effects of environment on galaxy evolution, as the majority of galaxies are found inside groups (Eke et al., 2004). They are also a crucial link in the hierarchical growth of structures from individual galaxies to dense clusters. Furthermore, from the hierarchical growth of structure, observations have shown that galaxies may have been pre-processed in groups beyond entering the cluster environment (Wilman et al., 2008; Lemaux et al., 2012). Therefore, we know that the group environment at this redshift must have some effect on galaxy evolution.

Third, the study of this epoch ($z \sim 1$) is preferred because most in-falling galaxies would not have spent a long time as a satellite (McGee et al., 2009). In addition, there are high in-fall rates into groups and the galaxies themselves still possess relatively high star formation rates and gas fractions (Cucciati et al., 2012). This allows us to more easily find any transitional objects that may be moving from the star-forming to the quiescent phase. As a result, $z \sim 1$ would be the among the best places to look at any potential environmental dependence.

The main results from the GEEC2 survey are summarized in Balogh et al. (2011). This survey contains a sample of 11 robustly-identified groups with extended X-ray emissions (Finoguenov et al., 2007; George et al., 2011). The groups in the GEEC2 survey are all located in the COSMOS survey field, which means that these objects have detailed

measurements in multiple photometric bands, as well as observations from the Spitzer and Hubble Space Telescope (Scoville et al., 2007). This archive data will be of great help in the analysis of the group galaxies.

Previous analysis of these groups at $z \sim 1$ has revealed a distinct population of intermediate ('green') galaxies (Balogh et al., 2011), which may indicate the presence of a transition population. These green galaxies have morphologies half-way between the blue-cloud and red-sequence galaxies and do not appear to be exceptionally dusty. A summary of the GEEC2 observations and the detailed characteristics of our sample will be presented in Chapter 2.

While the intermediate ('green') galaxies found in the GEEC2 survey may indicate the presence of a transition population between the star-forming and quiescent state, another possible origin for these 'green' galaxies is the result of the rejuvenation of early-type galaxies (Fang et al., 2012). We will constrain both of these theories using a combination of observations and modelling.

Attempts have been made to reproduce observed distributions of colours and star formation rates of satellite galaxies through semi-analytical models and detailed cosmological simulations (Font et al., 2008) Another complementary approach is to use simple quenching models and then attempt to constrain the properties of these satellite galaxies (Wetzel et al., 2012). This is the route we will pursue here as well.

The stellar synthesis models of Bruzual and Charlot will be used. In general, these codes compute the evolution of the spectrum of a galaxy based on their star formation histories, metallicity, and dust attenuation. They require several important inputs (Bruzual & Charlot, 2003):

- Initial Mass Function - the initial distribution of stellar masses created by the model (Salpeter, Chabrier)
- Stellar Evolution Prescriptions - the evolutionary tracks of the stars created in the model (Padova1994, Padova2000)
- Stellar Spectral Libraries - a library of the individual spectra of the stars created in the model (BaSeL, STELIB, Pickles)
- User defined parameters, such as star formation histories, metallicity, and dust attenuation

With these important items in place, the spectra for the model galaxies can be created for ages between 1×10^5 to 2×10^{10} years and at a resolution of 3200 to 9500Å (Bruzual

& Charlot, 2003). This will allow us to measure both specific spectra indicies, such as Hδ strength, as well as use broad-band photometric filters to determine the colour of these model galaxies.

The BC03 code was released first in 2003 (Bruzual & Charlot, 2003) and later updated in 2007 with a different treatment of the Thermally Pulsing Asymptotic Giant Branch (TP-AGB) stars (Bruzual, 2007b). We will use the updated CB07 code in this work.

1.6 Questions

Presented below are several of the important questions we will seek to answer with this work:

- The fractions of galaxies found along the 'red sequence' are higher for over-dense regions at fixed stellar masses, even at $z \sim 1$ (George et al., 2011; Muzzin et al., 2012; Tanaka et al., 2012; Presotto et al., 2012). Given the environmental dependence, can we observe the physical effects of the environment at this epoch?

- At $z > 0.8$, there had been competing evidence that the star formation rate (SFR) of the star-forming galaxies in locally-dense environments may be higher than in the field (e.g. Cooper et al., 2008; Elbaz et al., 2007; Sobral et al., 2011; Li et al., 2011) versus no enhancement (e.g. Patel et al., 2011; Webb et al., 2013; Dressler et al., 2013; Webb et al., 2013). Can we characterized the star-formation rates of the GEEC2 sample and determine if there is, in fact, any differences between the group and field population?

- What are the origins of the intermediate galaxies in the GEEC2 survey (Balogh et al., 2011)? Are they a transitory population between the red sequence and the blue cloud or could they perhaps be early-type galaxies experiencing a rejuvenation in star formation (via mixed mergers)?

- If the intermediate galaxies are a transitory population, can we put strong constraints on any environmental effects using stellar synthesis models? Does a delay in the effects of environmental quenching exist at $z \sim 1$, as suggested by simulations (Font et al., 2008) and observations (Wetzel et al., 2013) of the local universe?

1.7 Overview

The structure of the thesis will be as follows. In Chapter 2, we present a discussion of the GEEC2 observations and the sample used in our data analysis, including the determination of completeness weightings. In Chapter 3, the main analysis of the GEEC2 data will be presented, including our separation of the sample into quiescent ('red'), intermediate ('green'), and star-forming ('blue') populations, and the procedure to determine star-formation rates of galaxies. In Chapter 4, the main results from the GEEC2 survey are presented, including a comparison of specific star formation rates and Hδ strengths for different sub-populations and environment. In Chapter 5, we present the different satellite quenching and rejuvenation models and detail the procedure of using stellar synthesis models to produce these 'green' galaxies. In Chapter 6, the model results are presented, including the predicted quiescent, intermediate, star-forming fractions and their Hδ strengths. Finally, Chapter 7 will include a discussion of the GEEC2 sample and the model predictions, including the likely constraints based on the observed galaxy properties, and the potential for future observations.

Throughout this thesis, all magnitudes are in the AB system. The stellar synthesis model are done with the Chabrier IMF (Chabrier, 2003). A cosmology with $\Omega_m = 0.272$, $\Omega_\Lambda = 1 - \Omega_m$, and $h = H_\circ / \left(100\mathrm{km/s/Mpc}\right) = 0.702$ was assumed (Komatsu et al., 2011).

Chapter 2

Observations

The initial observations and data reduction from the Group Environment and Evolution Collaboration (GEEC2) survey has been completed by the collaborators. In this chapter, a basic overview of the goals and methodology of this survey is presented. Details are included where it is relevant and useful to understanding my later work with the reduced spectra and the intermediate ('green') galaxies. A complete overview can be found in Balogh et al. (2011).

2.1 GEEC2 Group Selection

The GEEC2 survey targets galaxy groups identified within the COSMOS field (Scoville et al., 2007). The survey used the groups presented in the George et al. (2011, 2012) X-ray catalogue. Groups are selected which lie within the redshift range $0.8 < z < 1$, have at least three spectroscopically-determined members, and possess a well-determined X-ray centre.

In the catalogue, there are ~ 21 groups that fits this selection criteria. In order to probe the possible environmental dependence at $z \sim 1$, groups with the lowest masses and the highest redshift are prioritized, for the reasons given in the introduction. Note that the X-ray selected groups in this work are a subset of the groups in the Knobel et al. (2012) spectroscopic catalogue, which were found using a general group-finding software.

2.2 GEEC2 Survey

Using the COSMOS photometric catalogue (Capak et al., 2007), precise photometric redshifts are obtained using a template-fitting technique to 30 broad, intermediate and narrow-band filters (Ilbert et al., 2009). In general, photometric redshift uncertainties ranges from $\sigma_{\rm photo} \sim 0.007$ for the brightest objects to $\sigma_{\rm photo} \sim 0.04$ for the faintest.

Each group had $3-4$ Gemini Multi-Object Spectrographs (GMOS) masks assigned, with $\sim 40-50$ slits in each. Faint galaxies with $21.5 < r < 24.75$ and photometric redshifts within $2\sigma_{\rm photo}$ were given priority 1 status. Other galaxies with $15 < r < 24.75$ and $0.7 < z_{\rm photo} < 1.5$ were given priority 2 status. Their spectra and the resulting spectroscopic redshifts will allow us to confirm whether these galaxies are indeed group members. Furthermore, the spectroscopic survey should lead to ~ 20 members for each group, a deep and complete sample which allows us to estimate the group mass and dynamical state.

The Gemini telescope's nod & shuffle mode was used (Glazebrook & Bland-Hawthorn, 2001), while observations are taken in the nodded positions. This allows for a more accurate sky-subtraction, as the telescope is rapidly switched between the target and the sky.

The data is then reduced in IRAF, using the GEMINI packages with minor modifications. Redshifts are measured by adapting the ZSPEC software. The subsequent redshift quality is quantified by a four-class method:

- Quality class 4 is assigned to galaxies with certain redshifts. Generally, this is reserved for galaxies with multiple, robust features.
- Quality class 3 is assigned to galaxies with very reliable redshifts, which we expect most of them to be correct. They may include objects with a good match to the Ca H&K lines for example, but with no obvious corroborating feature. One exception occurs for cases where the Ca H&K lines are detected in a region of telluric absorption, which will be relegated to quality class 2.
- Quality class 2 objects correspond to 'possible' redshifts. These include some spectra that are likely to be correct, such as, the Ca H&K line on top of telluric absorption and no other corroborating features.
- Quality class 1 is reserved for 'junk' spectra, with no chance of obtaining a redshift.

In this analysis we will only use galaxies with class 3 or 4 quality redshifts, which we expect to be reasonably secure. This represent 603 of the 810 unique galaxies in the GEEC2 survey for which a good spectrum was extracted.

The GEEC2 spectra are combined with those from the DR2 release of the 10K zCOSMOS spectroscopic survey where appropriate (Lilly et al., 2009). This catalogue provides spectra, photometry and redshifts for moderately bright galaxies ($i < 22.5$), over most of the COSMOS survey area.

In a similar fashion to the choices made with the GEEC2 sample, only the zCOSMOS 10k galaxies with secure redshifts are chosen. This includes the zCOSMOS quality classes 3, 4, and 9, which corresponds to secure redshift, very secure redshifts, and one-line redshifts (such as Hα or [OII] feature) respectively (Lilly et al., 2007, 2009). In addition, to maintain consistency with the GEEC2 survey, only galaxies located in the same redshift range, $0.8 < z < 1.0$, are selected.

2.3 GEEC2 Galaxy Properties

The stellar masses of these observed galaxies are determined by fitting the spectral energy distribution (SED) for each object, using the updated Bruzual (2007a) models and a Chabrier (2003) initial mass function (IMF).

The general procedure is to represent the star formation history with a series of exponential decay models with superposed bursts, while varying the other input parameters. The resulting match to the data would not be a single spectra, but a χ^2 weighted average over the entire series of models.

The probability distribution function (PDF) for every parameter of interest is obtained by combining these weights with their values. Then, the median of this probability distribution function (PDF) is taken to be the best estimate of the parameter in question, such as galaxy mass, metallicity, dust attenuation (Balogh et al., 2011).

2.4 GEEC2 Completeness Corrections

2.4.1 GEEC2 Spectroscopic and Redshift Completeness

In the GEEC2 survey, there are several potential sources of incompleteness.

First, we need to consider the the sampling completeness of the survey, which is a measure of the fraction of all likely group members in the photometric sample for which a spectrum had been obtained. This value is primarily dependent on a galaxy's magnitude (r) and position, with no significant colour dependence.

For the group sample, we consider all galaxies that have a photometric redshift consistent with the final group redshift, within twice the 68 per cent confidence limits of the photometric redshift. The targeting completeness within $R_{\rm rms}$ is computed on an individual group basis, in three r magnitude bins ($22 - 23.25$, $23.25 - 24$, $24 - 24.75$).

For the field sample, we consider all galaxies with photometric redshifts between $0.8 < z_{\rm phot} < 1.0$ that were found within the GMOS fields of view. The completeness is then defined as the ratio of this population with a spectrum. A second potential source of incompleteness is the failure to obtain a reliable redshift from a spectrum. Overall, the success rate for the GEEC2 survey is very high, > 80 per cent for $i < 24$. We found no significant dependence of this fraction on the galaxy colour.

2.4.2 GEEC2 Mass Completeness

Since the GEEC2 survey is r-selected, in the rest-frame at $z \sim 1$, this will turn out to be a very 'blue' selection. As a result, this could introduce some strong colour-dependence in the stellar mass completeness. To better understand this effect on the sample, we will need to calculate the stellar mass-to-light ratio for the individual galaxies.

To start, we will use the photometric colours from the COSMOS catalog that had been K-corrected to $z = 0.9$, the centre of the redshift range of interest for our survey. In the analysis, these colours are denoted with a superscript 0.9, for example, $(V - z)^{0.9}$. The $(V - z)^{0.9}$ colour straddles the 4000 Å break at $0.8 < z < 1$ and is a measure of the luminosity-weighted age of a galaxy. This colour is roughly comparable to the rest-frame $(u - B)$, but the V filter is now measuring rest-frame flux intermediate between GALEX NUV and ground-based u.

In Figure 2.1, the stellar mass-to-light ratio is shown as a function of $(V - z)^{0.9}$ colour, where the luminosity L_r is computed from the selection magnitude (r) and the luminosity distance. The mass-to-light ratio (M/L_r) relates the selection magnitude of the GEEC2 survey to the physical quantity of interest, which is the stellar mass of the galaxy. The fit is linear, separated into two sections.

The strong correlation with colour primarily reflects the different star formation histories for these galaxies. Bluer galaxies have a younger population of stars, which produce more light per unit mass. Note that at any fixed colour, the range in the mass-to-light ratios (M/L_r) can be caused by a variety of effects, including physical effects like dust and metallicity variations. In addition, there may be uncertainties associated with the SED-fitting procedure in the calculation of stellar masses, which could result from photometric

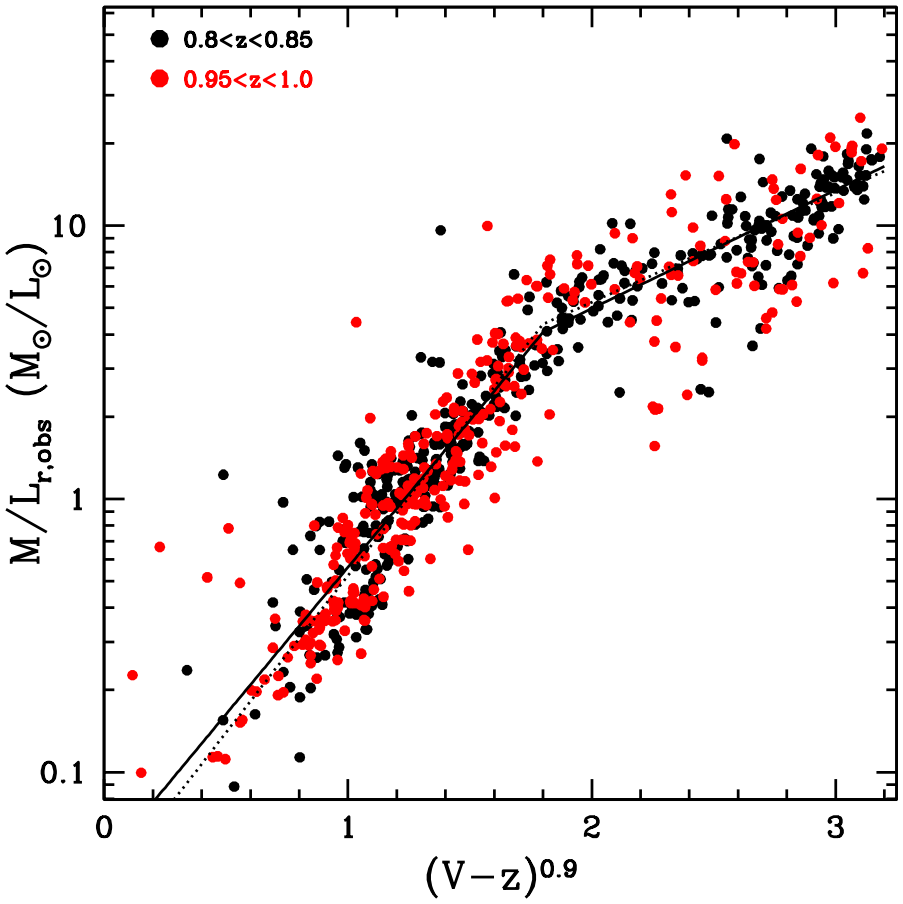

Figure 2.1: Plot of the stellar mass-to-light ratio as a function of colour, for galaxies with secure redshifts in our sample. The mass is derived from SED fitting using Bruzual (2007a) models with a Chabrier (2003) IMF, and the luminosity here does not include a K-correction. Black points represent galaxies at the lower end of our redshift range, $0.8 < z < 0.85$, while the red points correspond to the upper end at $0.95 < z < 1.0$. The solid and dotted lines (barely distinguishable over most of the range) are fits to the median M/L_r for the low and high redshift samples, respectively. The fit is bilinear, with a different slope for red and blue galaxies.

uncertainties or due to the random sampling of bursts in the population modeling (Balogh et al., 2011).

Since this function can also be modified by distance, we divide the galaxies into those at the lower end of our redshift range ($0.8 < z < 0.85$, black points) and at the upper end ($0.95 < z < 1.0$, red points). From Figure 2.1, the lines show the median M/L_r at the lower (solid line) and upper (dotted line) ends of the redshift range. There is no significant difference between the two.

Since the luminosity limit of our sample is set at $r < 24.75$, we can convert this to a stellar mass through the mass-to-light relationship. However, this range of stellar masses would depend strongly on colour. At fixed $(V - z)^{0.9}$ colour, the maximum value of M/L_r determines the 100 per cent mass completeness limit of the survey. For example, the reddest galaxies have M/L_r as high as 30 and the sample is only fully complete for $M_{\rm star} > 10^{10.8} M_{\odot}$ (Balogh et al., 2011).

2.4.3 GEEC2 Completeness Weightings

The stellar mass limits calculated from the stellar mass-to-light function for 'red' (quiescent) and 'blue' (star-forming) galaxies may be unnecessarily conservative. If we assume that the M/L_r distribution at fixed $(V - z)^{0.9}$ colour is not a strong function of stellar mass, but is instead due to metallicity and dust variations as discussed above, then we can use the distribution from Figure 2.1 to statistically correct for any missing galaxies with high mass-to-light ratios (M/L_r).

First, the cumulative distribution of limiting stellar masses is constructed. This is given by the r-band luminosity limit at the given redshift multiplied by the mass-to-light ratio (M/L_r). We can separate the limiting stellar masses into bins of colour ('blue' and 'red') and redshift ($z = 0.8$ and $z = 0.95$). This is given in Figure 2.2.

Each curve shows what fraction of the galaxies with the GEEC2 mass-to-light ratio (M/L_r) distribution will be included in the sample, for the case of a given colour and redshift. If the galaxies of that mass and colour are weighted by the inverse of this number, this is one method to statistically correct for galaxies with high M/L_r ratios that may be absent from the sample.

Using this method, if we are willing to accept statistical corrections as large as a factor of 5, we can extend the mass limit of blue galaxies by a factor ~ 4, and of red galaxies by a factor ~ 2.

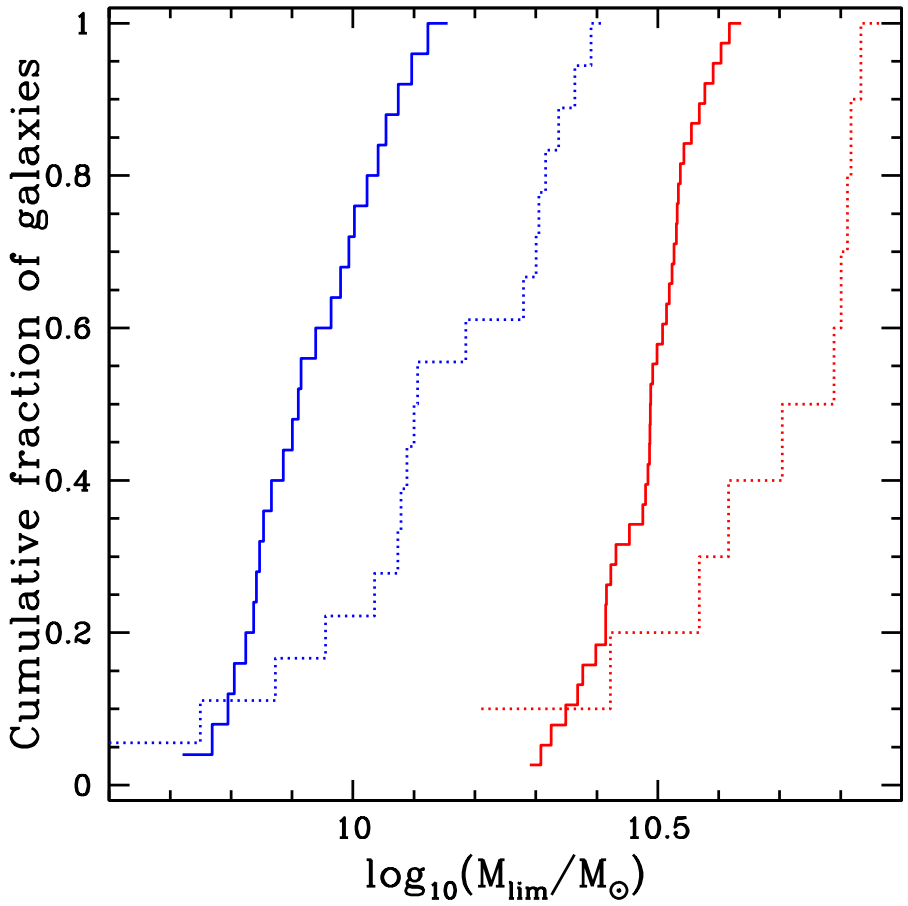

Figure 2.2: Each curve shows the cumulative distribution of limiting stellar mass (i.e. at a given stellar mass, the fraction of the M/L_r distribution that will be included in the sample) for a population of fixed $(V-z)^{0.9}$ colour and redshift. This is derived from the luminosity limit and the distribution of M/L_r (see Fig 2.1) for that population. Weighting galaxies of that mass by the inverse of this number then accounts statistically for galaxies with high M/L_r ratios that may be absent from the sample. The blue curves represent blue galaxies with $(V-z)^{0.9} \sim 1.7$, while the red lines correspond to galaxies with $(V-z)^{0.9} \sim 2.9$. Solid and dashed lines represent the lower and upper redshift range of the data, respectively ($z = 0.8$ and $z = 0.95$).

Note that this correction method means we are assuming that the distribution of dust, metallicity, and SED-fitting uncertainties is mass-independent for galaxies of a given colour over a small mass range. This does mean that the galaxies we are missing are preferentially those with high M/L_r ratios, for example, those with more dust than average. As a result, the 'corrected' sample may not be completely representative of the whole galaxy population at that stellar mass.

Although some caveats remain to the use of this method, the updated completeness limits and the use of the completeness weighting presented in this section will be very useful in the following analysis of the GEEC2 sample. The 'total' weighting, which combines the spectroscopic and mass completeness weightings will be used in the analysis of the group sample and the field population that is located with the GMOS field of view.

This analogous method can also be used later to calculate the completeness limits in terms of the [OII] star formation rates. Since star formation rate is correlated with the mass-to-light ratio (M/L_r), we can use the previously determined distribution of M/L_r ratios to calculate the completeness limits in term of star formation rates and include it in subsequent plots.

2.5 GEEC2 Group Properties

A total of 82.5 hours of data have been collected from Semesters 10A and 11A with the Gemini telescope, which allowed observation of a total of 11 groups. The groups in the GEEC2 sample have already been previously identified from sparse spectroscopy and deep X-ray observations. With the additional spectroscopy, the existing estimates of the centroid and the velocity dispersion have been improved.

Since these groups are significant over-densities with extended X-ray emission and well-determined centres, the amount of possible field contamination should be substantially lower than the $\sim$ 15 per cent expected from a general group-finding algorithm of the zCOSMOS field (Knobel et al., 2012).

The group dynamical masses can be computed from the calculated σ from our spectroscopy and the $R_{\rm rms}$:

$$M_{\rm dyn} = \frac{3R_{\rm rms}\sigma^2}{G} \tag{2.1}$$

The resulting group dynamical masses for the GEEC2 sample range from $\sim 2\times10^{12}M_{\odot}$ to $\sim 1.8\times10^{14}M_{\odot}$.

Group	RA	Dec	$z_{\rm mean}$	N_{mask}	N_{mem}	σ (km/s)	$R_{\rm rms}$ (Mpc)	C (%)	$M_{\rm dyn}(10^{13}M_{\odot})$
40	150.414	1.848	0.9713	2	15	690 ± 110	0.34 ± 0.04	64	11 ± 4.7
71	150.369	1.999	0.8277	3	21	360 ± 40	0.34 ± 0.03	82	3.0 ± 0.9
120	150.505	2.225	0.8358	3	31	480 ± 60	0.78 ± 0.07	69	12.7 ± 4.2
121	150.161	2.137	0.8373	3	5	210 ± 60	0.09 ± 0.01	100	0.2 ± 0.2
130	150.024	2.203	0.9374	3	34	600 ± 70	0.71 ± 0.06	76	17.8 ± 5.7
134	149.65	2.209	0.9467	3	23	450 ± 60	0.97 ± 0.07	70	13.3 ± 4.7
143	150.215	2.28	0.881	3	20	580 ± 60	0.23 ± 0.03	100	5.2 ± 1.7
150	149.983	2.317	0.9334	4	25	300 ± 40	0.89 ± 0.08	75	5.5 ± 2
161	149.953	2.342	0.944	4	8	170 ± 30	0.53 ± 0.12	70	1.0 ± 0.5
213	150.41	2.512	0.879	2	9	260 ± 100	0.84 ± 0.13	52	3.8 ± 3.4
213a	150.428	2.505	0.9256	2	8	110 ± 30	0.62 ± 0.09	40	0.4 ± 0.3

Table 2.1: Properties of the eleven galaxy groups in the GEEC2 survey. The position, median redshift $z_{\rm med}$, rest-frame velocity dispersion, and the number of group members are determined from GMOS spectroscopy, combined with available zCOSMOS 10k data. The number of GMOS masks observed in each field is given by $N_{\rm mask}$. $R_{\rm rms}$ is the rms projected distance of all group members from the centre. The next column lists the spectroscopic completeness of the group, where we list the percentage of candidates within $R_{\rm rms}$ of the group centre for which spectroscopic redshift was obtained, where a candidate is a galaxy with a photometric redshift consistent with the group redshift at the 2σ level. Finally we list the dynamical mass of the group, which is well correlated with the original X-ray masses (Balogh et al., 2011).

The remaining group properties in Table 2.1, including observational properties such as their right ascension, declination, mean redshift, and the number of the masks used. Uncertainties on σ and $R_{\rm rms}$ are computed using a jackknife method, iterating over the list of group members. As a result, these uncertainties do not include systematic biases due to the clipping process, which are likely to be at least ~ 15 per cent (Wilman et al., 2005).

From the X-ray catalog of Finoguenov et al. (2007); George et al. (2011), we find that there are 50 total X-ray detected groups in the redshift range $0.8 < z < 1.0$. Therefore, we have sampled 11 out of the 50 groups, or ~ 22 per cent of the total number of groups with X-ray detections, i.e. all groups that would be in an analogous mass-range. This number will be much lower if we are considering all possible groups in this redshift range.

Also, note that the number of priority 1 galaxies selected in the GEEC2 survey, with photometric redshift with 2σ of the group redshift, was 497. Out of this, only 145 turned out to be spectroscopically confirmed group members. Therefore, the fraction of photometrically selected group members that were later spectroscopically confirmed is 30.2 per cent.

2.6 Galaxy Colours

As stated in the introduction, most galaxies are distributed into two main populations in a colour-magnitude diagram. The first group is the 'red sequence' of galaxies, which tend to have negligible present star formation. The second main concentration is the 'blue cloud' of star-forming galaxies. It is therefore important to consider our sample in terms of these two populations and find any galaxies that might be intermediate between the two.

For the rest of this thesis, we will use the following terms to describe the three populations, star-forming ('blue'), intermediate ('green'), and quiescent/passive ('red').

While this choice could be made based on estimates of the galaxy's star formation rate, it is easier and more straightforward to start with a classification based on directly observable quantities, such as colour. It has been previously shown that that the star-forming and quiescent populations are well-separated in a colour-colour plane (e.g. Labbé et al., 2005; Wolf et al., 2005; Balogh et al., 2009; Whitaker et al., 2012a).

In Figure 2.3, we show the distribution of galaxies in the colour-colour plane. The x-axis colour, $(V-z)^{0.9}$, is a very good indicator of luminosity-weighted age (Balogh et al., 1999). On the other hand, the y-axis colour, $(J-[3.6])^{0.9}$, is chosen to be sensitive to dust extinction. A higher (redder) $(J-[3.6])^{0.9}$ colour would indicate increasing levels of dust extinction (Huang et al., 2011).

All galaxies with good redshifts $0.8 < z < 1$ within a mass range of $M_{\rm star} > 10^{9.8} M_{\odot}$ are plotted, including all group and field galaxies within the GMOS fields-of-view. We also highlight with purple circles galaxies detected in deep MIPS data, with 24μm flux greater than 0.071 mJy (Sanders et al., 2007), which is an indication of dust obscured emissions from young stars and is a good star formation indicator. The results are shown in Figure 2.3.

Figure 2.3 also demonstrates that selecting quiescent galaxies based only on an optical colour that straddles the 4000 Å break (e.g. $(V-z)^{0.9} > 2.4$) would include a significant population of dust-reddened galaxies with significant star formation. This is shown by the large number of 'red' galaxies with MIPS 24 micron detections. With the help of this colour-colour plot, we can begin to identify truly quiescent galaxies, without possible contamination from very dusty galaxies.

To determine the two populations, we first fit a line to the main distribution of galaxies, shown in Figure 2.3 as the blue dotted line. The equation of this line is $y = 0.89x - 0.28$, where $x = (V-z)^{0.9}$ and $y = (J-[3.6])^{0.9}$. The red dotted line in Figure 2.3 has an identical slope, but with an offset of -1.02 mag to fit the second concentration of galaxies observed.

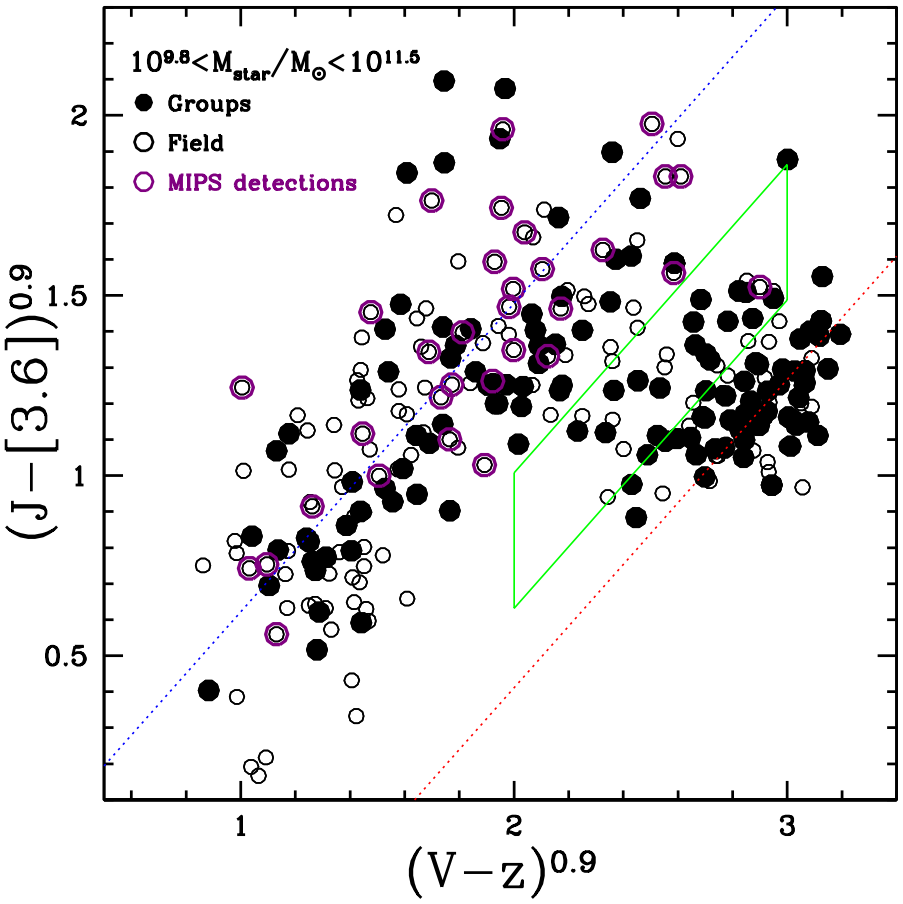

Figure 2.3: The distribution of galaxy colours in the $(J-[3.6])^{0.9}$ vs. $(V-z)^{0.9}$ plane, selecting only galaxies within the GMOS field of view. Group members are indicated by the *filled circles*, field members are shown with *open circles*. The blue and red dotted line indicates our star-forming and quiescent sequences respectively, where the equation for the star-forming sequence is $y = 0.89x - 0.28$, where $x = (V-z)^{0.9}$ and $y = (J-[3.6])^{0.9}$. Galaxies with 24 micron MIPS detection within 3″ are outlined in purple. The green box represents our identification of the intermediate population.

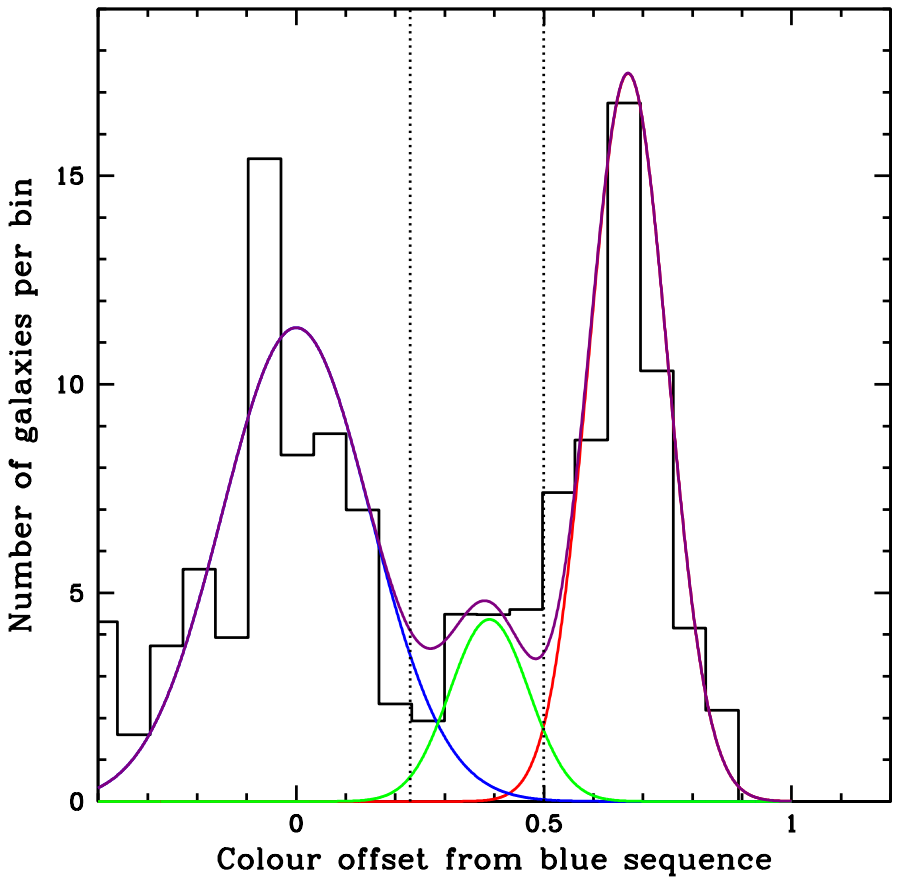

Figure 2.4: The distribution of group galaxies positions (with masses $9.8 < \log(M_{\rm star}/M_{\odot}) < 11.5$) in the colour-colour plane, measured as the perpendicular offset from the peak of the blue sequence. The histogram data includes the relevant statistical weights. Also plotted are Gaussian fits to the star-forming ('blue'), red ('quiescent'), and intermediate ('green') population, and the summed function of all three fits.

Next, the distance of each galaxy from the two main distributions is measured as the perpendicular distance from the blue sequence lines. The distribution of these distances is shown in Figure 2.4, with a clear separation between the two peaks.

We also observe a small group of intermediate population, located in between the two main distributions. We will refer to these as the 'green' or intermediate galaxies, as in Balogh et al. (2011). After fitting the three populations with Gaussian functions, we define the boundaries of the intermediate population so it has the minimal overlap with the star-forming and quiescent sequence. This is shown by the dotted lines in Figure 2.4.

The resulting green box in Figure 2.3 represents our definition of the intermediate population. Note that there are additional vertical limits drawn using in the $(V-z)^{0.9}$ axis, in order to prevent very 'blue' or very 'red' objects from being identified as intermediate galaxies.

Hubble Space Telescope (HST) images of these important intermediate galaxies are presented in Figure 2.5. They were found to contain morphologies that are intermediate between the star-forming and quiescent population. For example, many of these intermediate galaxies contain disks, but they are smaller and less structured than those from the star-forming population.

The morphology of these objects is an important tool to help differentiate between the two possible origins of the intermediate population, the quenched star-forming galaxies and rejuvenated quiescent galaxies. For example, the quenching process may leave behind a disk while the rejuvenation process (through mixed mergers and accretion) would not. Preliminary work has been started by other members of the collaboration on the analysis of the morphology of these intermediate galaxies.

With the galaxies from the sample classified into star-forming ('blue'), intermediate ('green'), and quiescent/passive ('red'), we can begin to focus on the detailed analysis of the spectra and feature of these objects.

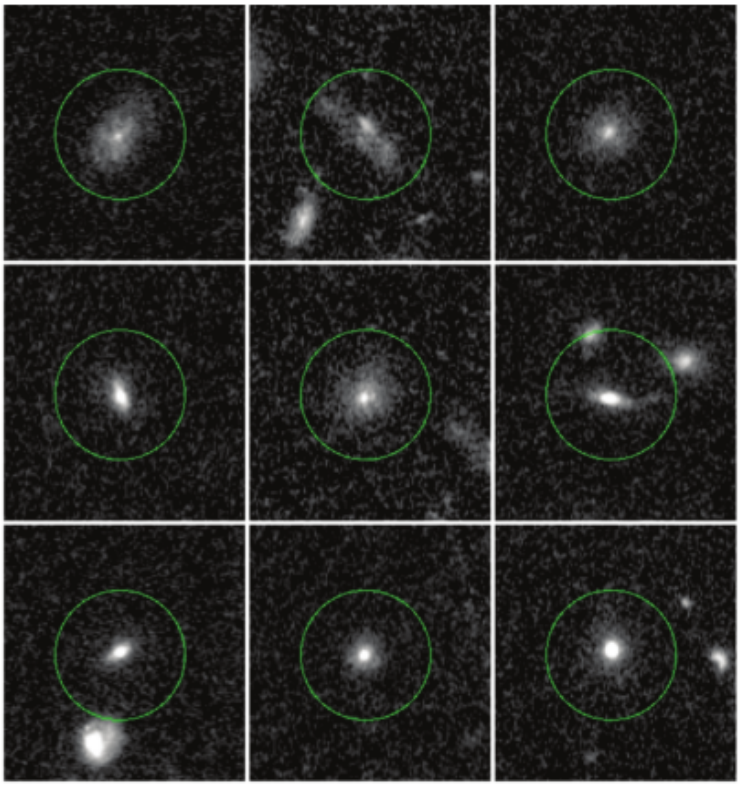

Figure 2.5: HST images of a selection of intermediate group galaxies. The images are 6.0 arcseconds across, corresponding to $\sim$ 47 kpc at $z = 0.9$. The intermediate galaxies possesses morphologies that are intermediate between the star-forming and quiescent population, with disks that are smaller and less structured than the star-forming population. Reproduced from Figure 10 of Balogh et al. (2011).

Chapter 3

Data Analysis

3.1 Group and Field Populations

From the galaxies in the GEEC2 survey, we can define the group and field populations. The group population consists of galaxies that have been identified in the previous analysis as a member of the 11 groups from Table 2.1.

For field galaxies, our sample is defined as all galaxies in the combined GEEC2 and zCOSMOS 10k catalog with reliable spectra, lying within the range $0.8 < z < 1$. Note that this field does not represent isolated galaxies, but rather a random selection of representative galaxies. Therefore, the percentage of group galaxies would then be the normal percentage expected at this redshift, which should be ~ 20 per cent for groups with $N \geq 2$ and ~ 5 per cent for groups with $N \geq 5$ (Knobel et al., 2009).

This field sample should be a fair representation of the 'average' population of galaxies at this redshift and so would provide a good basis for comparison to the group sample. When appropriate, we will limit the field galaxies to those found within the field-of-view of the GEEC2 GMOS fields, in order to simplify the analysis and homogenize the sample. This also allows us to use the spectroscopic and mass completeness to correct the field sample in a similar way to the group population.

Based on the previous quiescent, intermediate, and star-forming classification, the resulting number of galaxies in each colour and mass bins is shown in Figure 3.1, as a function of stellar mass. The asymmetrical error bars are calculated using the binomial error method from Cameron (2011).

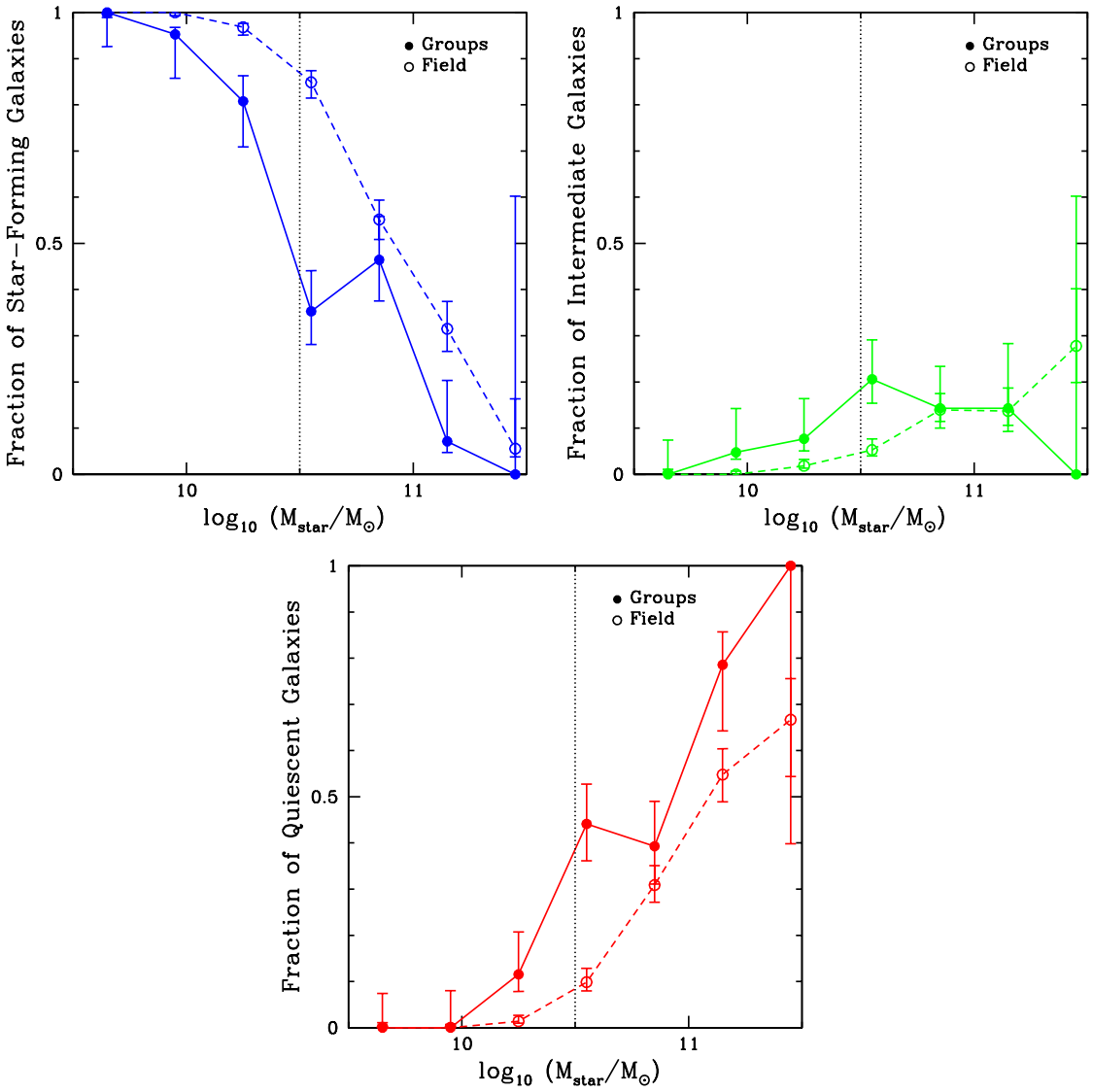

Figure 3.1: Plots of the fraction of star-forming *(top left)*, intermediate *(top right)*, and quiescent *(bottom)* galaxies in the group and field populations, based on the colour definitions in Figure 2.3 and restricted to galaxies with $0.8 < z < 1$, secure redshifts, and with total weights (spectroscopic and mass completeness) of between 0 and 5. The group population *(filled circles and solid line)* consists of galaxies identified as a group member. The field population *(open circles and dashed line)* consists of all galaxies (including objects from the zCOSMOS 10k catalog) not specifically identified as part of a group in Table 2.1. Also shown with the data points are their error bars. The black dotted line at $10^{10.5} M_{\odot}$ shows where the sample is reasonably complete, even for quiescent ('red') galaxies.

Log (M_*)	Blue-Group	Blue-Field	Green-Group	Green-Field	Red-Group	Red-Field
9.5 - 9.8	23	160	-	-	-	-
9.8 - 10.1	20	272	1	-	-	-
10.1 - 10.4	21	211	2	4	3	3
10.4 - 10.7	12	129	7	8	15	15
10.7 - 11.0	13	75	4	19	11	42
11.0 - 11.3	1	23	2	10	11	40
11.3 - 11.6	-	1	-	5	1	12

Table 3.1: The number of galaxies in each mass bin, based on the colour definitions in Figure 2.3. The count is restricted to GEEC2 and zCOSMOS galaxies lying in the GMOS fields-of-view and with total weights (spectroscopic and mass completeness) of between 0 and 5.

We observe a strong environmental dependence on the fraction of quiescent galaxies, as they comprise a larger proportion in groups then in the field for all stellar masses. In addition, the fraction of intermediate ('green') population was found to represent $\sim 15-20$ per cent of the overall galaxy population or up to $\sim$ 30 per cent of the total combined quiescent + intermediate population in the GEEC2 sample.

Finally, there is no significant difference observed in the fraction of intermediate galaxies between the group and field sample.

3.2 Spectroscopic Indices

For the GEEC2 sample, the relevant spectral line indices in this wavelength range were measured for all galaxies with secure redshifts. The reduced one-dimensional spectra had been provided in the FITS file format, previously reduced by the GEEC2 and zCOSMOS collaborations. We also make use of a catalog file with the combined GEEC2 and zCOSMOS galaxy properties, such as stellar mass, photometric redshifts, spectroscopic redshifts, and magnitudes in various photometric bands.

The reduced 1D spectra are first shifted into each galaxy's rest-frame with the IRAF DOPCOR command using the spectroscopic redshifts provided by the catalog. The shifted 1D spectra are then imported into IDL, where the relevant spectroscopic indices can be measured using a custom-written script that implements the bandpass approach. For this analysis, we are focused on the [OII] and Hδ lines, which are redshifted into the relevant area. The procedure for the bandpass process is as follows:

First, the continnum flux levels of the spectra both red-ward and blue-ward of the feature are found. This is done by averaging the flux over the relevant wavelength ranges in the red and blue continuum.

Next, the continuum flux level in the area of the spectral line can be defined by drawing a line between the centres of the red and blue continuum ranges. This is done because the continuum levels on the line itself can be hard to measure and define, especially for strong features. The relevant wavelength ranges for the the [OII] and Hδ features are presented in Table 3.2.

The equivalent width for the Hδ and [OII] lines is determined using the following equation:

$$W_\lambda = \int \left(1 - \frac{F_\lambda}{F_c}\right) d\lambda, \tag{3.1}$$

where F_c is the flux level of the continuum and F_λ is the total flux per unit wavelength.

Operationally, the flux over the line index is integrated over the wavelength ranges listed in Table 3.2 for each spectral feature. The same method can also be used to determine the integrated flux of the linear fit to the continuum. The contribution from the line is then simply the difference between the two values.

For the following discussion, we adopt the sign convention such that a positive [OII] equivalent width indicates an emission feature, while a positive Hδ equivalent width corresponds to an absorption feature.

Index	Blue Continuum	Line Definition	Red Continuum
[OII]	3653 - 3713	3722 - 3733	3741 - 3801
Hδ	4030 - 4082	4082 - 4122	4122 - 4170

Table 3.2: This table list the wavelength intervals used for the estimation of the blue and red continuum, as well as the line definitions for the [OII] and Hδ spectroscopic indices used in this work. The values in the table are provided in units of Angstroms.

3.2.1 Calculation of Errors in Equivalent Widths

The measurement errors in the equivalent widths of the stacked spectra can be calculated using the formula from Vollmann & Eversberg (2006).

$$\sigma(W_\lambda) = \sqrt{1 + \frac{\overline{F_c}}{\overline{F}}} \; \frac{\Delta\lambda - W_\lambda}{S/N} \tag{3.2}$$

where $\Delta\lambda$ is the wavelength interval used to measure the spectral feature, W_λ is the measured equivalent width, and the S/N term is the total signal-to-noise ratio over the line index in question. This is defined as the mean value of the flux per pixel, divided by the variance and multiplied by the square root of the number of pixels in the line index definition.

3.2.2 Weighted-Median and Stacked-Spectra Methods

Since the signal-to-noise ratio for these faint spectra are relatively low ($S/N \sim 1$ per pixel), any measurements of spectroscopic indices (including their derived quantities, like the star formation rate) can have considerable uncertainty. It is therefore valuable to consider quantities averaged over the various subpopulations in the GEEC2 sample, and we do this in two different ways

For the first method ('Weighted-Median'), the relevant indices for each galaxy spectrum are measured individually, using the procedure outlined in Chapter 3.2. We then compute a median that includes a combination of the galaxy's spectroscopic and mass-completeness weights. The description of these weights had been described in Chapter 2.4.3.

For this weighted-median method, the total weighting is defined as the product of the galaxy's spectroscopic and mass-completeness weights. Then, the relevant physical quantities are sorted in order of increasing value of this total weight. The sum of the total weights in the sample is calculated. The point at which the cumulative weighting is equal to half of the sum is considered to be the weighted-median value for the parameter in question.

The uncertainties in this method can be determined using the bootstrap method. We randomly re-sample the distribution of galaxies in the particular population we are interested in. This is done 500 times for each case and the median value re-calculated for each iteration. The standard deviation of this new distribution of median values can provide a robust error estimate for the original measurement.

The second method ('Stacked-Spectra') involves stacking the individual spectra in the sample and then directly measure the relevant features on the combined spectrum. In this case, we also incorporate the effects of the weighting using the following procedure:

First, the flux values of each individual spectra is multiplied by their total weight, which is the product of their spectroscopic and mass-completeness weighting. Then, the spectra are combined by taking the average flux of each pixel, using the IRAF function SCOMBINE.

This resulting stacked spectra is used for the subsequent calculations for the equivalent widths of [OII] and Hδ , in a similar fashion to that of the individual spectra. The other associated measurements, such as the stellar mass, would also be weighted averages of the galaxies used to created the stacked spectra.

Note that the error estimate from Vollmann & Eversberg (2006) would represent only the uncertainty in the mean value due to the signal-to-noise of the stacked spectra, and does not include any variance that may be associated with the distribution of pixel values entering the stacking process. As a result, this uncertainty is comparatively much lower than the bootstrap method used for the weighted-median method.

3.3 Star Formation Rates

3.3.1 [OII] Star Formation Rates

The star formation rates of these galaxies in the GEEC2 survey can be obtained directly from the [OII] feature, as its luminosity is coupled to the H II regions, the sites of star-formation inside galaxies. However, this line is more strongly affected by dust extinction and metallicity than comparable indicators, like the Hα recombination feature.

To compensate, the work by Gilbank et al. (2010, 2011) presents an empirical conversion between observed [OII] luminosities and the star formation rate at $z = 0.1$ in a statistical manner, calibrating the result to values derived using Hα and UV data:

$$\frac{\mathrm{SFR}}{\mathrm{M}_\odot\ yr^{-1}} = \frac{\mathrm{L}_{[\mathrm{O\ II}]}}{3.80 \times 10^{40} \mathrm{erg\ s^{-1}}} \frac{1}{a\ \tanh[(x-b)/c] + d}, \tag{3.3}$$

with $a = -1.424,\ b = 9.827,\ c = 0.572,\ d = 1.700,\ x = \log(M_{\mathrm{star}}/M_\odot)$.

Note that this only includes the average dust correction for galaxies for that stellar mass and does not correct for individual dust attenuations or metallicity. This correction also does not take into account any changes in the properties of these galaxies between $z = 0.1$ and $z \sim 1$.

To determine the [OII] star formation rates for the GEEC2 sample, we first calculate the [OII] luminosity by multiplying the equivalent width measurement from the spectra with the luminosity of the continuum at its redshifted position. In the range $0.8 < z < 1.0$, the r and i photometric bands bracket the [OII] line. Therefore, we can use those two magnitudes from the catalogue to estimate the continuum luminosity at the redshift [OII] position for each galaxy:

First, we convert the two magnitudes (r and i) into fluxes. Then, we do linear interpolation between the two bands, as measured from the broad-band images. The continuum flux for the [OII] feature is found by going to the corresponding redshifted wavelength of the [OII] feature (with a rest-frame wavelength of 3727 Å) for each galaxy.

Next, we can multiply the continuum flux with the [OII] equivalent widths in order to determine the [OII] flux. [OII] luminosities can then be obtained by using the luminosity distances calculated for each object, using the standard cosmology and a cosmology calculator. This resulting luminosities can be inserted into Equation 3.3 to output the resulting [OII] star formation rate.

3.3.2 FUV + IR Star Formation Rates

Since the group galaxies in the GEEC2 sample are located within the larger zCOSMOS survey and as such, many objects have both FUV and MIPS-based Spitzer Infra-red measurements (Scoville et al., 2007; Knobel et al., 2012). The combination of these two measurements can be one of the best measurements of the total star formation rate of a galaxy, taking into account the UV flux from young stars and the IR emissions from dust attenuation and scattering.

In order to calculate the FUV + IR SFR, we use the rest-frame K-corrected UV and optical photometric data from the zCOSMOS catalog. To do this, the K-corrections were applied to the filter that most closely matches the rest wavelength of the desired filter, rather than taking the synthetic magnitude from the template fit. The distribution of FUV magnitudes also allows us obtain a reasonable upper limit (FUV $\gtrsim 25$) for galaxies that are undetected in rest-frame FUV flux.

Next, MIPS 24 micron data is converted into total IR luminosity with the templates from Chary & Elbaz (2001). The corresponding code can be found at `http://david.elbaz3.free.fr/astro_codes/chary_elbaz.html`. We use the individual redshifts of each galaxy, as well as the standard cosmology and their observed MIPS 24 micron flux.

Finally, we combine FUV and the total IR luminosities into star formation rate estimates with the prescription of Hao et al. (2011):

$$L(\mathrm{FUV})_{\mathrm{obs}} + 0.46 \times L(\mathrm{TIR})_{\mathrm{obs}} \tag{3.4}$$

The conversion between total luminosity and star formation rates is taken from Salim et al. (2007), for the Chabrier IMF.

3.3.3 FUV + Dust Attenuation Star Formation Rates

We can also estimate the star formation rates for galaxies which are only FUV detected, but lack the corresponding MIPS 24 micron detection. Since the detection limit for the MIPS data is relatively high, upper limits based on the 24 micron data may be overly conservative. Therefore, we estimate the possible dust attenuation from the UV slope, which would include the use of the NUV band and the $(\text{FUV-NUV})^0$ colour.

The relationship from Salim et al. (2009) was used, which had had dust attenuation estimated using the $(\text{FUV-NUV})^0$ colour:

$$A_{\text{FUV}} = 3.68(\text{FUV} - \text{NUV})^0 + 0.29 \text{ for } (\text{FUV} - \text{NUV})^0 < 1 \tag{3.5}$$

The original, non-dust attenuated FUV fluxes can then be obtained and turned into a star formation rate using the previous conversion factor from Salim et al. (2007).

Chapter 4

Results

4.1 Star Formation Rates

4.1.1 Normalization Difference between [OII] and FUV-based Star Formation Rates

The star formation rate of the galaxies in the GEEC2 survey can be measured through their spectra. As summarized in the previous chapter, this value is obtained through the [OII] feature and the prescription for dust attenuation correction from Gilbank et al. (2010, 2011), which had calibrated their [OII] result to the same values derived using Hα and UV data in the local universe.

However, this correction only includes the average dust correction for galaxies of that stellar mass. Furthermore, it does not take into account any changes in the properties of these galaxies between $z = 0.1$ and $z \sim 1$. To test this formula, we can compare the [OII] star formation rates and the FUV-based measurements of the star formation rates (FUV + IR and FUV + dust attenuation estimate) for the GEEC2 sample.

In Figure 4.1, the log difference in the star formation rates measured between the two methods, $\log_{10}$ ($SFR_{[FUV+IR]}$) - $\log_{10}$ ($SFR_{[OII]}$), is shown as a function of stellar mass. The mass-independent offset is presented with the black line.

Note that those points with purple outline have both FUV and MIPS IR measurements. Points without purple outline are detected in the FUV only. Points with upper limit arrows are objects not detected in the FUV, but their calculations used the FUV limit of the

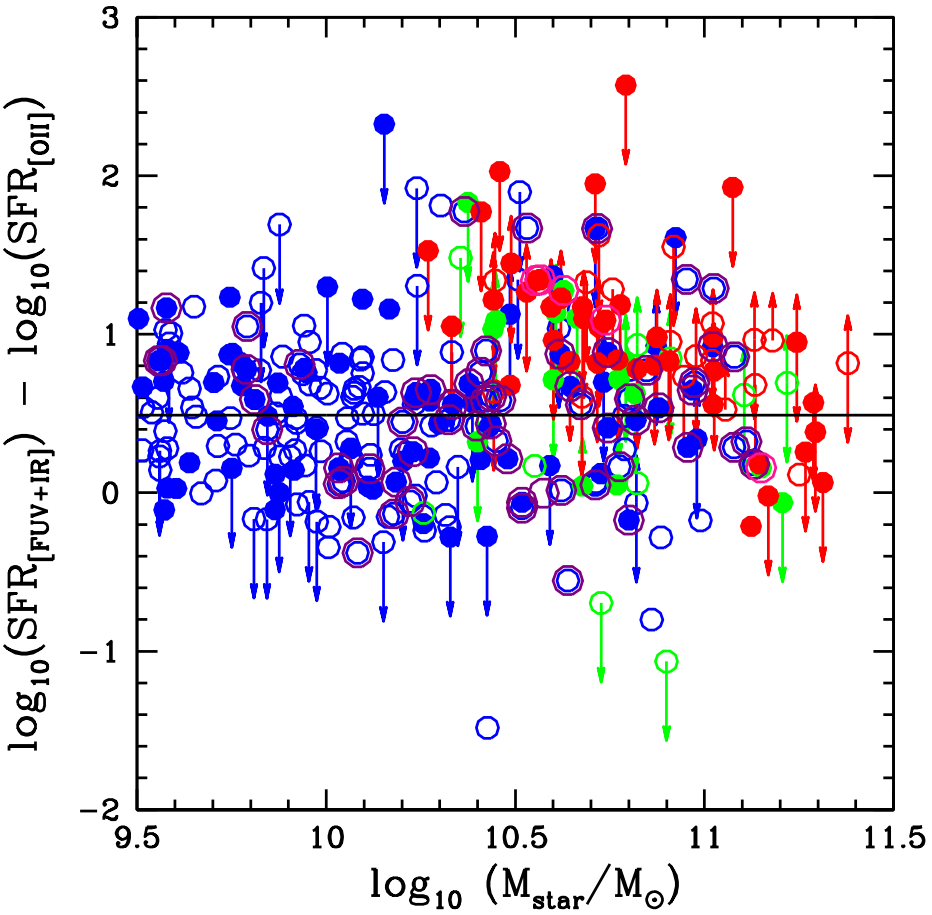

Figure 4.1: Log_{10} ($\mathrm{SFR}_{[\mathrm{FUV+IR}]}$) - $\log_{10}$ ($\mathrm{SFR}_{[\mathrm{OII}]}$) is plotted as a function of stellar mass for galaxies at $0.8 < z < 1$ in the GMOS fields-of-view. Group members are shown as *filled symbols*, and field members within our GMOS fields-of-view are shown as *open symbols*. Only galaxies with total weight (spectroscopic and mass-completeness) of between 1 and 5 are included. Points are colour-coded according to their classification as red, blue, and green. Galaxies with 24 micron MIPS detection within 3″ are outlined in purple. The black line indicates the mass-independent offset between the FUV + IR and OII star formation rates. Note that those galaxies with a negative [OII] equivalent width or with [OII] detections less than the measurement error are converted into lower limits, while undetected FUV galaxies are shown as upper limits. The mass-independent offset is presented as the *black line*.

survey at 25 magnitude. Finally, points with lower limits are galaxies with a negative [OII] equivalent width or with [OII] detections less than the measurement error.

It is not clear which method would provide the more 'correct' answer, but in principle the combination of FUV and IR measurement should be more direct, with the infrared bolometric corrections being the largest systematic uncertainty with this method. However, at this redshift range, $0.8 < z < 1.0$, the total infrared luminosity estimated from the 24 micron line should remain relatively accurate (Magdis et al., 2011).

In addition, the Gilbank et al. (2010) calibration would be expected to underestimate the true star formation rates if these relatively massive galaxies at $z = 1$ are dustier than galaxies of similar mass at $z = 0$, which may not be unreasonable as recent studies have found that the average dust attenuation peaks at $z \sim 1$ (Cucciati et al., 2012). Furthremore, this normalization offset between the [OII] dust corrected star formation rates and other measurements have also been noted in (Patel et al., 2011; Karim et al., 2011).

From the GEEC2 sample, this offset is found to be ~ 3.1 and is roughly mass-independent. In this calculation, we have neglected all the galaxies that only had upper limits for the star formation rate measurements. For the reason listed above, the [OII] - derived SFR are multiplied by this normalization factor in all subsequent analysis.

4.1.2 The Correlation between the Specific Star Formation Rates and Stellar Mass

In Figure 4.2 we show the specific star formation rate for individual galaxies as a function of their stellar mass, considering galaxies within the GMOS fields of view and with secure redshifts $0.8 < z < 1$. The specific star formation rate (or star formation rate per unit stellar mass) is a useful measure here, as this removes any potential mass biases introduced into measurements of star formation.

Galaxies are colour-coded according to their classification into star-forming ('blue'), intermediate ('green'), and quiescent ('red'). The solid and dotted lines represent the completeness limits at $z = 0.8$ and $z = 1$, respectively.

We observe that the star-forming galaxies form a well-defined sequence, in good agreement with previous results from Elbaz et al. (2007) at the high mass end and Whitaker et al. (2012a) above their completeness limit of $M_{\rm star} \sim 10^{10} M_{\odot}$. The GEEC2 data shows that the Whitaker trend seems to extend to lower masses, $M_{\rm star} \approx 10^{9.5} M_{\odot}$, although survey completeness may be playing an important role.

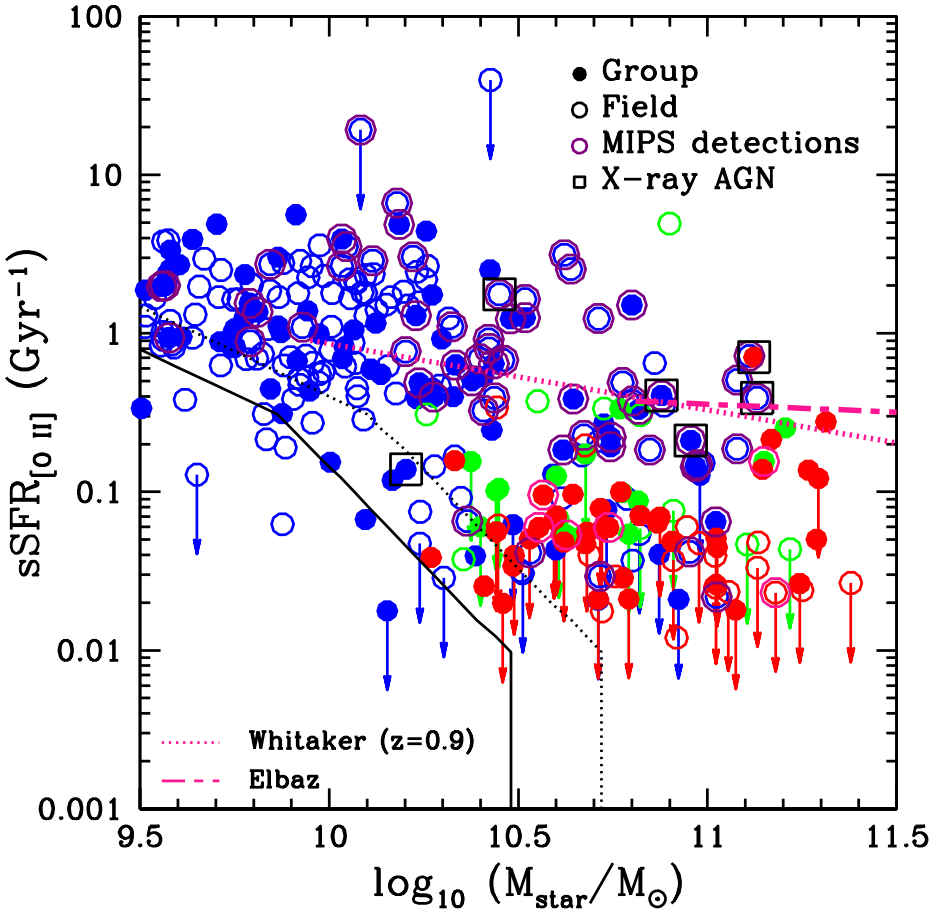

Figure 4.2: The specific star formation rate measured from the [OII] feature is shown as a function of stellar mass for galaxies at $0.8 < z < 1$ with secure redshifts. Group members are shown as *filled symbols*, and field members within our GMOS fields-of-view are shown as *open symbols*. Only galaxies with total weight (spectroscopic and mass-completeness) of between 1 and 5 are included. The solid line and dotted lines represent our 50 per cent completeness limit due to the M/L_r distribution at fixed specific star formation rate (sSFR), at $z = 0.8$ and $z = 1$, respectively. Points are colour-coded according to their classification as star-forming ('blue'), intermediate ('green'), and quiescent ('red'). Galaxies with significant X-ray sources within 5″ are outlined in black, while galaxies with 24 micron MIPS detection within 3″ are outlined in purple. The star-forming sequence from Elbaz et al. (2007) *(thick pink dashed line)* and Whitaker et al. (2012a) *(thin pink dashed line)* at $z = 0.9$ are included for comparison, up to their stated mass completeness limits. Note that those galaxies with a negative [OII] equivalent width or with [OII] detections less than the measurement error are converted into upper limits.

We also note that a small number of blue galaxies do not have a detected [OII] emission, as shown by the arrows denoting upper limits. At the high mass end, this may be caused by the [OII] luminosity being dominated by the continuum component as well as difficulties in the detection of the relatively weaker [OII] feature from their spectra. Variations in dust extinction from the average could also contribute, as well as the large uncertainties (and the low signal to noise ratio) of the spectra, especially for fainter galaxies.

In addition, we observe that the intermediate galaxies are not well separated from the quiescent population, as the [OII] feature is rarely detected in either population. We shall see later that a real separation does exist when taking into account the stacked properties of the intermediate ('green') and quiescent ('red') populations.

Finally, the slope of the sSFR-stellar mass relationship potentially holds important clues about the processes regulating galaxy formation, and can put strong constraints on feedback models (Bower et al., 2012). However, the measured slope will depend sensitively on a survey's completeness limits and their definition of star-forming galaxies.

In particular for the GEEC2 sample, we are certainly missing galaxies with still substantial star formation at $M_{\rm star} < 10^{10} M_{\odot}$, as denoted by the completeness limits. This means that the overall slope of the star-forming sequence is likely to be flatter than observed here, despite the inclusion of statistical weights to partially offset this.

4.1.3 Stacked Measurements

Next, we can looked at the stacked properties of the galaxies in individual mass bins, using the weighted-median method. In Figure 4.3, we show the weighted median specific star formation rate (sSFR) for the star-forming and intermediate galaxies, stacked in equal mass bins, with errors calculated using the bootstrap method.

For the most massive star-forming group bin, which contains only one galaxy, the error of that individual measurement is shown. For the intermediate galaxies, cases where the weighted median measurements would indicate an undetected [OII] emission are shown as upper limits.

We observed that for $M_{\rm star} > 10^{10.3} M_{\odot}$, the star-forming and intermediate field populations show slightly higher specific star formation rates than their group counterparts. Below $M_{\rm star} \sim 10^{10.3} M_{\odot}$, the blue group and field population do not show a statistically significant difference, which may be caused by incompleteness in our sample, since we could only detect galaxies with high specific star formation rates (sSFRs) in this mass range.

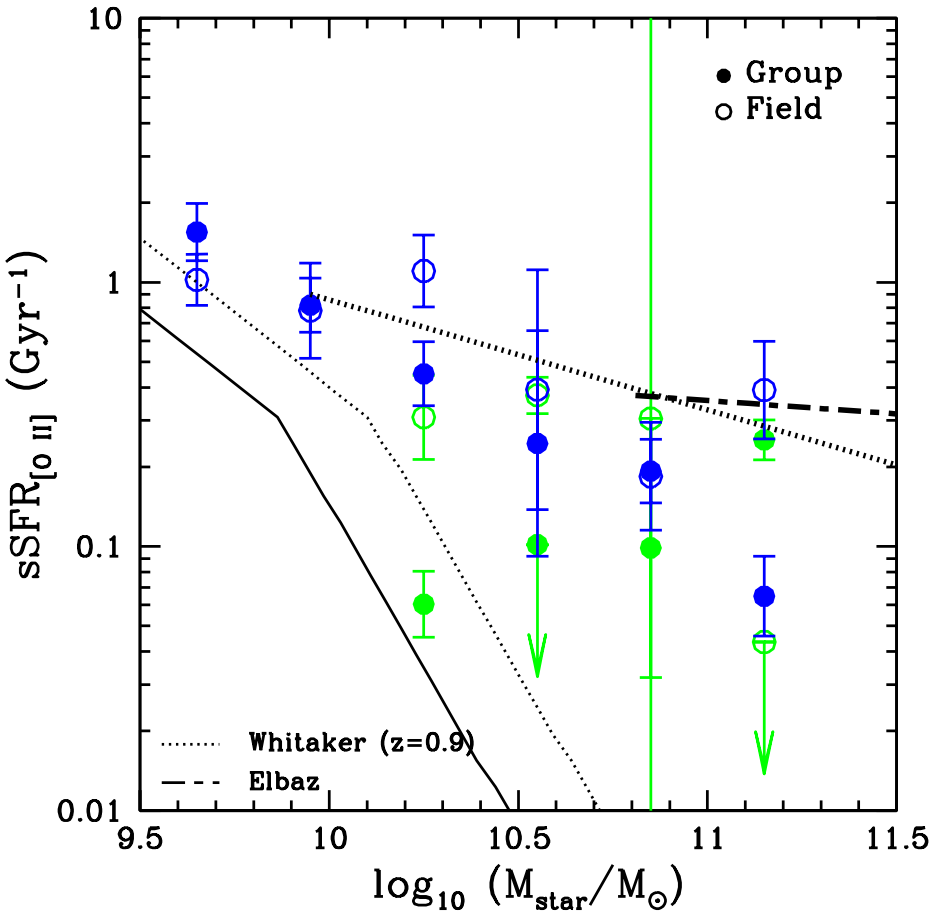

Figure 4.3: The binned weighted-median sSFR is shown as a function of stellar mass for galaxies at $0.8 < z < 1$, within the GMOS fields-of-view and total weights (spectroscopic and mass-completeness) between 1 and 5. Group galaxy bins are shown with *filled symbols* and field galaxies as *open symbols*. The solid line and dotted lines represent our 50 per cent completeness limit due to the M/L_r distribution at fixed sSFR, at $z = 0.8$ and $z = 1$, respectively. The star-forming sequence from Elbaz et al. (2007) *(thick dashed line)* and Whitaker et al. (2012a) *(thin dashed line)* at $z = 0.9$ are included for comparison, up to their stated mass completeness limits. The blue points are the binned values for the blue galaxies and the green points indicate green galaxy bins. For the green galaxies, cases where the weighted median would indicate an undetected [OII] emission are shown as upper limits. Note that for the most massive blue group bin, which contains only one galaxy, the error of the measurement is shown.

4.1.4 Distribution of Star-Forming Group and Field Galaxies

To determine the cause for this possible divergence in the specific star formation rates of the star-forming group and field population, we used the Whitaker et al. (2012a) relationship between stellar mass and specific star formation rates at $z = 0.9$ and calculate the difference between their sequence and the individual galaxies' specific star formation rates.

The distribution of the residuals for the high mass blue galaxy population ($M_{\rm star} > 10^{10.3} M_{\odot}$) is shown in Figure 4.4, including the relevant spectroscopic and mass-completeness weights. Qualitatively, the main difference between the two shapes is the lack of high specific star formation rate (sSFR) galaxies in the group sample. This may be some indication of environment-driven evolution in the star-forming population, which would cause a quenching in the star formation rates.

Quantitatively, the two distributions can be compared by calculating their weighted means. The associated error of this measurement is provided using the bootstrap method, by re-sampling the distribution 500 times and calculating the mean each time. The standard deviation of this new distribution will be the quoted error for the measurement.

The field population has a mean log specific star formation rate (sSFR) residual of 0.27 ± 0.1, while the log mean sSFR residual for the group population is -1.48 ± 1.6. These two values are within the error bounds of the two measurements, so we could not say conclusively that one distribution has a higher specific star formation rate than the other. More measurements of star-forming group galaxies may help in this regard, by reducing the final error bounds.

In addition, performing the standard Kolmogorov-Smirnov (KS) test on the unweighted sample shows that the group and the field have a 17% chance of originating from the same distribution. Therefore, the small offset we observe between the star-forming main sequence of $z \sim 1$ group and field galaxies is not yet statistically significant.

4.1.5 Starburst Fractions of Group Galaxies

As well as measuring the bulk properties of galaxies, the fraction of galaxies undergoing starbursts is also important in the study of the evolution of galaxies. This section will discuss the individual star formation rates and the starburst fraction of the group galaxies in the GEEC2 sample, using the two main methods of measuring star formation rates.

First, the result for the FUV + IR and the FUV + dust attenuation estimates are presented in Figure 4.5. As before, the MIPS detected galaxies are outlined in purple

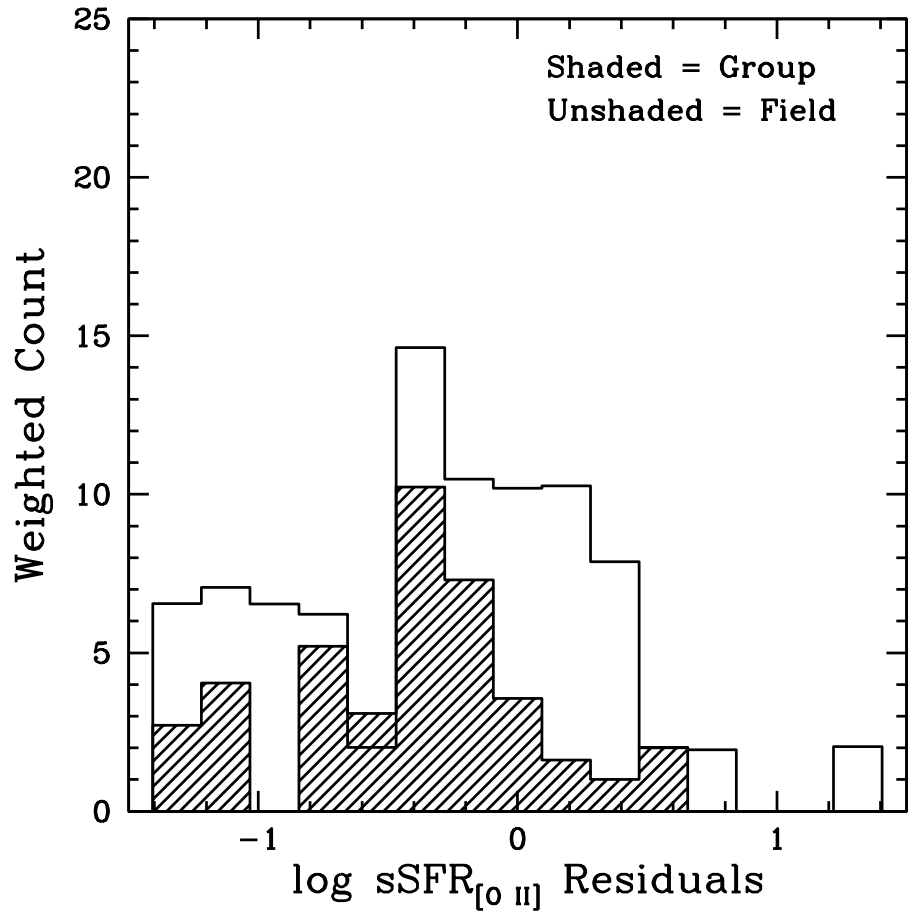

Figure 4.4: A histogram showing the residuals to the Whitaker et al. (2012a) line at $z = 0.9$, shown in Figure 4.3, for the high mass blue galaxy population ($M_{\rm star} > 10^{10.3} M_{\odot}$). The data includes the spectroscopic and mass-completeness weights, drawn from the same population as Figure 4.2. The histogram for the group galaxies is shaded, while the field galaxies are unshaded.

while those without are detected in the FUV only. Those galaxies undetected in the FUV are converted into upper limits with the survey detection limit of 25 mag and the dust attenuation estimate done in a consistent fashion.

We notice that most of the star-forming group galaxies are detected in FUV, while many of the intermediate and most of the quiescent galaxies are not. The star-forming group galaxies agree with the star forming sequence for field galaxies at $z = 0.9$ of Whitaker et al. (2012b), as seen in Figure 4.5, especially where the GEEC2 sample is complete ($> 10^{10.5} M_{\odot}$). This is similar to the result previously obtained for the [OII] star formation rates.

This process can also be done for the field population with secure redshifts. Since all the galaxies from the zCOSMOS and GEEC2 catalogue have photometric and Spitzer data available, we can also extend this analysis to galaxies not within the GMOS field of view. This is shown in Figure 4.6. We note that the star-forming sequence from Whitaker et al. (2012b) fits the field population as well.

The star-forming group sample contain 90 galaxies in total. If we take the limit of $4\times$ the specific star formation rate (sSFR) of the star-forming population from Rodighiero et al. (2011) to be the threshold for starburst galaxies, then only 4.4 per cent fit this criteria (4 out of 90). In the field, this value is 5.1 per cent (44 out of 871). Although our group sample is small, this result is in agreement with the findings of other groups which have not found an enhancement in star-formation in higher density regions (e.g. Dressler et al., 2013; Webb et al., 2013).

Next, the result for the [OII] - based star formation rate measurements are presented in Figure 4.7, with the starburst threshold overplotted. If we again take the limit of $4\times$ the specific star formation rate (sSFR) of the star-forming population to be the threshold for starburst galaxies as before, then only 6.7 per cent fit this criteria (6 out of 90).

Measurements using the [OII] method matches the results from the FUV + IR measurements and shows that starbursts may not play a big role in the process of environmental quenching. This result suggests that the use of simple quenching models, where star formation is quenched with an exponential function after in-falling into the group, may be an appropriate approximation.

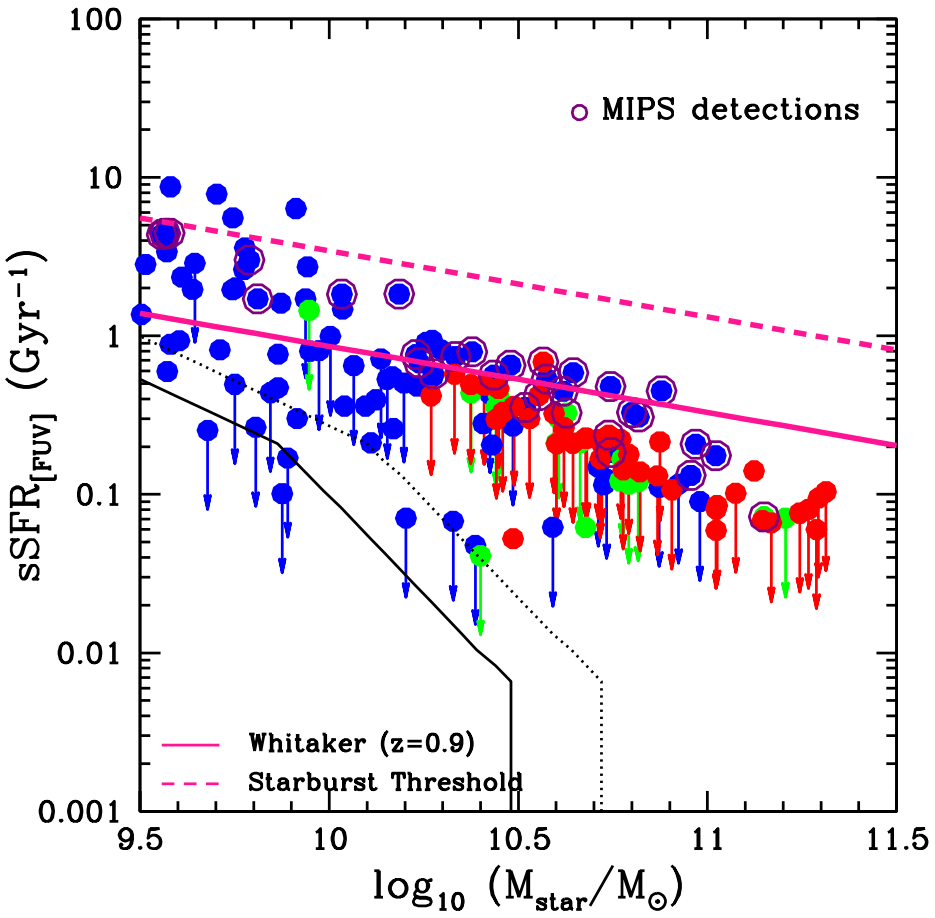

Figure 4.5: The specific star formation rate measured from the FUV + IR (where available) and FUV + Salim's dust attenuation estimate is shown as a function of stellar mass for group galaxies at $0.8 < z < 1$ with secure redshifts. The solid line and dotted lines represent our 50 per cent completeness limit due to the M/L_r distribution at fixed sSFR, at $z = 0.8$ and $z = 1$, respectively. Galaxies with 24 micron MIPS detection within $3''$ are outlined in purple. The star-forming sequence from Whitaker et al. (2012a) *(thin pink dashed line)* at $z = 0.9$ are included for comparison, along with the $4\times$ sSFR threshold from Rodighiero et al. (2011). Note that those points with upper limits are not detected in the FUV.

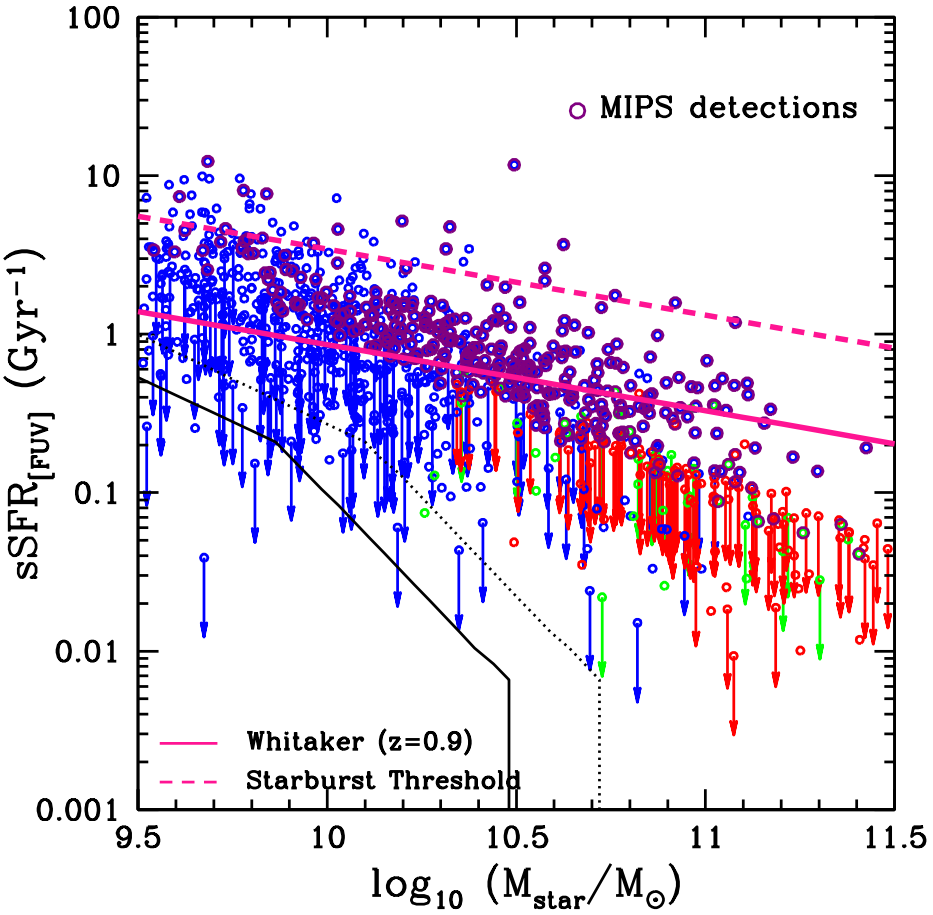

Figure 4.6: The specific star formation rate measured from the FUV + IR (where available) and FUV + Salim's dust attenuation estimate is shown as a function of stellar mass for field galaxies at $0.8 < z < 1$ with secure redshifts. The solid line and dotted lines represent our 50 per cent completeness limit due to the M/L_r distribution at fixed sSFR, at $z = 0.8$ and $z = 1$, respectively. Galaxies with 24 micron MIPS detection within $3''$ are outlined in purple. The star-forming sequence from Whitaker et al. (2012a) *(thin pink dashed line)* at $z = 0.9$ are included for comparison, along with the $4\times$ sSFR threshold from Rodighiero et al. (2011). Note that those points with upper limits are not detected in the FUV.

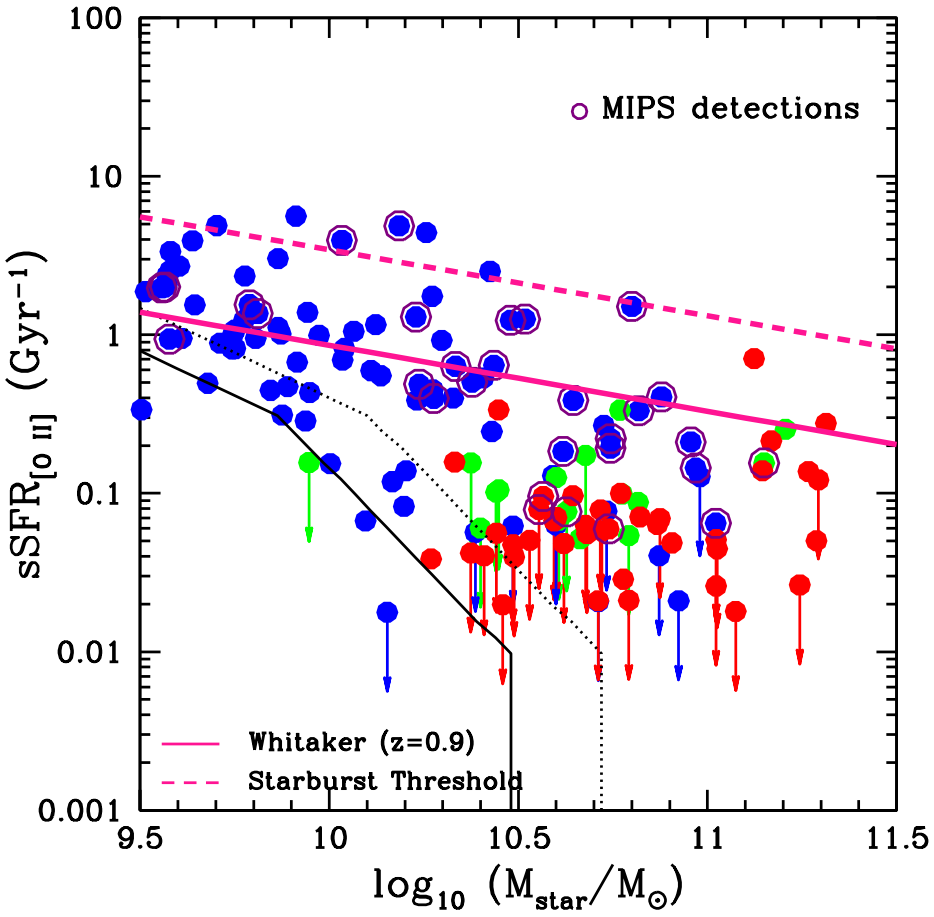

Figure 4.7: The specific star formation rate measured from the [OII] feature is shown as a function of stellar mass for group galaxies at $0.8 < z < 1$ with secure redshifts. The solid line and dotted lines represent our 50 per cent completeness limit due to the M/L_r distribution at fixed sSFR, at $z = 0.8$ and $z = 1$, respectively. Galaxies with 24 micron MIPS detection within 3″ are outlined in purple. The star-forming sequence from Whitaker et al. (2012a) *(thin pink dashed line)* at $z = 0.9$ are included for comparison, along with the 4× sSFR threshold from Rodighiero et al. (2011). Note that those galaxies with a negative [OII] equivalent width or with [OII] detections less than the measurement error are converted into upper limits.

4.2 Spectroscopic Properties of Star-Forming, intermediate, and Quiescent Galaxies

Next, it is instructive to consider the average spectroscopic properties of each population in the GEEC2 sample. Figure 4.8 shows an example of the stacked spectra for the six sub-populations. The signal-to-noise ratios ranges between 7.0 per Å (in the range of 4050 Å to 4100 Å) for the relatively small sample of intermediate ('green') field stacked spectra to 12.7 per Å for the more numerous star-forming 'blue' group stacked spectra.

The average spectra confirm that intermediate ('green') galaxies have features that are intermediate between star-forming and quiescent galaxies. They seem to have less prominent absorption lines, which means that their spectra do not closely resemble the typical post-starburst type galaxies.

In addition, for the intermediate galaxies, some [OII] emission is present at a low level. The strength of the [OII] line seems to be much greater in the field population rather than for the group population. Therefore, some star formation is still ongoing inside these intermediate galaxies, as compared to the quiescent spectra.

Using their stacked spectra, the average spectral properties for the star-forming ('blue'), intermediate ('green'), and quiescent ('red') populations can be determined by measuring the [OII] and Hδ strengths.

Note that for the star-forming population, we have decided to separate the population into a low mass and high mass sample at $\log(M_{\rm star}/M_{\odot}) = 10.3$. This decision was motivated by the differences observed in the distribution of specific star formation rates in Chapter 4.1.2 between the high mass and low mass 'blue' galaxies, which may have been caused in part by the onset of incompleteness. It is instructive to see if there are also differences in their stacked spectra as well.

Another important point to note is that our stacked spectra contain enough signal to distinguish the presence of weak emission-filling in the Hδ absorption line of blue galaxies. We correct for this in the calculation of the average Hδ equivalent width, by the fitting of Gaussian functions to this emission component. The equivalent width of the emission line is then added to the total equivalent width obtained using the automated bandpass method, as described in Chapter 3.2.

For the lower mass blue galaxies bin, the emission component was measured to be 1.5 Å for the group galaxies and 1.3 Å for the field galaxies. For the higher mass bin, the emission component was measured to be $\sim$ 1.8 Å for the group and field population.

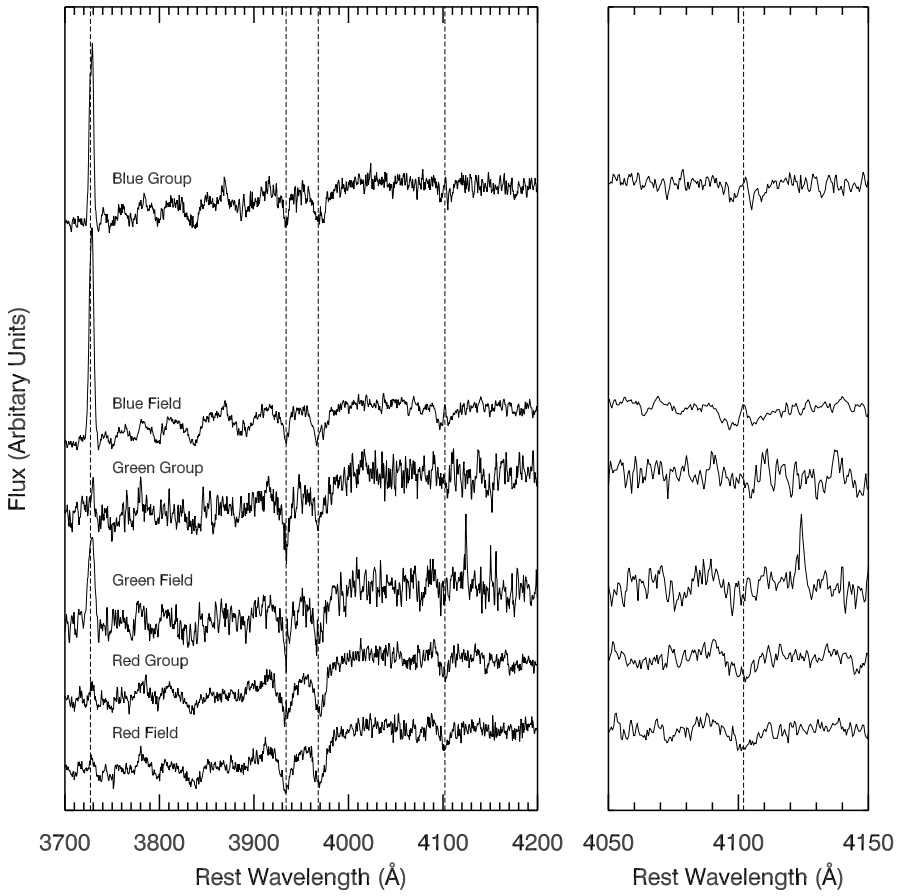

Figure 4.8: Rest-wavelength stacked spectra for galaxies at $0.8 < z < 1$ and $9.5 < \log(M_{\rm star}/M_{\odot}) < 11.6$, including the spectroscopic and mass-completeness weights, for the six main classification used in this work. The spectra are arbitrarily normalized within the wavelength range of $4050 - 4100$ Å. The location of the important lines (in order: [OII] , Calcium H&K, and Hδ) are also indicated on this plot. The figure on the right show an expanded section of the spectra around the Hδ line.

4.2.1 [OII] Measurements

First, the specific star formation rates (sSFR) calculated from these eight populations are shown in Figure 4.9, with filled and open circles for the group and field galaxies, respectively. This is done for both the stacked-spectra and weighted-median method, as described in Chapter 3.2.2. Note that for the stacked spectra method, the [OII] luminosity is the weighted average value for the [OII] continuum level and the stellar mass used for the dust correction formula is also the weighted average of the sample.

We see that for the star-forming galaxies, where the statistical uncertainty on the stacked spectra is negligible, we observe a significant difference between the average specific star formation rate (sSFR) of the low and high mass blue sample. This is a reflection of the relationship between sSFR and stellar masses observed previously.

For the quiescent ('red') and low-mass star-forming ('blue') populations, the weighted-median specific star formation rate (sSFR) shows at most a weak dependence on environment. On the other hand, while the group galaxies have only ~ 3 per cent lower sSFR than the field sample for the low mass blue population, the difference is ~ 55 per cent for the high mass sample from the stacked spectra method.

The apparently high significance of this difference is misleading, however, as the error bar only reflects the fact that the [OII] feature is measured with high signal-to-noise in the stacked spectrum. Intrinsic variations in the line strength amongst galaxies means that average star formation rates is not as well determined as the error suggested, as already seen in Figures 4.3 and 4.4.

Interestingly, the intermediate galaxies show an even larger difference, as green group galaxies have an average specific star formation rates (sSFR) a factor ~ 3 lower than the field, when measured using the stacked spectra. This result does need to be treated carefully, as this is a relatively small population defined by sharp boundaries amongst a continuous distribution of galaxy colours (refer to Figure 2.4).

Both statistical and systematic (i.e. the connection between colours and underlying star formation history) uncertainties mean that the 'green' population likely contains contamination from the adjacent 'blue' and 'red' populations. Since the quiescent fraction is a strong function of environment, this can lead to an apparent environmental dependence amongst these green galaxies.

When we compare the specific star formation rates (sSFR) from the weighted-median of the individual galaxy measurements (see Chapter 3.2), shown as the squares in Figure 4.9, the difference between group and field still exists. However, the error bars now include the bootstrap contribution to the error due to the scatter of the parent distribution.

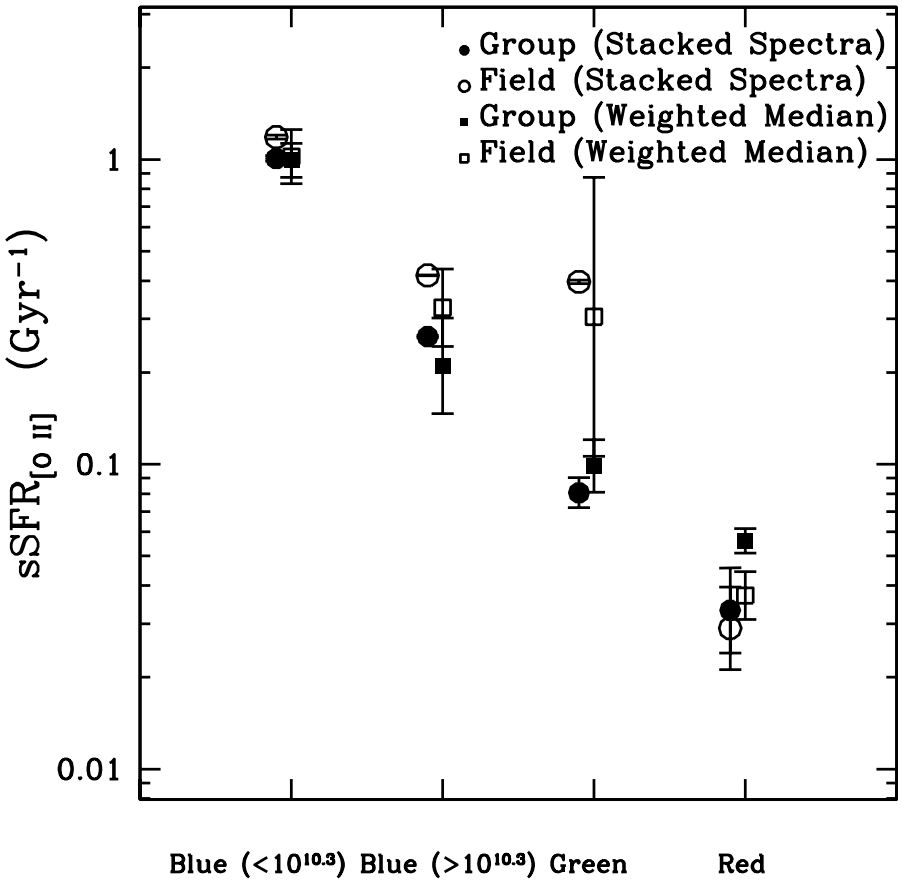

Figure 4.9: The sSFR for the red, green, and blue populations. The galaxies are restricted to $0.8 < z < 1$ and include galaxies within the GMOS fields-of-view and total weights (spectroscopic and mass-completeness) of between 0 and 5. Bins of group galaxies are shown with *filled symbols* and field galaxies as *open symbols*. The red and green bins contain galaxies with masses $9.5 < \log(M_{\rm star}/M_{\odot}) < 11.6$. For the blue population, another cut was made, separating the two populations at $\log(M_{\rm star}/M_{\odot}) = 10.3$. The *circle* indicate the results from stacked-spectra measurement of [OII] sSFR. The *squares* are data from the same bin, except combined using the weighted median method.

The larger error bars indicate that these differences in the sSFR may not be statistically significant, given the small sample sizes and the wide spread in the properties of the binned galaxies. Therefore, with the dataset from the GEEC2 sample, we cannot yet claim any significant suppression of the specific star formation rates (sSFR) amongst group galaxies of a given spectral type, relative to the field.

4.2.2 Hδ Measurements

Next, we consider the Hδ absorption line. This spectral feature is most prominent in A-type stars and is a signature of recent star formation, especially for galaxies with low instantaneous specific star formation rates (sSFR). An especially strong Hδ signature, with an equivalent width greater than 5 Å, may indicate a truncation in star formation. This is due to the domination of intermediate age A-type stars (Couch & Sharples, 1987; Balogh et al., 1999; Lemaux et al., 2012).

In Figure 4.10, we show the Hδ equivalent width measured using the stacked spectra as the circular points. One potential source of concern is that the corrections to the telluric absorption at the A-band may not be perfect. They often leave significant residuals which unfortunately overlap with Hδ over the redshift range, $0.818 < z < 0.895$. To ensure that this contamination is not affecting our results, we remove galaxies in the redshift range $0.818 < z < 0.895$ and show our updated results for this restricted sample with triangular points.

We find differing environmental signatures in Hδ between the red, green, and blue populations, though they are not highly significant given our uncertainties. The high mass star-forming ('blue') galaxies ($M_{\rm star}/M_{\odot} > 10^{10.3}$) show a weaker absorption for the group sample, as compared to the field, which may be related to the observed differences in their specific star formation rates (sSFR) from Figure 4.9. However, this significant difference disappears when we consider the sample unaffected by telluric absorption, so we must treat this result with caution.

Another point to note from the Hδ measurements is that the intermediate 'green' population is not dominated by post-starburst galaxies ($W_{\circ}$(Hδ)$>$ 5 Å), as we had observed from a visual inspection of their stacked spectra. Surprisingly, the Hδ strength of the green population is much less than that of the blue population, which suggests that the last period of significant star formation occurred $\gtrsim 1-2$ Gyr ago. How this result fits into the general interpretation that intermediate galaxies are quenched star-forming galaxies will depend on the exact star-formation history associated with the quenching.

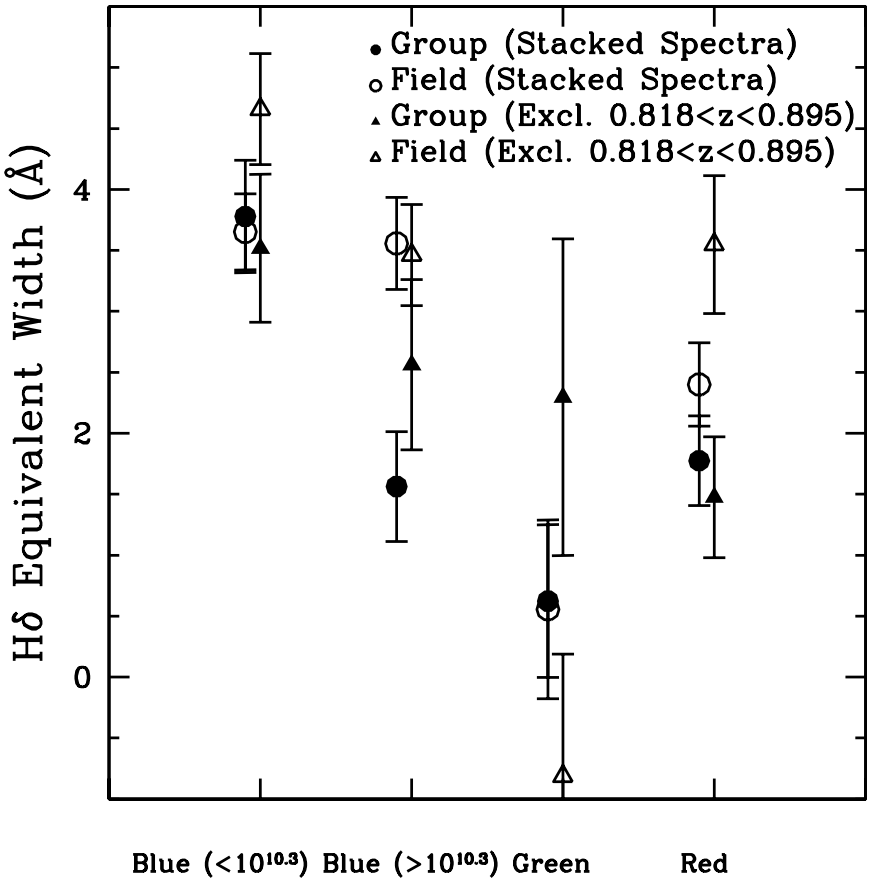

Figure 4.10: The Hδ equivalent widths for the red, green, and blue populations. The galaxies are restricted to $0.8 < z < 1$ and include galaxies within the GMOS fields-of-view and total weights (spectroscopic and mass-completeness) of between 0 and 5. Bins of group galaxies are shown with *filled symbols* and field galaxies as *open symbols*. The red and green bins contain galaxies with masses $9.5 < \log(M_{\rm star}/M_{\odot}) < 11.6$. For the blue population, another cut was made, separating the two populations at $\log(M_{\rm star}/M_{\odot}) = 10.3$. In addition, the measurement of the blue galaxies includes a correction for Hδ emission, computed using a Gaussian fit to the stacked spectra. The *triangles* represents the removal of galaxies in the redshift range $0.818 < z < 0.895$, in order to avoid the telluric-dominated spectra.

In addition, the intermediate field galaxies have a weaker measured Hδ line than even the quiescent galaxies, though this result should be treated with caution. The systematic errors are not included in the error bars, as demonstrated by the substantial shift we observe after the removal of the telluric dominated galaxies. There is also a small number of these intermediate field objects, which means any results obtained from this sample should be treated with caution, as this may be a fully representative sample of field galaxies.

Chapter 5

Modelling Galaxies - I - Procedure

From the GEEC2 sample, we observed the presence of an intermediate ('green') population, which may indicate the presence of a transition population between the star-forming and quiescent state. These intermediate galaxies tend to have lower star formation rates than the star-forming population, but do not show the strong Hδ strengths associated with post-starburst galaxies. If this scenario is correct, then we could attempt to model these objects with quenched star formation histories.

Another possible origin for these 'green' galaxies is the result of the rejuvenation of early-type galaxies (Fang et al., 2012), perhaps through wet merger events. For example, these quiescent objects could have an additional 'burst' of star-formation, which would push them into the intermediate ('green') region.

We will constrain both of these theories using a combination of observations and detailed stellar synthesis models.

5.1 Stellar Synthesis Models

The stellar synthesis code in this work uses the Bruzual (2007a) models (also known as CB07), an update to the GALAXEV BC03 code (Bruzual & Charlot, 2003). As explained in the introduction, this program takes in a user-defined star formation history and outputs the model galaxy's physical characteristics throughout its lifetime, such as its flux through different filters, its resulting spectra, as well as other important data. The Hδ strength can also be measured in the model synthesis code, since it uses the bandpass method in an analogous wavelength range to our analysis in Chapter 3.2.

In addition, note that the classification system used in the GEEC2 survey can be reproduced for these model galaxies using the CB07 stellar synthesis code. The $(V-z)^{0.9}$ and $(J-[3.6])^{0.9}$) colours can be recreated by red-shifting the V, z, J, and [3.6] filter response functions to $z = 0.9$. When compiled into the CB07 code, the magnitude through these photometric filters can be outputted for all time steps. Then, the two colours of interest can be calculated and assigned to these model galaxies. Our updated choice of the colour cuts required to separate galaxies into the quiescent, intermediate, and star-forming populations will be discussed in Chapter 5.4.

The observations can then be compared to the model results and used to constrain the possible star formation histories of the galaxies in the GEEC2 survey. Given the low signal-to-noise of spectra at $z \sim 1$, this method is best used on bins of galaxies with similar stellar mass, colour, and environment.

For this work, we will be looking at the collective properties of six main types of galaxies: quiescent group, quiescent field, intermediate group, intermediate field, star-forming group, and star-forming field.

5.2 Satellite Quenching Model

Once the framework is in place, we need to create standard star-formation histories for these quenched satellites. If we assume that these objects were 'blue' before entering the group environment, then we need to create sample star-formation histories for actively star forming objects. This may not be inappropriate assumption, given the in-fall times required to be observed as a group member at $z \sim 1$ and the previously observed trends in the stellar mass function of star-forming and quiescent galaxies with redshift.

In this work, two different sets of star formation histories are used. First, the star formation model from Behroozi et al. (2012) is assumed. They used cosmological models and fit models for the stellar mass-halo mass relation to determine the most likely star formation histories for different mass haloes. Using the data set found at `http://www.peterbehroozi.com/data.html`, the closest star formation history for haloes that produce central galaxies with stellar masses of $10^{9.5}$, $10^{10.0}$, $10^{10.5}$, $10^{11.0}$, and $10^{11.5}$ $M_{\odot}$ at $z = 1.0$ were chosen.

For the sake of comparison, the staged star formation model of Noeske et al. (2007b) is also used. In their paper, they have fitted to the observed distribution of specific star formation rates (sSFR) at $z = 0$ with an empirical function. In the Noeske model, the

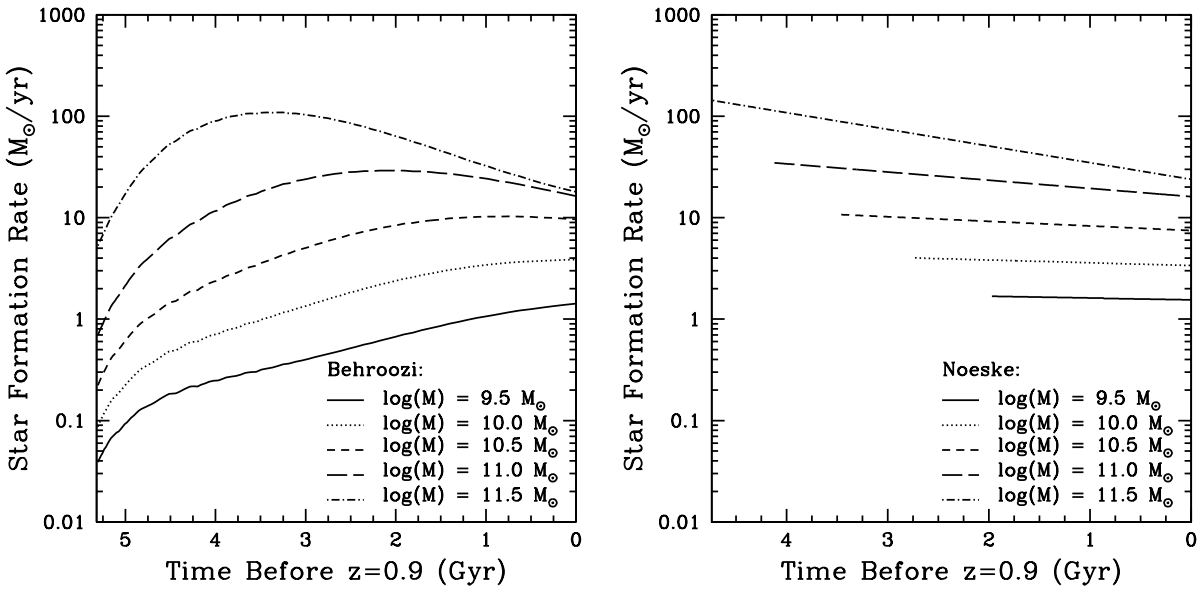

Figure 5.1: *Left:* The star formation rate histories for galaxies with stellar masses of $10^{9.5}M_{\odot}$, $10^{10.0}M_{\odot}$, $10^{10.5}M_{\odot}$, $10^{11.0}M_{\odot}$, and $10^{11.5}M_{\odot}$, taken from the Behroozi et al. (2012) models, from $z = 7.95$ to $z = 1.0$. Note that the lower mass objects have increasing star formation rates up to the time of observation, while the higher mass models have already peaked. *Right:* The star formation rate histories for the galaxies with stellar masses of $10^{9.5}M_{\odot}$, $10^{10.0}M_{\odot}$, $10^{10.5}M_{\odot}$, $10^{11.0}M_{\odot}$, and $10^{11.5}M_{\odot}$, taken from the Noeske et al. (2007b) models. Note that galaxies of different stellar masses have different 'formation' times and exponential timescales (τ).

star formation history of a galaxy is an exponential function, with parameters (such as the formation times and exponential timescale τ) that will be dependent on the galaxy's mass.

Except for the observation time, which is set to $z = 0.9$, all other parameters are kept as in the original paper. Note that in general for Noseke's model, lower mass objects have their major period of star formation start later, possesses a longer τ, and have a higher specific star formation rates at $z = 0.9$. Conversely, higher mass objects have their major period of star formation start earlier, possesses a shorter τ, and have a lower specific star formation rates at $z = 0.9$.

A plot of the shape of the star formation histories for the Noeske and Behroozi models can be found in Figure 5.1. Model galaxies with stellar masses of $10^{9.5}M_{\odot}$, $10^{10.0}M_{\odot}$,

$10^{10.5} M_\odot$, $10^{11.0} M_\odot$, and $10^{11.5} M_\odot$ have been included.

5.2.1 Satellite In-fall Rates

To calculate the quenched population of galaxies, an additional input is needed. The satellite in-fall rates can tell us what proportion of galaxies needs to be quenched and when this quenching would start.

We used the semi-analytic galaxy formation models of Bower et al. (2006) for groups at this redshift ($z \sim 1$). They indicate that the in-fall rate should roughly be constant over the past ~ 6 Gyr. For the sake of simplicity, we will therefore assume that there is a uniform distribution of in-fall times between the formation time of the satellite galaxy and the time of observation at $z \sim 1$.

Note that this amount of time between formation and observation varies for Noeske's model, which have different formation times for galaxies with different stellar masses. However, all of Behroozi's models start at $z = 7.95$ and galaxies of different masses would have the same distribution of in-fall times.

The satellite accretion histories are normalized such that all group galaxies are assumed to have accreted by the time of observation ($z \sim 1$). In all cases, the accreted fraction rises from 0 at the time of formation to 1 at $z \sim 1$.

In Noeske's model, a lower mass object is 'formed' later and thus would have a steeper accretion curve, in order to have been observed in the group environment at $z \sim 1$. The dependence of the slope of the accretion curve and the mass of the satellite galaxy can be seen in Figure 5.2.

5.2.2 Procedure

Using the Behroozi et al. (2012) star formation histories and the Noeske et al. (2007b) staged galaxy formation model, we produce star formation histories for galaxies with stellar masses of $10^{9.5}$, $10^{10.0}$, $10^{10.5}$, $10^{11.0}$, and $10^{11.5}$ $M_\odot$ at the time of observation.

This is shown in the left and right plot in Figure 5.1 for the Behroozi and Noeske star formation histories respectively. Note that for their presentation in this plot, the star-formation histories have been normalized such that the integral of their star formation rate from their formation to the time of observation is equal to their stated stellar mass.

Next, the 'natural' rate of star formation is modified once a galaxy has entered the group. We assume that the satellite galaxy undergoes a 'quenching' process. We chose a

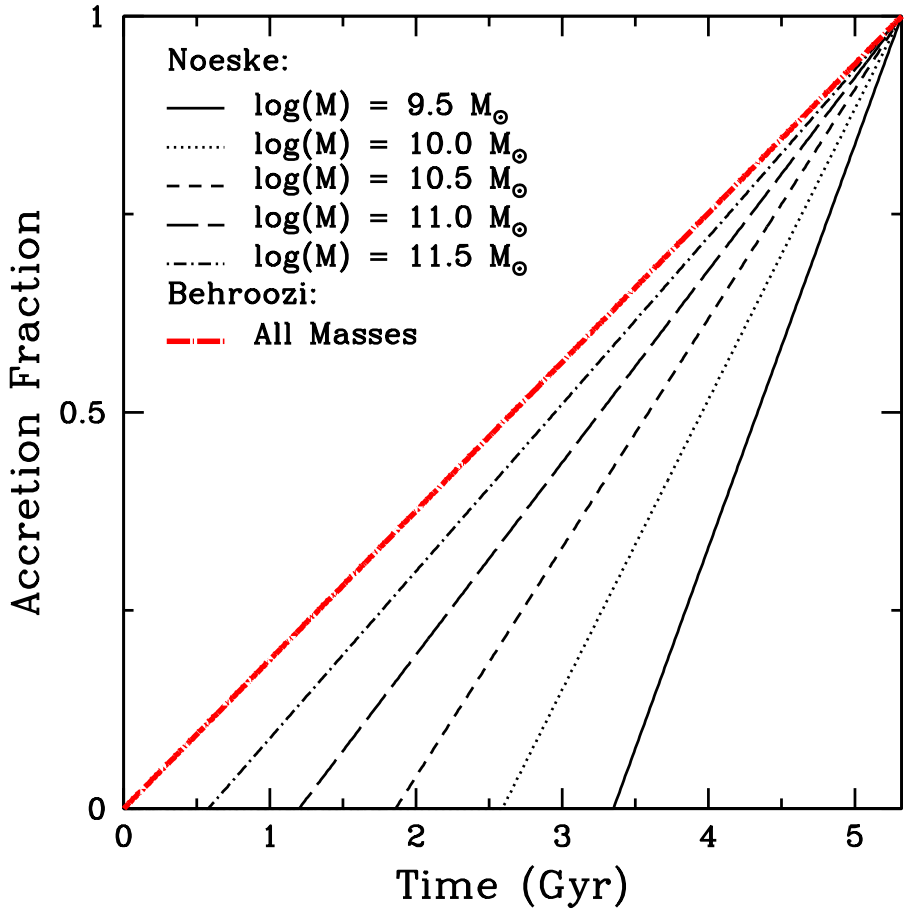

Figure 5.2: Sample accretion curves for different model galaxies with Noeske's star formation histories. Galaxies with stellar masses of $10^{9.5}M_{\odot}$, $10^{10.0}M_{\odot}$, $10^{10.5}M_{\odot}$, $10^{11.0}M_{\odot}$, and $10^{11.5}M_{\odot}$ are presented. Also included is the mass-independent accretion curve used for the galaxies with Behroozi's star-formation histories.

sharper second exponential timescale (τ_2), where star formation declines in an exponential fashion after quenching begins. An immediate cut-off in star formation can be modelled with a $\tau_2 = 0$ Gyr.

In addition, this process can be modified by the addition of a delay before quenching begins, as advocated by Wetzel et al. (2012). These changes can have a large effect on the fractions of quiescent, intermediate, and star-forming galaxies, as well as the strengths of their Hδ feature. This means that these different choices of parameters can then be constrained by our observations.

A set of models are created with a range of quenching start times, spaced out at time intervals of 0.02 Gyr from the galaxy's formation time to the time of observation. Each individual model can be identified with a specific point on the accretion curve. They are simulated independently and then their properties are combined to create our final results.

Note that the stellar synthesis code does not really care about the absolute values from the star-formation histories, only their overall shapes. Therefore, for these individual star formation histories, we use the unquenched models for each stellar mass satellite galaxy as the benchmark. The stellar masses at the end of the models (excluding stellar remnants), are normalized with the same factor, such that the stellar mass for the unquenched model would be at $10^{9.5}$, $10^{10.0}$, $10^{10.5}$, $10^{11.0}$, and $10^{11.5}$ $M_{\odot}$ respectively.

By keeping track of the resulting stellar mass of these models at the time of observation ($z \sim 1$), these objects would then be matched to the correct mass bin. We choose bins of equal sizes in log space, for example, $10^{9.5}$ $M_{\odot}$ would correspond to galaxies with a stellar mass of $10^{9.25}$ $M_{\odot}$ to $10^{9.75}$ $M_{\odot}$.

This is necessary because for some extreme cases, the 'earliest' quenched objects might not have enough stellar mass to remain in their original mass bins. For the proportion of initial objects at each mass bin and the resulting impact of these 'cross-over' models, we use the stellar mass functions for star-forming group galaxies from Giodini et al. (2012).

The next step is to run the BC07 stellar synthesis models. Then, a weighted average of their resulting colour and spectral features at the time of observation is calculated. The weights are needed in order to properly incorporate the stellar-mass function and the differing in-fall rates for the Noeske star formation histories.

Note that this procedure assumes that all the group galaxies would be star-forming at the time of accretion, as we use star formation histories for actively star forming galaxies as the initial inputs. If these group galaxies transition to a passive state through a process not related to environment, then this model might over-predict the number of star-forming ('blue') galaxies. We have tested this by assuming that the incoming population consist of

a representative sample from the field at $z \sim 1$ and we found that this modification would not substantially change our conclusions.

5.3 Rejuvenation Model

Another hypothesis for the creation of these intermediate ('green') galaxies is investigated in this work. We can assume that these intermediate galaxies are not formed through the process of quenching satellite galaxies, but rather from the rejuvenation of star formation in red, passive galaxies. For example, this can occur through wet minor mergers or through gas accretion (Salim & Rich, 2010; Fang et al., 2012).

Since these intermediate galaxies are a subset of the quiescent population, we can use the stellar synthesis models to constrain the size and frequencies of the required bursts of star formation, based on their observed properties of these intermediate galaxies and the expected timescale that such rejuvenated early-type galaxies spend inside the 'green' region.

The stellar synthesis models can create 'passive' galaxies by having a initial burst of star formation in the beginning, and then zero star formation thereafter. Intermediate ('green') galaxies are formed by adding in a smaller burst of star formation 3 Gyr later. As a result, these models will allow us to constrain the proportion of passive galaxies that would be required to undergo this process, as well as the required properties of these bursts.

5.4 Choice of Model Colour Cuts

To directly compare between the model galaxies and the populations of the GEEC2 survey, we need to determine the best way of separating the quiescent, intermediate, and star-forming populations. While we can retain the definitions from the GEEC2 survey, there is a more efficient method in terms of the number of models required to be run. This new method can reduce the large number of parameters to be explored, such as the quenching parameters, stellar mass, dust, and metallicity.

We first test the effect of dust and metallicity, which were the primary motivations behind the original classification. We follow the track of an instantaneous burst model through the $(J - [3.6])^{0.9}$ vs $(V - z)^{0.9}$ plane, while varying the model parameters for the dust and metallicity. This is presented using the dust and metallicity arrows in Figure 5.3,

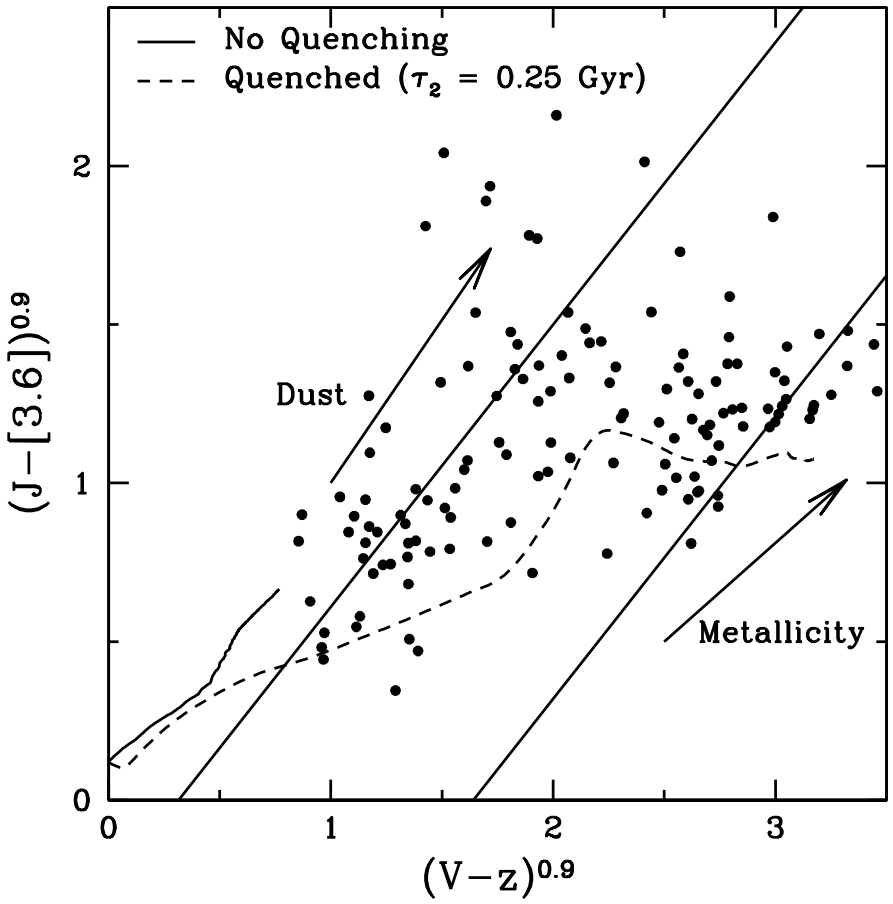

Figure 5.3: Model tracks for a star-forming galaxy in the Behroozi model (with a stellar mass of $10^{10} M_{\odot}$) vs a sample quenched model with $\tau_2 = 0.25$ Gyr in the $(J - [3.6])^{0.9}$) vs $(V - z)^{0.9}$ plane. The group galaxies from the GEEC2 survey are presented as *black filled circles*. Also plotted are the dust (from $\tau_v = 0$ to $\tau_v = 5.0$) and metallicity arrows (from $Z = 0.004$ to $Z = 0.08$). We see that the data points can be spanned with a combination of these simple models and the contribution from dust and metallicity.

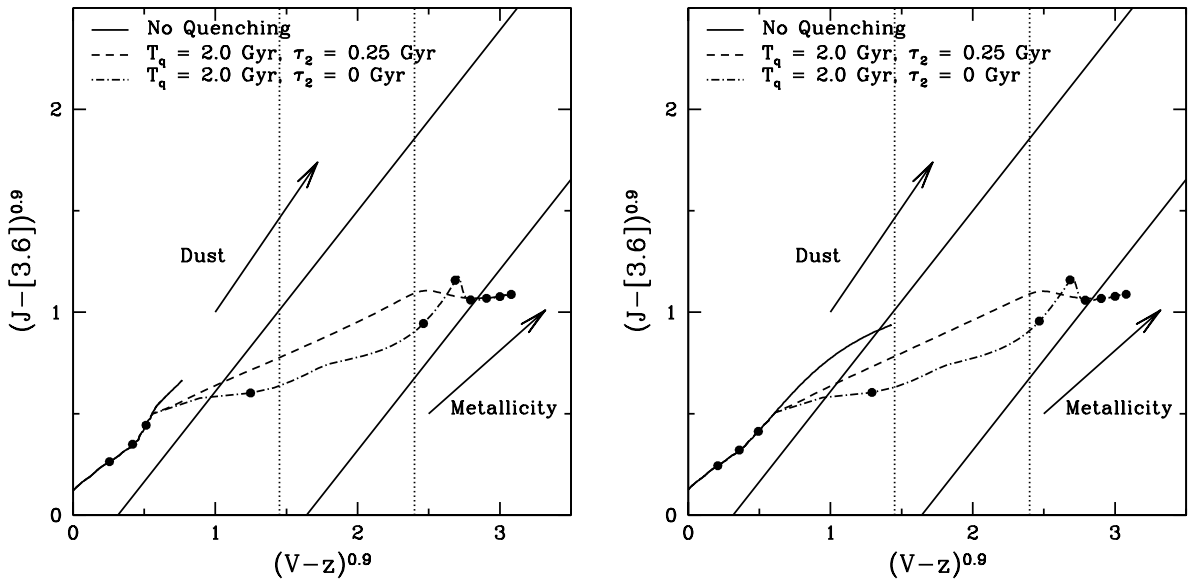

Figure 5.4: *Left:* The effects of the quenching process for a sample galaxy with the Behroozi models, a stellar mass of $10^{10.0} M_{\odot}$, and the starting time for the quenching process (T_q) at 2.0 Gyr after formation. The model track is shown in the $(J-[3.6])^{0.9}$) vs $(V-z)^{0.9}$ plane. The quenching timescale (τ_2) is set at 0 Gyr (immediate-cutoff) and 0.25 Gyr. Also plotted are the average dust (from $\tau_v = 0$ to $\tau_v = 5.0$) and metallicity arrows (from $Z = 0.004$ to $Z = 0.08$). *Black dots* show time intervals of 0.50 Gyr for the earliest quenched model ($T_q = 2.0$ Gyr). *Right:* The effects of the same quenching process on a sample galaxy, but with a stellar mass of $10^{11.5} M_{\odot}$.

which shows the positional change in the colour-colour plot as a result of dust (from an extinction $\tau_v = 0$ to $\tau_v = 5.0$) and metallicity (from $Z = 0.004$ to $Z = 0.08$).

We can see that the stellar synthesis models have dust and metallicities vectors that are roughly parallel to the star-forming sequence in Figure 2.3. As we have anticipated, our original separation into quiescent, intermediate, and star-forming galaxies has largely incorporated the effect of dust and metallicity. The star-forming sequence and the 'red' sequence can be reproduced by our basic star-forming model and the quenched model with the addition of these two factors, as shown overlaid on the group galaxies in Figure 5.3.

This result also has the beneficial consequence of simplifying the amount of analysis and modelling required. We can collapse the colour classification onto the x-axis, $(V-z)^{0.9}$, since the effect of dust and metallicity would only move the galaxies diagonally along the two sequences. Therefore, we can create one set of model galaxies with no dust and a standard metallicity content and still maintain the correspondence to our previous colour classifications.

To find out the new classifications along the $(V - z)^{0.9}$ axis, we first plot the model tracks for different stellar mass galaxies, with the two extreme cases of $10^{9.5}$ and $10^{11.5}$ $M_{\odot}$. This is shown in Figure 5.4.

For the Behroozi models, the highest mass star-forming models have already peaked in star formation. They would have evolved more than the lower mass case, which have their star formation rates still increasing, as we can see in Figure 5.1. The boundary for the Behroozi case is therefore set at $(V - z)^{0.9} = 1.45$ and any galaxy beyond this threshold would be considered to be intermediate ('green'). This boundary also works well for the Noeske models as well, as this is also close to the limit for the highest mass and longest evolving Noeske star-forming models.

Next, we want to set the approximate boundary between the intermediate (and potentially transitioning) population and the quiescent population. We can follow the track of sample model galaxies after they have been environmentally quenched, as shown in Figure 5.4 for a gentler truncation ($\tau_2 = 0.25$ Gyr) and an immediate cut-off model ($\tau_2 = 0$ Gyr).

The result shows that the quenching process takes the galaxies quickly from the star-forming ('blue') to the quiescent ('red') sequence, from the dots indicating the time intervals of 0.50 Gyr. As a result, a classification system with a colour cut in the $(V - z)^{0.9}$ axis seems reasonable. Also, we see little dependence on the y-axis $(J - [3.6])^{0.9}$) or the time at the start of the environmental quenching. We have therefore set the boundary between the quiescent and intermediate population at $(V - z)^{0.9} = 2.4$, the point at which the

evolution of these quenched model noticeably slows down, as shown by the sequence of dots in Figure 5.4.

We have tested shifting these two boundaries and determining the changes in the properties of the model galaxies. The exact location of these two boundaries does not significantly affect our results.

Chapter 6

Modelling Galaxies - II - Results

6.1 Satellite Quenching Models with the No-Delay Scenario

To begin with, we assume a simple satellite quenching model for the Behroozi models, where the galaxy switches over to a second exponential timescale (τ_2) immediately after accretion. In this case, three values for the quenched exponential timescale are chosen, $\tau_2 = 0$ Gyr (immediate cut-off), $\tau_2 = 0.25$ Gyr, and $\tau_2 = 0.5$ Gyr. The resulting fractions of quiescent, intermediate and star-forming galaxies of this model are presented in Figure 6.1.

These no-delay models tend to under-produce star-forming galaxies, even for the longest $\tau_2 = 0.5$ Gyr. The quenching process acts very quickly, as compared to the lifetime of the satellite galaxies. If there is no delay, then all galaxies accreted would quickly enter into the 'green' phase and then become quiescent. The mass dependence in the fraction of quiescent, intermediate and star-forming galaxies comes primarily from the loss of galaxies from the various mass bins, since these quenched objects no longer have their 'original' stellar mass.

The proportion of intermediate galaxies depend most strongly on the value of τ_2, as we have seen from plots of the model tracks in Figure 5.4. An immediate cut-off model moves through the 'green' region in a rapid fashion, compared to a less rapid truncation, and we would therefore expect to observe a small number of these intermediate ('green') galaxies. It is not possible to simultaneously match the proportion of star-forming/quiescent galaxies and the immediate-colour ('green') fraction, as the $\tau_2 = 0.5$ Gyr model already produces an excess of 'green' galaxies and still not enough star-forming galaxies.

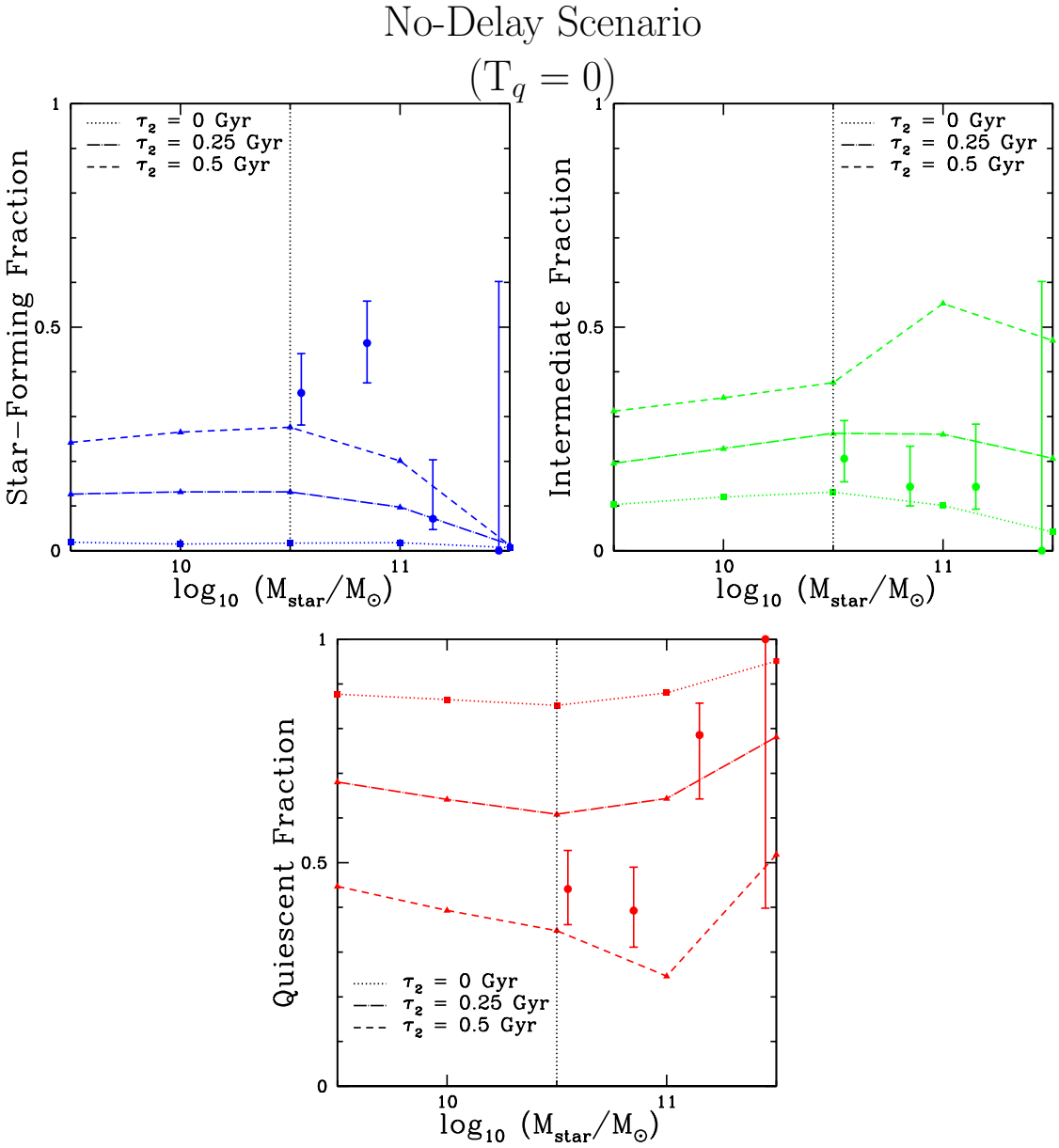

Figure 6.1: Satellite quenching model with varying τ_2 + **no delay** and its impact on the star-forming *(top left)*, intermediate *(top right)*, and quiescent *(bottom)* galaxy fractions for the Behroozi models. The *filled triangles* indicates different mass bins, with *dotted line* connecting models with $\tau_2 = 0$ Gyr (immediate cut-off), *thick dashed line* connecting models with $\tau_2 = 0.25$ Gyr, and *thin dashed lines* connecting models with $\tau_2 = 0.5$ Gyr. The observed group fractions from GEEC2 are presented as points with error bars. The black dotted line at $10^{10.5} M_\odot$ shows where the sample is reasonably complete, even for passive galaxies.

6.2 Satellite Quenching Model with Quenching Delay

The next step is to introduce a delay, which means that a period of time must pass between the time of accretion of the satellite into the group and the beginning of the quenching process (i.e. where the second exponential function takes over). This has been suggested, especially at $z = 0$, to match the observed distribution of star formation rates (Wetzel et al., 2012, 2013) and the quiescent fraction (De Lucia et al., 2012).

There are many different kinds of delays that could be implemented into this model. The delay timescale could be a constant value, such as the 3 Gyr suggested for the local universe by Wetzel et al. (2012). The delay timescale could also be dependent upon the dynamical time. In general, this is given by the following formula, which calculates the time required for a test mass released from rest to reach the centre of a homogeneous sphere (Binney & Tremaine, 2008):

$$t_{\rm dyn} = \sqrt{\frac{3\pi}{16G\rho}} \propto \sqrt{\frac{1}{G\rho}} \tag{6.1}$$

The effects of quenching can also related to the in-fall time of an object inside the group environment. For example, we can assume a velocity dispersion of $\sigma^2 = \frac{GM(<R)}{3R}$ at a given radius R. The time required to travel from $R = r$ to $R = 0$ is given by the following equation, after substituting in the density of the enclosed sphere:

$$t_{\rm infall} = \sqrt{\frac{9}{4\pi G\rho}} \propto \sqrt{\frac{1}{G\rho}} \tag{6.2}$$

The boundaries of groups are often defined using a threshold related to the critical density of the universe (such as 200 times ρ_c for R_{200} and M_{200}). Therefore, the dynamical time can also be related to the Hubble time ($1/H$). This is because H is related to critical density of the universe, $\rho_c = \frac{3H^2}{8\pi G}$. Rearranging provides the following equation:

$$t_{\rm Hubble} = \frac{1}{H} = \sqrt{\frac{3}{8\pi G\rho_c}} \propto \sqrt{\frac{1}{G\rho_c}} \tag{6.3}$$

If we assume that the quenching process is related to the dynamical time, as advocated by Tinker & Wetzel (2010), then it would evolve proportional to the redshift at the time of accretion as $(1 + z_{\rm infall})^{-\frac{3}{2}}$. This is because $t_{\rm dyn} \propto \rho^{-\frac{1}{2}}$ while $\rho \propto (1 + z)^3$ in a matter dominated universe.

For group in the GEEC2 sample, if we use the R_{rms} and M_{dyn} from Table 2.1, the

corresponding average dynamical time in the local universe is $t_{\rm dyn} \sim 0.72$ Gyr. At $z = 1$, this value would be much smaller, with $t_{\rm dyn} \sim 0.25$ Gyr. This is slightly lower than the corresponding values calculated from 200 times the critical density (ρ_c).

However, we know from Wetzel et al. (2012) that the delay timescale seems to be best fitted with a value of ~ 3 Gyr at $z = 0$. Note that this value of 3 Gyr is higher than the dynamical time in the local universe, but it may take some time for the physical processes associated with quenching, such as the stripping of hot gas, to affect the star formation rates of satellites after their first in-fall. This delay could also be related to the orbits of these satellites, which would then also evolve in a similar fashion as the dynamical time with redshift.

Therefore, one of the delay timescales in our models will evolve as $3 \times (1 + z_{\rm infall})^{-\frac{3}{2}}$ Gyr. The results from this evolving delay timescale and a constant 3 Gyr delay is presented below.

6.2.1 3 Gyr Delay

A 3 Gyr delay was added to the model, while maintaining the previous values for the quenched exponential timescale, $\tau_2 = 0$ Gyr (immediate cut-off), $\tau_2 = 0.25$ Gyr, and $\tau_2 = 0.5$ Gyr. The result of this change can be seen in Figure 6.2.

For all cases, not enough quiescent galaxies have been produced by $z \sim 0.9$, since a large proportion of satellite galaxies would not have begun to feel the quenching process and therefore would stay on the star-forming ('blue') sequence. The formation timescale of these model galaxies at $z = 7.95$ and the age of the universe at $z \sim 1$ would likely prohibit such a long delay timescale.

6.2.2 Delay Dependent on Dynamical Time

While the satellite quenching model with a 3 Gyr delay may work well in the local universe, this value must be lower at $z \sim 1$. The delay timescale would then evolve with redshift as $(1 + z_{\rm infall})^{-\frac{3}{2}}$, which can be individually calculated for each galaxy at their time of accretion. Once again, the three quenched exponential timescale are kept, $\tau_2 = 0.0$ Gyr (immediate cut-off), $\tau_2 = 0.25$ Gyr, and $\tau_2 = 0.5$ Gyr. The resulting colour fractions are presented in Figure 6.3.

The star-forming and quiescent fractions appear to be much better matched to the observations than the first two scenarios. A delay timescale evolving with the dynamical

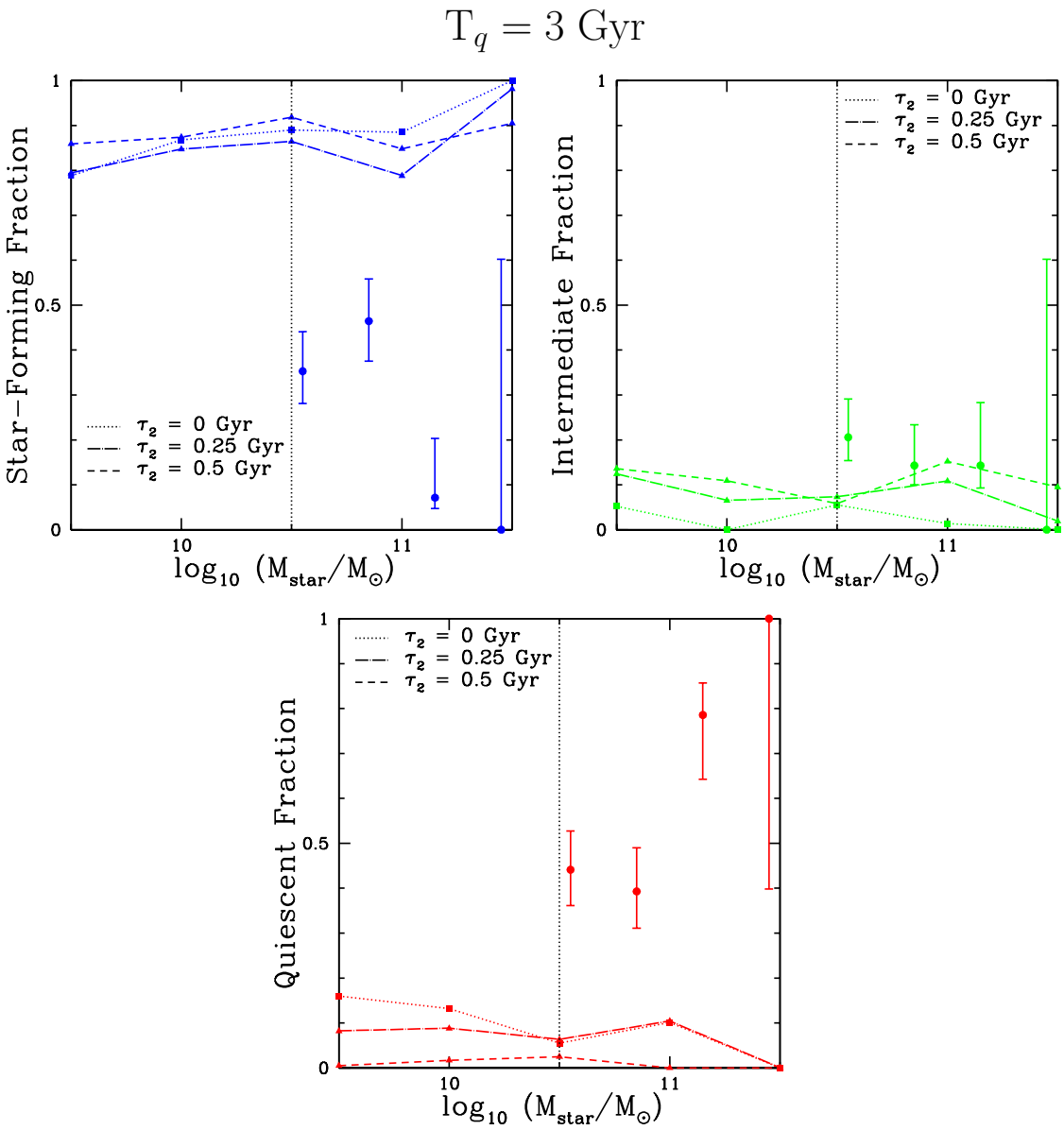

Figure 6.2: Satellite quenching model with varying τ_2 + **a 3 Gyr delay** and its impact on the star-forming *(top left)*, intermediate *(top right)*, and quiescent *(bottom)* galaxy fractions for the Behroozi models. The *filled triangles* indicates different mass bins, with *dotted line* connecting models with $\tau_2 = 0$ Gyr, *thick dashed line* connecting models with $\tau_2 = 0.25$ Gyr, and *thin dashed lines* connecting models with $\tau_2 = 0.5$ Gyr. The observed group fractions from GEEC2 are presented as points with error bars. The black dotted line at $10^{10.5} M_\odot$ shows where the sample is reasonably complete, even for passive galaxies.

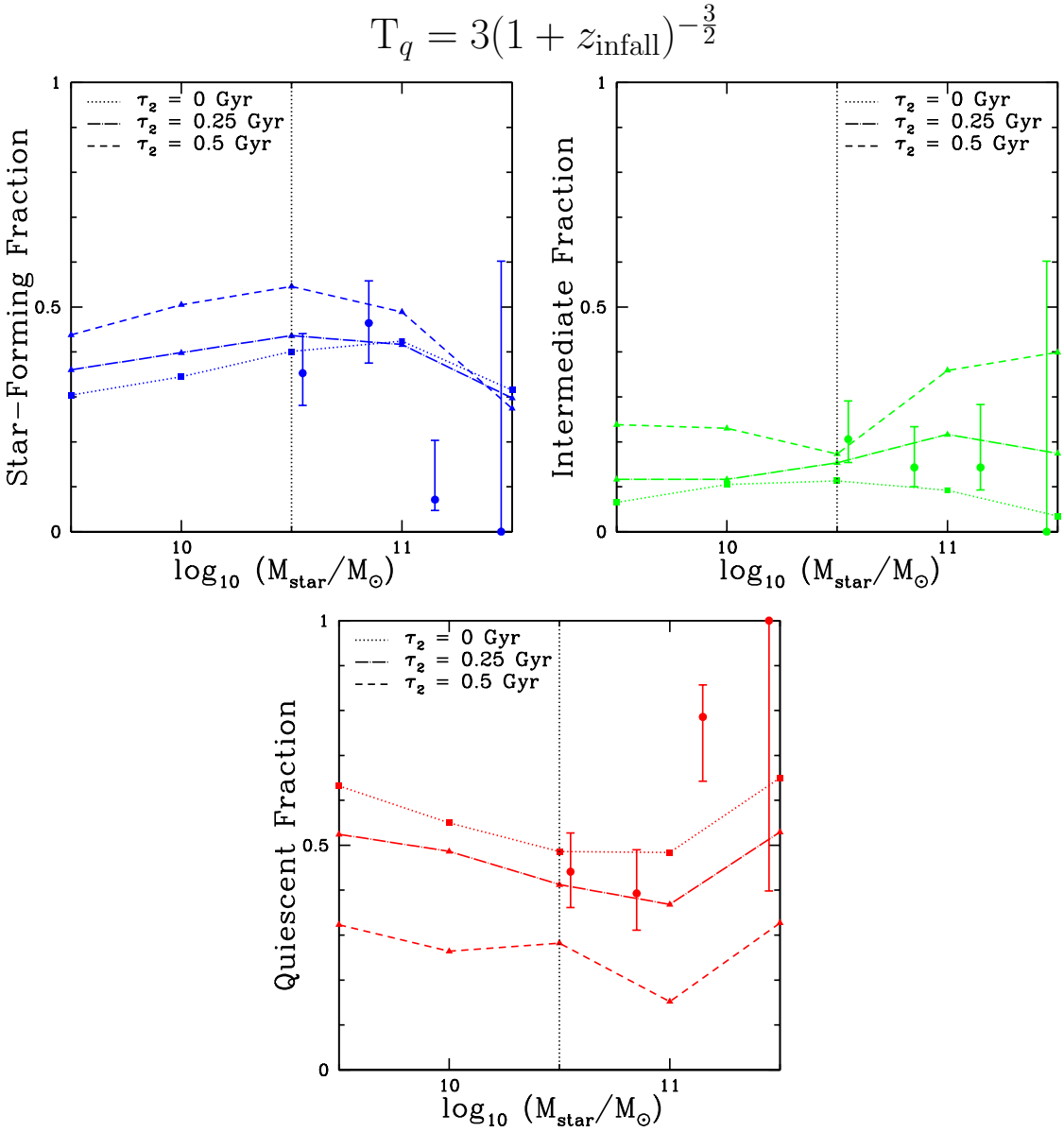

Figure 6.3: Satellite quenching model with varying τ_2 + **a delay timescale that is dependent on the dynamical time** and its impact on the star-forming *(top left)*, intermediate *(top right)*, and quiescent *(centre)* galaxy fractions for the Behroozi models. The *filled triangles* indicates different mass bins, with *dotted line* connecting models with $\tau_2 = 0$ Gyr, *thick dashed line* connecting models with $\tau_2 = 0.25$ Gyr, and *thin dashed lines* connecting models with $\tau_2 = 0.5$ Gyr. The observed group fractions from GEEC2 are presented as points with error bars. The black dotted line at $10^{10.5} M_\odot$ shows where the sample is reasonably complete, even for passive galaxies.

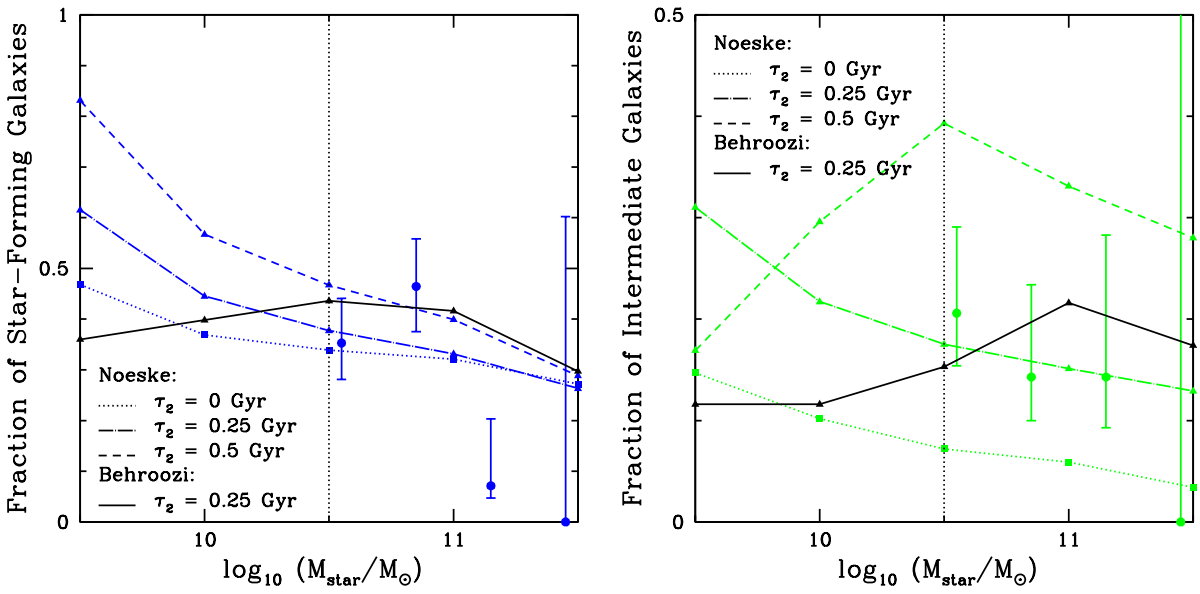

Figure 6.4: Comparison of the star-forming *(left)* and intermediate *(right)* fraction in Noeske's and Behroozi models for the satellite quenching model with varying τ_2 + a delay timescale that is dependent on the dynamical time. A *blue dotted line* connects Noeske models with $\tau_2 = 0$ Gyr, a *blue thick dashed line* connects Noeske models with $\tau_2 = 0.25$ Gyr, and a *blue thin dashed lines* connects Noeske models with $\tau_2 = 0.5$ Gyr. The *black solid line* is the reference Behroozi model with $\tau_2 = 0.25$ Gyr. The observed group fractions from GEEC2 are presented as points with error bars. The black dotted line at $10^{10.5} M_\odot$ shows where the sample is reasonably complete, even for passive galaxies..

time could explain the star-forming and quiescent population. Combined with the correct value of τ_2, this model could also produce the correct amount of intermediate galaxies.

From the GEEC2 sample, a value of $\tau_2 = 0.25$ Gyr seem to be most likely. Models with $\tau_2 = 0.5$ Gyr or $\tau_2 = 0.0$ Gyr models perform worse, as they tend to over-produce or under-produce intermediate ('green') galaxies respectively.

6.3 Comparison with Noeske's Models

The Noeske star formation histories provide similar results for the scenario with a delay dependent on the dynamical time, as shown in Figure 6.4 for the fraction of star-forming and intermediate galaxies. The similar results for the intermediate galaxies galaxies is to be expected, since the proportion is strongly dependent on the second quenching timescale (τ_2).

The more interesting result is the fraction of star-forming galaxies. The mass dependence in the star-forming fraction with the Noeske models comes from the different formation time of satellite galaxies, which causes a variation in the steepness of the accretion curve, as seen previously in Figure 5.2. Therefore, the main mass dependence in the the fraction of quiescent and star-forming galaxies comes from the varying proportion of galaxies that had 'felt' the effects of quenching.

The results using the Noeske's star formation histories seem to match the Behroozi's in the high mass end, with both models fitting the GEEC2 data points. However, these two models do make different predictions in the low mass end, where the GEEC2 sample is not fully complete. This will need to be tested with deeper observations of group galaxies.

6.4 Rejuvenation Model

An alternate to the satellite quenching model is the possibility of having quiescent ('red') galaxies undergo a process that restarts star formation, for example, through the process of wet minor mergers or through gas accretion (Salim & Rich, 2010; Fang et al., 2012). We create a model of a quiescent galaxy by creating an instantaneous burst model and letting it evolve for 3 Gyr.

Then, we could re-introduce a smaller burst of star formation, which would cause an short evolution in the galaxy's colour. The addition of the new star formation would push the 'red' galaxy into the intermediate region, which we would then observe in the GEEC2 survey as an intermediate galaxy.

The major results from the rejuvenation model can be seen in Figure 6.5. First, we find that the length in the 'green' region is a smooth function of the burst size, which ranges from ~ 0.02 Gyr for a 0.1 per cent burst to ~ 0.3 Gyr for a 10 per cent burst. This can then be converted to an estimate of the number of bursts required to create the population of intermediate galaxies observed.

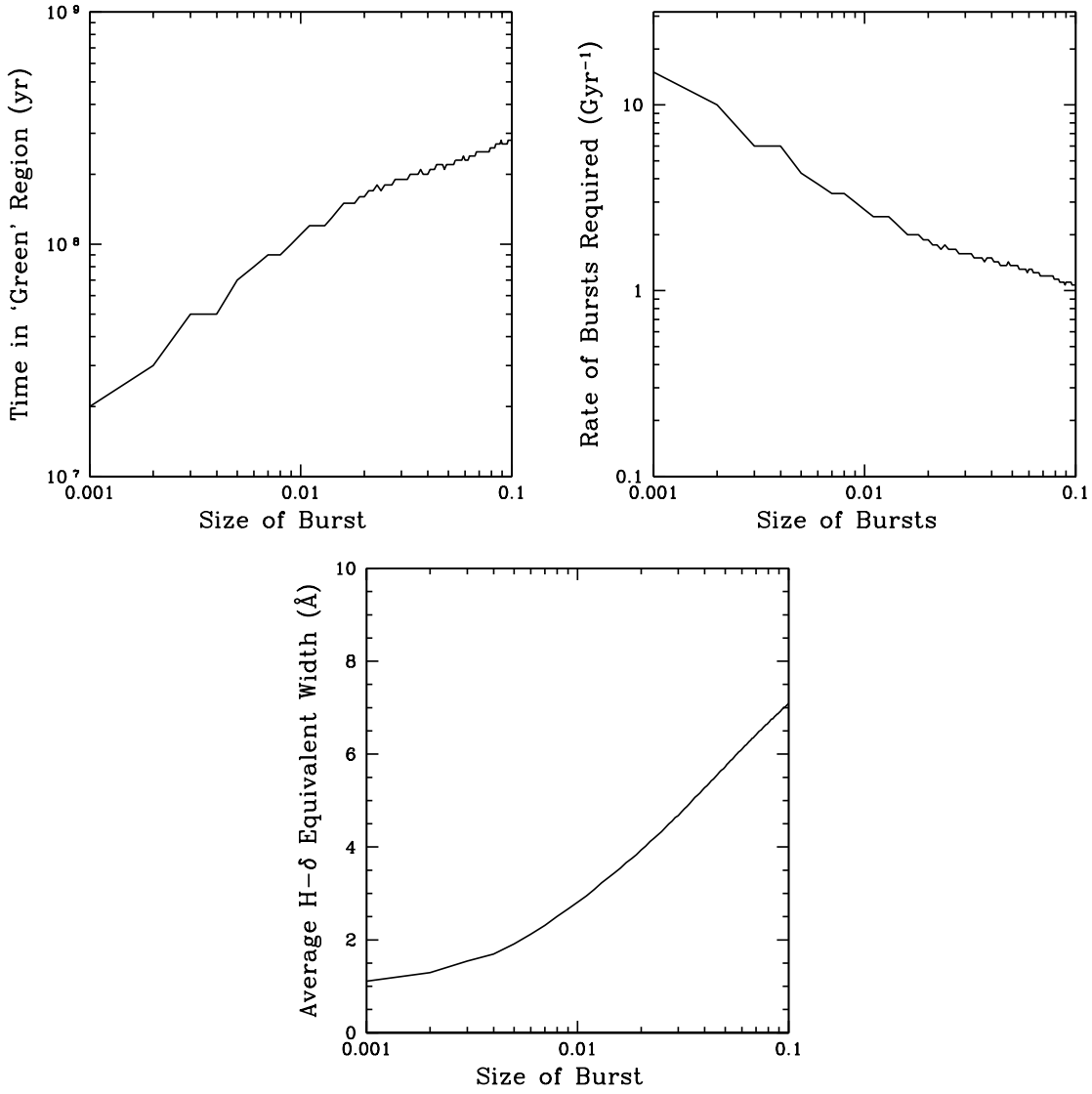

Figure 6.5: Summary of results from the rejuvenation model. *Top left:* The length of time that the rejuvenated galaxy is observable in the 'green' region, as a function of the size of the burst. *Top right:* The number of bursts required per Gyr to explain the proportional of intermediate galaxies in the GEEC2 survey, as a function of the size of the burst. *Bottom:* The average Hδ strengths of these rejuvenated galaxies, as a function of the size of the burst.

For example, a ~ 1 per cent burst would spend ~ 0.1 Gyr in the 'green' region. Since intermediate galaxies compose up to $\sim 15 - 20$ per cent of the overall galaxy population or up to ~ 30 per cent of the total combined quiescent + intermediate population in the GEEC2 sample, this would mean that these quiescent galaxies have to switch to the 'green' phase ~ 3 times per Gyr. We can also compute that value for each individual model in Figure 6.5, where the number of bursts ranges from ~ 10 for a ~ 0.1 per cent burst to only ~ 1 for a ~ 10 per cent burst.

6.5 Hδ Analysis

We consider the strength of the Hδ feature for the different models in Figure 6.6, by performing the same weighted averages and mass binning done for the fraction of quiescent, intermediate and star-forming galaxies.

The quenching models produce Hδ strengths higher than from the GEEC2 sample of intermediate ('green') galaxies. This is a roughly 2σ deviation to the $\tau_2 = 0.25$ Gyr models. The large uncertainties in the measurement for green galaxies are caused by our small sample of these 'green' galaxies as well as the low signal-to-noise measurements of their spectra.

Interestingly, the models also predict higher Hδ strengths for the star-forming galaxies as well. This might be caused by an incomplete measurement of the emission component in the GEEC2 sample. However, this effect should be unimportant for the intermediate ('green') group galaxies.

While the sample of intermediate galaxies is small, and the measurement of this weak line is generally of low signal to noise, it appears that the rejuvenation model (with a ~ 1 per cent burst), predicts a more reasonable range of Hδ values. This is likely because the relatively small sizes of the burst compared to the stellar population, while enough to push a galaxy into the 'green' window, is not enough to lead to a significant increase in the Hδ value.

From Figure 6.5, the strength of the Hδ feature ranges from ~ 1.6Å for a ~ 0.1 per cent burst to ~ 6.5Å for a ~ 10 per cent burst. For example, a 10 per cent burst would make galaxy extremely strong in the Hδ absorption feature, far stronger than the range we would expect from our GEEC2 'green' group sample.

A ~ 1 per cent burst would also require roughly a maximum of ~ 3 events per Gyr, assuming all the observed 'green' galaxies are the rejuvenated variety. This may not be completely unrealistic at this redshift and mass ratio (Lin et al., 2008).

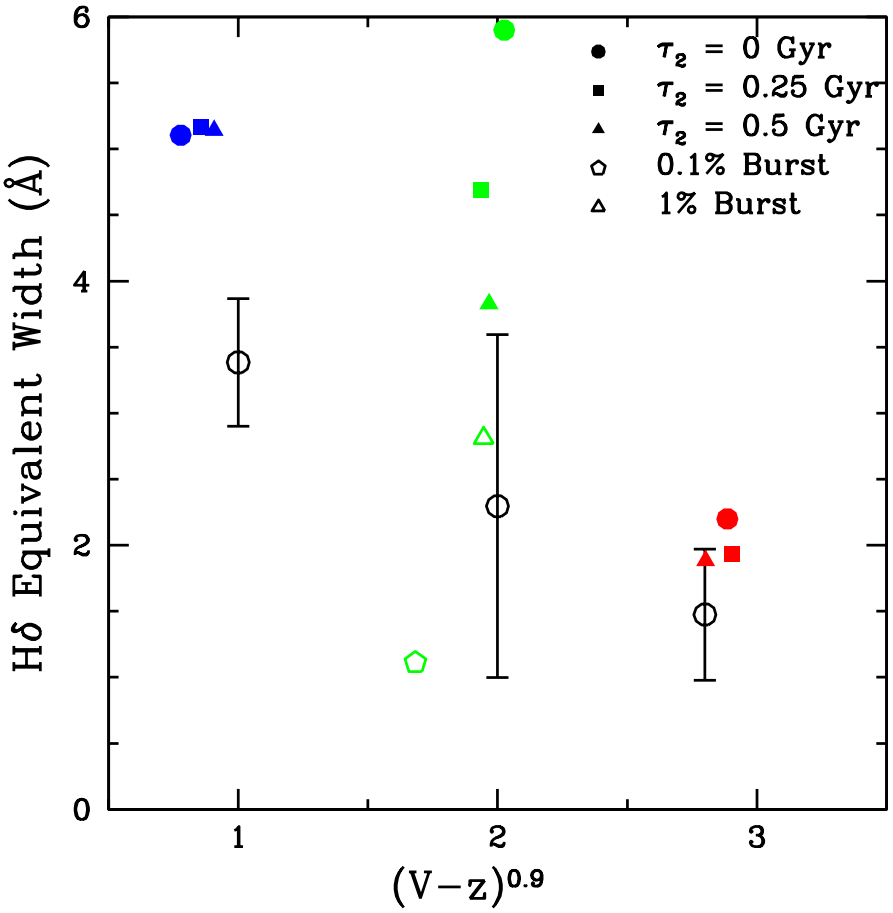

Figure 6.6: Satellite quenching model with a varying τ_2 and a delay timescale that is dependent on the dynamical time and its impact on the $(V-z)^{0.9}$ colour and Hδ equivalent widths. The results for models with a mass of $\log(M_*) = 10.5 M_\odot$ are presented. The *filled circles* indicates the population of quiescent, intermediate and star-forming galaxies with $\tau_2 = 0$ Gyr, the *filled squares* for models with $\tau_2 = 0.25$ Gyr, and the *filled triangles* for models with $\tau_2 = 0.5$ Gyr. The *open pentagon* shows the expected Hδ value for the intermediate galaxies with a 0.1 per cent burst, while the *open triangle* show the same for the 1 per cent burst. The *open circles* with the error bars are the measured Hδ widths from the GEEC2 survey (their location on the x-axis is arbitary).

Chapter 7

Discussion

7.1 Star-Forming/Intermediate/Quiescent Fractions

From the GEEC2 sample, we observe the presence of an intermediate ('green') population, which may represent a transition from the blue cloud to red sequence (Bell et al., 2004; Georgakakis et al., 2008; Lemaux et al., 2012). If the intermediate population is indeed a transition from the star-forming fraction, then the ratio of the 'green' and 'blue' galaxies fractions should give some indication of the rate at which this transformation is occurring. This possible transition fraction is largest for the highest mass galaxies, and is ~ 20 per cent at $M_{\rm star} \sim 10^{10.5} M_{\odot}$.

In addition, there is no strong evidence that the fraction is any higher within groups, given the uncertainties. If the green galaxies do represent a 'transition' population, then many of them may be associated with the mass-quenching population, from the model of Peng et al. (2010). Since this mass-quenching would be generally independent of environment, this process would produce the same amount of intermediate objects in both the field and groups.

Another strong possibility, as shown by the modelling, is that some of these galaxies may represent predominantly quiescent (early-type) galaxies that have been partially rejuvenated. For example, this could happen following a minor merger event which provides fuel for additional star formation. This process could also produce roughly the same amount of intermediate objects in both the field and groups.

On the other hand, the 'field' population in the GEEC2 survey are galaxies within the GMOS field of view that are not identified as one of the 11 main groups as well

as objects from the zCOSMOS 10k catalog. As a representative sample, many of the field 'green' galaxies may be satellites as well. Even though the data itself shows no significant difference between the 'group' and field population, the possibility remains that this population is environment-driven. This result would need to be tested with highly complete spectroscopic surveys of the field at this redshift.

Of course, even though most of the intermediate population do not appear to be directly related to the group environment, the fact that we observe higher fractions of passive galaxies inside groups (for $M_{\rm star} < 10^{10.7} M_{\odot}$) implies that environment would have to play a significant role.

7.2 Star Formation Rates

We have measured star formation rates using two main methods, [OII] based and FUV + IR based. The FUV method includes both a direct measurement of infrared emission from Spitzer 24 micron MIPS data, as well as an estimate of the dust attenuation from the UV colour (FUV-NUV). Both methods of determining star formation rates provide results consistent with each other, after a calibration was made to account for the differences in the properties of galaxies in the local universe and at $z \sim 1$.

First, the measurements of the star formation rates give validity to our separation into star-forming ('blue), intermediate ('green'), and quiescent ('red'). We found that the star-forming galaxies have high specific star formation rates, followed by the intermediate, and then the quiescent galaxies. Furthermore, the data from both the star-forming group and field population seem to match the star-forming sequence found in similar works (Elbaz et al., 2007; Whitaker et al., 2012a).

Second, both the group and the field show a similar fraction of starburst galaxies (~ 5 per cent). There were no indications that the group population is home to a higher number of starbursts than the field population, as seen in other studies (Dressler et al., 2013; Webb et al., 2013).

Third, while there are indications that the star formation rates inside groups are lower than in the general field for the star-forming galaxies, this result is not yet statistically significant given the amount of galaxies present in the GEEC2 sample. With more data, it may be possible to properly distinguish between these two populations.

7.3 Modelling the Intermediate Galaxies

With the combination of observational results and theoretical modeling, we can begin to determine which models are favoured and which models can be safely excluded. From the perspective of the GEEC2 survey, the number of galaxies in our sample, and the mass range where we are complete, the choice of the Behroozi and Noeske star formation histories have led to the same conclusion.

For the quenching models, a combination of a delay timescale that scales with the dynamical time and a second exponential timescale (τ_2) $\sim$ 0.25 Gyr seems to best match observations. Models with a lower value of the delay timescale, such as the no-delay scenario, would require a much larger τ_2 to reduce the number of quiescent galaxies. However, the quenching timescale is strongly constrained by the proportion of intermediate galaxies observed. Furthermore, a very long delay timescale, such as a constant 3 Gyr from the local universe, may be hard to reconcile with observed fractions of quiescent galaxies at $z \sim 1$.

Stronger constraints can be imposed by combining these two scenarios, the rejuvenated early-type galaxy model and the satellite quenching model. It is possible that the intermediate population would contain a mixture of these two models. For example, if a certain proportion of intermediate galaxies are rejuvenated early-types, then the amount of 'transition' or environmentally quenched intermediate galaxies would have to be even lower and vice versa. Therefore, the second exponential timescale (τ_2) can be constrained to be < 0.25 Gyr and the 'burst' rate to be $\lesssim 3$ per Gyr.

For future observations, there are two main avenues to pursue. First, we will need to increase the signal-to-noise ratio for Hδ measurements and to reduce the error bars for the measurements of the fraction of quiescent, intermediate and star-forming galaxies for our group galaxies. This can be accomplished by simply observing more groups and identifying more satellite galaxies. Having a larger sample would allow us to further constrain the parameters of any quenching or rejuvenation model.

Second, we will need to go deeper in our surveys at $z \sim 1$, in order to find lower mass satellite galaxies. This is especially true for the quiescent galaxies and the intermediate ('green') population, as the GEEC2 survey is only complete at a much higher stellar mass limit compared to actively star-forming galaxies.

A push to lower mass satellites will allow us to differentiate between the mass-dependent quenching models and the mass-independent rejuvenation models. In addition, the use of Noeske and Behroozi star formation histories predicts different trends of the fraction of quiescent and star-forming galaxies with mass. If we can determine the fractions of

quiescent, intermediate and star-forming satellites galaxies with stellar masses less than $10^{10.5} M_{\odot}$, we can verify the predictions that our models have made.

Finally, the effects of the rejuvenation process is different from that of environment quenching. For example, the rejuvenation of early-type galaxies should affect the field population equally. With a deep and complete group and field sample, we can robustly compare the properties of these two population and better constrain our two scenarios.

Chapter 8

Conclusions

For the first part of this thesis, we used data from the Group Environment Evolution Collaboration 2 (GEEC2) survey, which provided highly complete GMOS spectroscopy for 11 galaxy groups at $0.8 < z < 1$. We then divided the galaxies into three subpopulations in a colour-colour plot: star-forming ('blue'), intermediate ('green'), and quiescent ('red'). In particular, we looked at the fractions of each sub-populations, comparing the group and field sample. We also studied the spectra of these objects, measuring their Hδ and [OII] strengths to present a picture of their star formation history. We conclude the following:

- The strongest environmental dependence is on the fraction of quiescent galaxies. This fraction is higher inside groups than in the field for all stellar masses.
- For the normal star-forming galaxies, the average specific star formation rates (sSFR) for the high mass ($M_{\rm star}/M_{\odot} > 10^{10.3}$) group sample is ~ 55 per cent lower than the field population, but the difference is not statistically significant. For the low mass star-forming galaxies, where our sample is incomplete, we observe no difference in the specific star formation rate (sSFR) between the group and the field.
- The intermediate galaxy population represents approximately the same fraction of the star-forming population at all stellar masses, in both the group and the field. Neither the group or field spectra show very strong Hδ absorption, which indicates that their populations are not dominated by post-starburst galaxies.
- Green galaxies in the group exhibit a factor of ~ 3 lower sSFR than the field, calculated using their stacked spectra. This suggests that the origins of at least some of these transitional systems may be caused by quenching of star-formation that is environmentally dependent.

- The star-forming group and field galaxies seem to match the star forming sequence for field galaxies at $z = 0.9$ of Whitaker et al. (2012b), especially in the region where the GEEC2 sample is complete ($> 10^{10.5} M_{\odot}$).

- For the FUV + IR measurements, if we take the limit of 4× sSFR threshold from Rodighiero et al. (2011) to be the threshold for starburst galaxies, then only 4.4 per cent fit this criteria (4 out of 90), compared to 5.1 per cent (44 out of 871) in the field. From the [OII] star formation rate measurements, only 6.7 per cent are starburst galaxies (6 out of 90). This result gives validity to our assumption that quenching is the primary factor in the transition between star-forming and quiescent states.

For the second part of this thesis, two set of models were created to help explain the intermediate ('green') population, the quenching scenario and the rejuvenated early-type scenario. For the quenching models, we used the Behroozi et al. (2012) and Noeske et al. (2007b) star formation histories to model star-forming galaxies. We tested the use of different quenching timescales (τ_2), and the addition of delays, such as a simple 3 Gyr delay and a delay that is dependent on the dynamical time. We conclude the following:

- For the quenching scenario, the fraction of intermediate ('green') galaxies is strongly dependent on the second quenching timescale (τ_2).

- The star-forming/intermediate/quiescent fractions rule out the no-delay scenario, which would require a long τ_2 that over-produces immediate-colour galaxies. They also rule out the 3 Gyr delay model, which does not produce a sufficient amount of quiescent galaxies.

- The observed fractions are best matched with a dynamical delay time and $\tau_2 = 0.25$ Gyr. However, this best-fitting quenching model predict the intermediate ('green') galaxies Hδ strength higher than the observed Hδ strengths (a $\sim 2\sigma$ deviation). This may be caused by the low number of these 'green' galaxies observed, the low signal-to-noise ratios of their spectra, or a portion of the observed intermediate galaxies to have originated from another source.

- For the rejuvenation scenario, it is found that the time observed in the 'green' region is a smooth function of the burst size. A large number of small bursts or a smaller number of large bursts can both explain the population of intermediate ('green') galaxies.

- The observed Hδ strength for the 'green' population can be used to constrain the burst size, which is best matched with a burst size of ~ 1 per cent, at a rate of ~ 3 times per Gyr.

- The combination of environmental quenching and rejuvenation may be at work in the GEEC2 sample. The fraction of quiescent galaxies suggests that environmental quenching is present, but the models do not match the Hδ strength perfectly. On the other hand, the rejuvenation scenario points to a high 'burst' rate of ~ 3 per Gyr and would not lead to any environmental dependence. If both of these processes are taking place, then we can constrain the 'burst' rate to be $\lesssim 3$ per Gyr and $\tau_2 < 0.25$ Gyr.

The models investigated in this work, although simple, can be used as a starting point to a better understanding of the star-formation histories of these group galaxies. From the results, we know that environmental quenching must act quickly once it has begun, in order to explain the fraction of intermediate galaxies observed. The models also suggest that any delay at $z \sim 1$ must be shorter than at $z = 0$, which indicates that this process may be related to the dynamical time or to the orbit of galaxies in the haloes.

In order to better constrain the quenching scenario and the rejuvenated early-type scenario, we will need to increase the signal-to-noise ratio for the Hδ measurements and reduce the error bars for the measurements of the fraction of quiescent, intermediate and star-forming galaxies for group and field galaxies. Furthermore, we will need to go deeper in new surveys at $z \sim 1$, in order to find lower mass satellite galaxies and remain reasonably complete for these quiescent objects. These new data-sets will allow us to better differentiate between the different mass-dependent quenching and rejuvenation processes.

References

Arnouts S. et al., 2007, Astron. Astrophys., 476, 137

Balogh M. L. et al., 2009, MNRAS, 398, 754

Balogh M. L. et al., 2011, MNRAS, 412, 2303

Balogh M. L., Morris S. L., Yee H. K. C., Carlberg R. G., Ellingson E., 1999, ApJ, 527, 54

Behroozi P. S., Wechsler R. H., Conroy C., 2012, ArXiv e-prints ArXiv:1207.6105B

Bell E. F., McIntosh D. H., Katz N., Weinberg M. D., 2003, ApJS, 149, 289

Bell E. F. et al., 2004, ApJ, 608, 752

Binney J., Tremaine S., 2008, Galactic Dynamics: Second Edition. Princeton University Press

Blanton M. R., Moustakas J., 2009, Ann. Rev. Astron. Astrophys., 47, 159

Bower R. G., Benson A. J., Crain R. A., 2012, MNRAS, 422, 2816

Bower R. G., Benson A. J., Malbon R., Helly J. C., Frenk C. S., Baugh C. M., Cole S., Lacey C. G., 2006, MNRAS, 370, 645

Brammer G. B. et al., 2009, ApJL, 706, L173

Bruzual G., 2007a, in From Stars to Galaxies: Building the Pieces to Build Up the Universe, ed. A. Vallenari, R. Tantalo, L. Portinari, & A. Moretti, pp. 303–+

Bruzual G., 2007b, in Astronomical Society of the Pacific Conference Series, Vol. 374, From Stars to Galaxies: Building the Pieces to Build Up the Universe, Vallenari A., Tantalo R., Portinari L., Moretti A., eds., p. 303

Bruzual G., Charlot S., 2003, MNRAS, 344, 1000

Cameron E., 2011, Proc. Astron. Soc. Aust., 28, 128

Capak P. et al., 2007, ApJS, 172, 99

Carroll B. W., Ostlie D. A., 2006, An introduction to modern astrophysics and cosmology

Cassata P. et al., 2008, Astron. Astrophys., 483, L39

Chabrier G., 2003, Publ. Astron. Soc. Pac., 115, 763

Chary R., Elbaz D., 2001, ApJ, 556, 562

Combes F., 2004, in IAU Symposium, Vol. 217, Recycling Intergalactic and Interstellar Matter, Duc P.-A., Braine J., Brinks E., eds., p. 440

Cooper M. C. et al., 2008, MNRAS, 383, 1058

Couch W. J., Sharples R. M., 1987, MNRAS, 229, 423

Cucciati O. et al., 2012, Astron. Astrophys., 539, A31

Davis M. et al., 2003, in Society of Photo-Optical Instrumentation Engineers (SPIE) Conference Series, Vol. 4834, Society of Photo-Optical Instrumentation Engineers (SPIE) Conference Series, Guhathakurta P., ed., pp. 161–172

De Lucia G., Weinmann S., Poggianti B. M., Aragón-Salamanca A., Zaritsky D., 2012, MNRAS, 423, 1277

de Vaucouleurs G., 1961, ApJS, 5, 233

Dressler A., 1980, ApJ, 236, 351

Dressler A., Oemler, Jr. A., Poggianti B. M., Gladders M. D., Abramson L., Vulcani B., 2013, ApJ, 770, 62

Eke V. R. et al., 2004, MNRAS, 355, 769

Elbaz D. et al., 2007, Astron. Astrophys., 468, 33

Faber S. M., Jackson R. E., 1976, ApJ, 204, 668

Faber S. M. et al., 2007, ApJ, 665, 265

Fang J. J., Faber S. M., Salim S., Graves G. J., Rich R. M., 2012, ApJ, 761, 23

Finoguenov A. et al., 2007, ApJS, 172, 182

Font A. S. et al., 2008, MNRAS, 389, 1619

Georgakakis A. et al., 2008, MNRAS, 385, 2049

George M. R. et al., 2012, ApJ, 757, 2

George M. R. et al., 2011, ApJ, 742, 125

Gilbank D. G., Baldry I. K., Balogh M. L., Glazebrook K., Bower R. G., 2010, MNRAS, 405, 2594

Gilbank D. G., Baldry I. K., Balogh M. L., Glazebrook K., Bower R. G., 2011, MNRAS, 412, 2111

Giodini S. et al., 2012, Astron. Astrophys., 538, A104

Glazebrook K., Bland-Hawthorn J., 2001, Publ. Astron. Soc. Pac., 113, 197

Hao C.-N., Kennicutt R. C., Johnson B. D., Calzetti D., Dale D. A., Moustakas J., 2011, ApJ, 741, 124

Hopkins P. F., Hernquist L., Cox T. J., Di Matteo T., Robertson B., Springel V., 2006, ApJS, 163, 1

Huang J.-S., Zheng X. Z., Rigopoulou D., Magdis G., Fazio G. G., Wang T., 2011, ApJ, 742, L13

Hubble E. P., 1926, ApJ, 64, 321

Huchra J., Davis M., Latham D., Tonry J., 1983, ApJS, 52, 89

Ilbert O. et al., 2009, ApJ, 690, 1236

Juneau S. et al., 2005, ApJL, 619, L135

Karim A. et al., 2011, ApJ, 730, 61

Kennicutt, Jr. R. C., 1998, ApJ, 498, 541

Knobel C. et al., 2012, ApJ, 753, 121

Knobel C. et al., 2009, ApJ, 697, 1842

Komatsu E. et al., 2011, ApJS, 192, 18

Labbé I. et al., 2005, ApJL, 624, L81

Le Fèvre O. et al., 2005, Astron. Astrophys., 439, 845

Lemaux B. C. et al., 2012, ApJ, 745, 106

Li I. H. et al., 2011, MNRAS, 411, 1869

Lilly S. J. et al., 2009, ApJS, 184, 218

Lilly S. J. et al., 2007, ApJS, 172, 70

Lin L. et al., 2008, ApJ, 681, 232

Madgwick D. S. et al., 2002, MNRAS, 333, 133

Magdis G. E. et al., 2011, Astron. Astrophys., 534, A15

McGee S. L., Balogh M. L., Bower R. G., Font A. S., McCarthy I. G., 2009, MNRAS, 400, 937

Mo H., van den Bosch F. C., White S., 2010, Galaxy Formation and Evolution

Muzzin A. et al., 2012, ApJ, 746, 188

Noeske K. G. et al., 2007a, ApJ, 660, L43

Noeske K. G., et al., 2007b, ApJL, 660, L47

Park C., Hwang H. S., 2009, ApJ, 699, 1595

Patel S. G., Kelson D. D., Holden B. P., Franx M., Illingworth G. D., 2011, ApJ, 735, 53

Peng Y.-j. et al., 2010, ApJ, 721, 193

Peng Y.-j., Lilly S. J., Renzini A., Carollo M., 2012, ApJ, 757, 4

Percival W. J. et al., 2001, MNRAS, 327, 1297

Presotto V. et al., 2012, Astron. Astrophys., 539, A55

Rodighiero G. et al., 2011, ApJL, 739, L40

Salim S. et al., 2009, ApJ, 700, 161

Salim S., Rich R. M., 2010, ApJL, 714, L290

Salim S. et al., 2007, ApJS, 173, 267

Salmi F., Daddi E., Elbaz D., Sargent M. T., Dickinson M., Renzini A., Bethermin M., Le Borgne D., 2012, ApJL, 754, L14

Sanders D. B., et al., 2007, ApJS, 172, 86

Schechter P., 1976, ApJ, 203, 297

Scoville N. et al., 2007, ApJS, 172, 1

Smith R. J., Lucey J. R., Price J., Hudson M. J., Phillipps S., 2012, MNRAS, 419, 3167

Sobral D., Best P. N., Smail I., Geach J. E., Cirasuolo M., Garn T., Dalton G. B., 2011, MNRAS, 411, 675

Somerville R. S., Hopkins P. F., Cox T. J., Robertson B. E., Hernquist L., 2008, MNRAS, 391, 481

Strateva I. et al., 2001, Astron. J., 122, 1861

Tanaka M. et al., 2012, PASJ, 64, 22

Tinker J. L., Wetzel A. R., 2010, ApJ, 719, 88

Tully R. B., Fisher J. R., 1977, Astron. Astrophys., 54, 661

van den Bosch F. C., Aquino D., Yang X., Mo H. J., Pasquali A., McIntosh D. H., Weinmann S. M., Kang X., 2008, MNRAS, 387, 79

Vollmann K., Eversberg T., 2006, Astronomische Nachrichten, 327, 862

Webb T. et al., 2013, ArXiv e-prints ArXiv:1304.3335

Wetzel A. R., Tinker J. L., Conroy C., 2012, MNRAS, 424, 232

Wetzel A. R., Tinker J. L., Conroy C., van den Bosch F. C., 2013, MNRAS, 432, 336

Whitaker K. E., Kriek M., van Dokkum P. G., Bezanson R., Brammer G., Franx M., Labbé I., 2012a, ApJ, 745, 179

Whitaker K. E., van Dokkum P. G., Brammer G., Franx M., 2012b, ApJL, 754, L29

Wilman D. J., Balogh M. L., Bower R. G., Mulchaey J. S., Oemler A., Carlberg R. G., Morris S. L., Whitaker R. J., 2005, MNRAS, 358, 71

Wilman D. J. et al., 2008, ApJ, 680, 1009

Wolf C., Gray M. E., Meisenheimer K., 2005, Astron. Astrophys., 443, 435